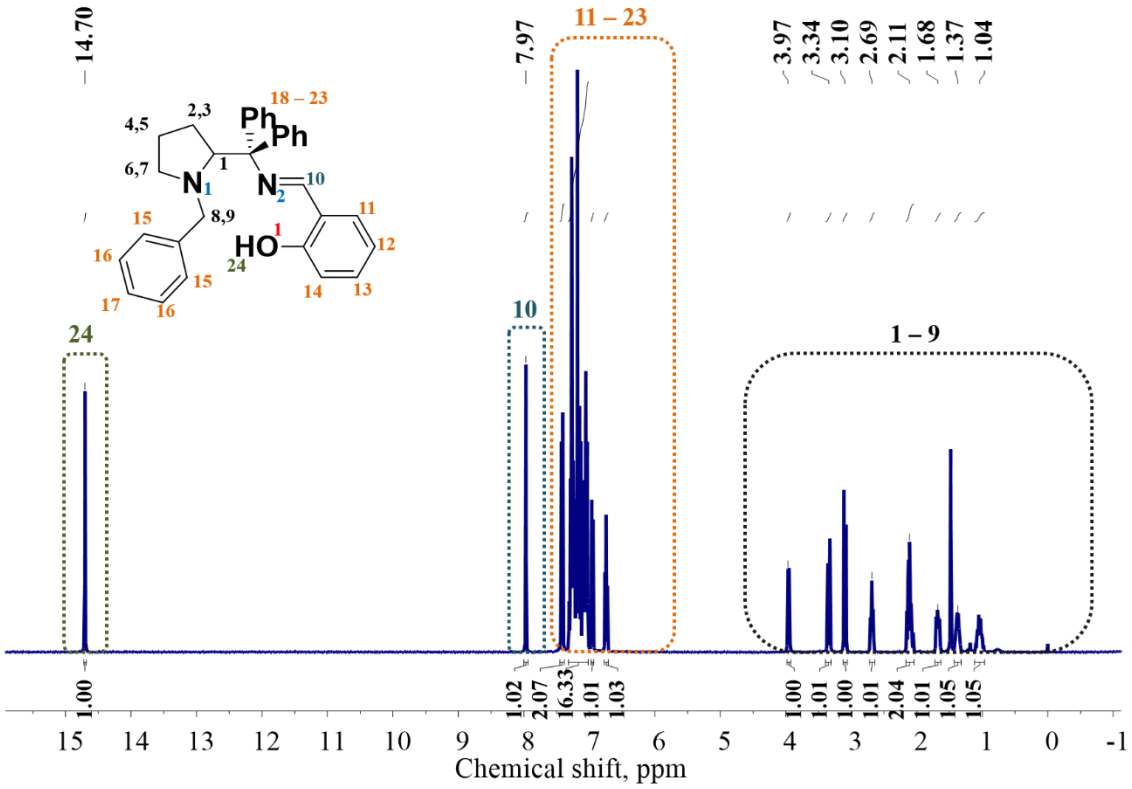

Figura S1.[1]H NMR spectrum of HL1 in $CDCl_3$ at room temperature.

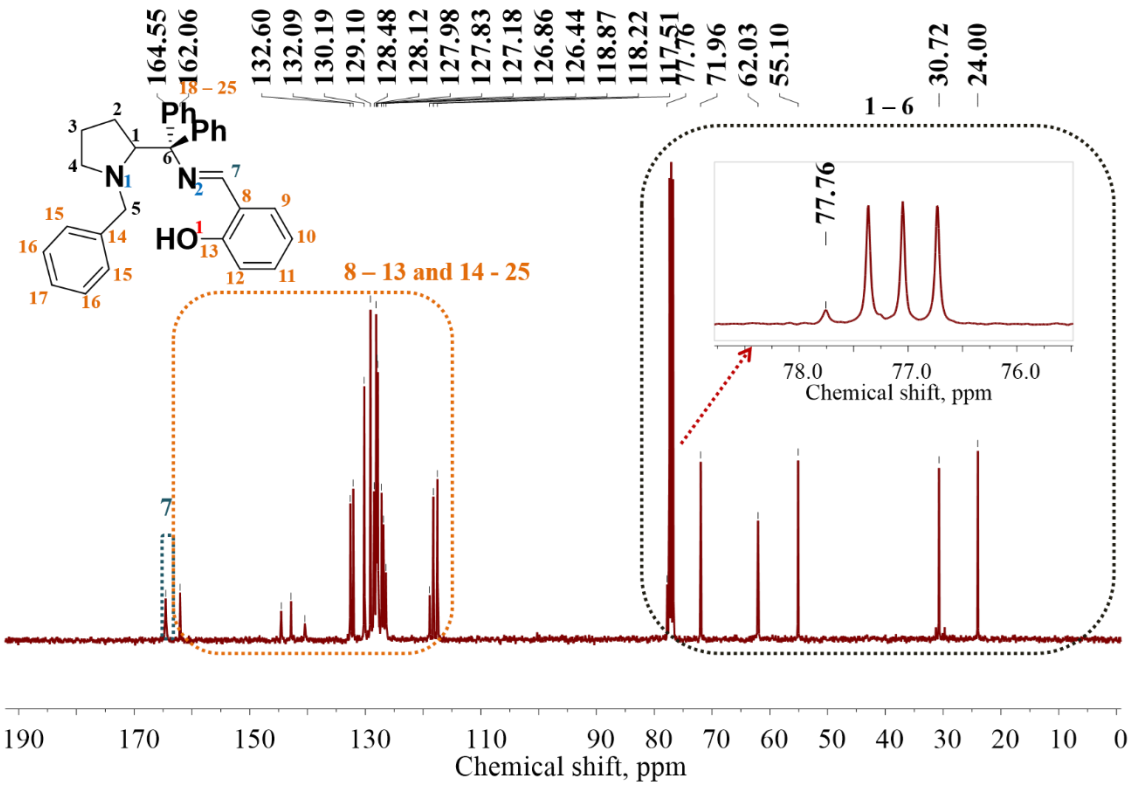

Figura S2.[13]CNMR Spectrum of HL1 in $CDCl_3$ at room temperature.

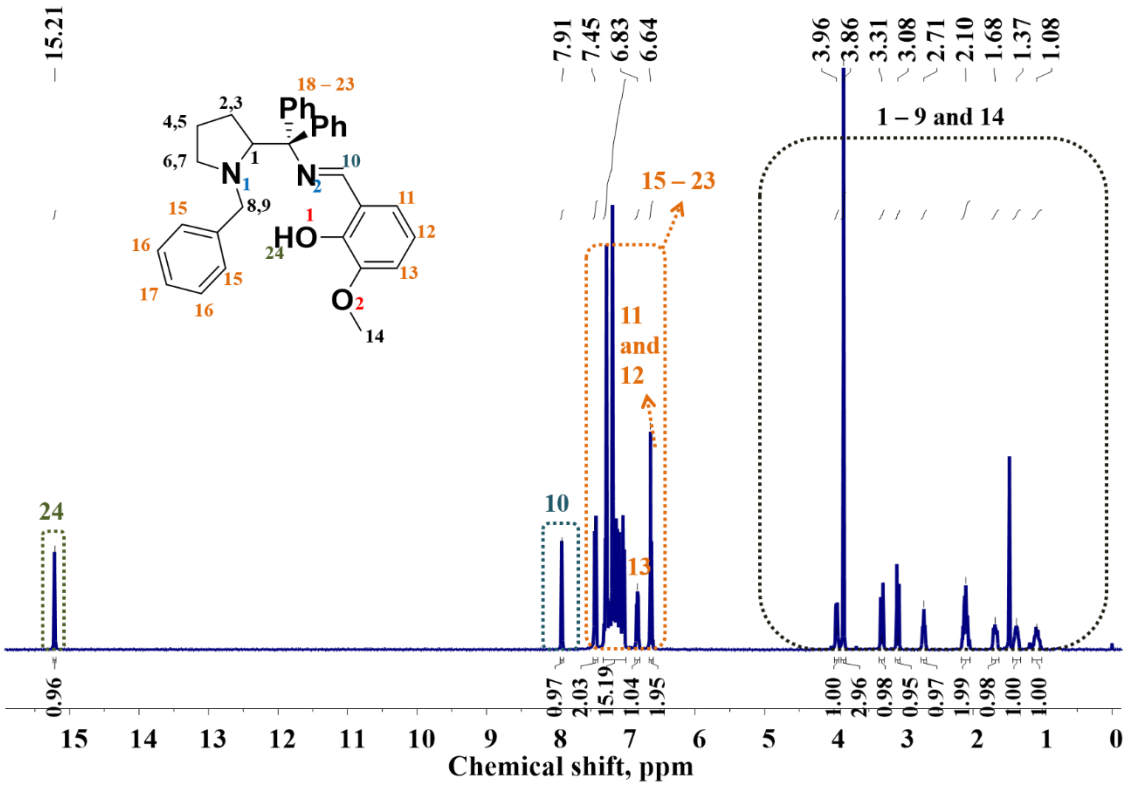

Figura S3. ^{1}H NMR spectrumof HL2 in $CDCl_3$ at room temperature.

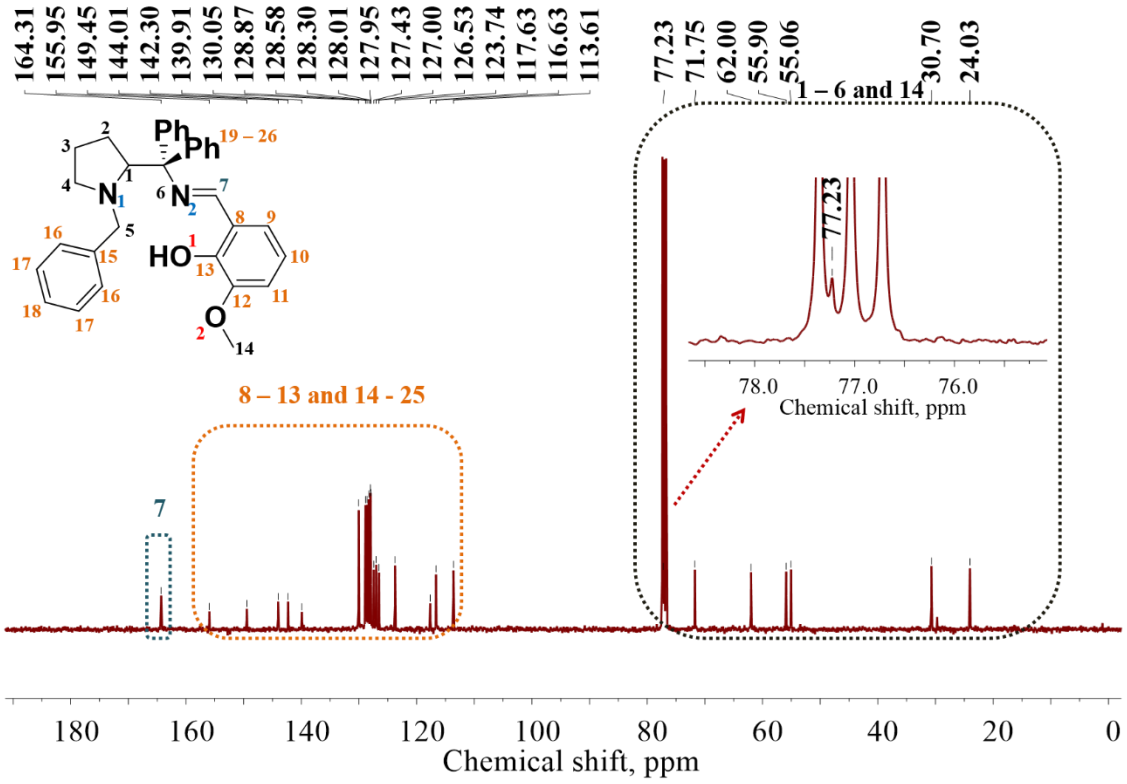

Figura S4. ^{13}CNMR spectrumof HL2 in $CDCl_3$ at room temperature.

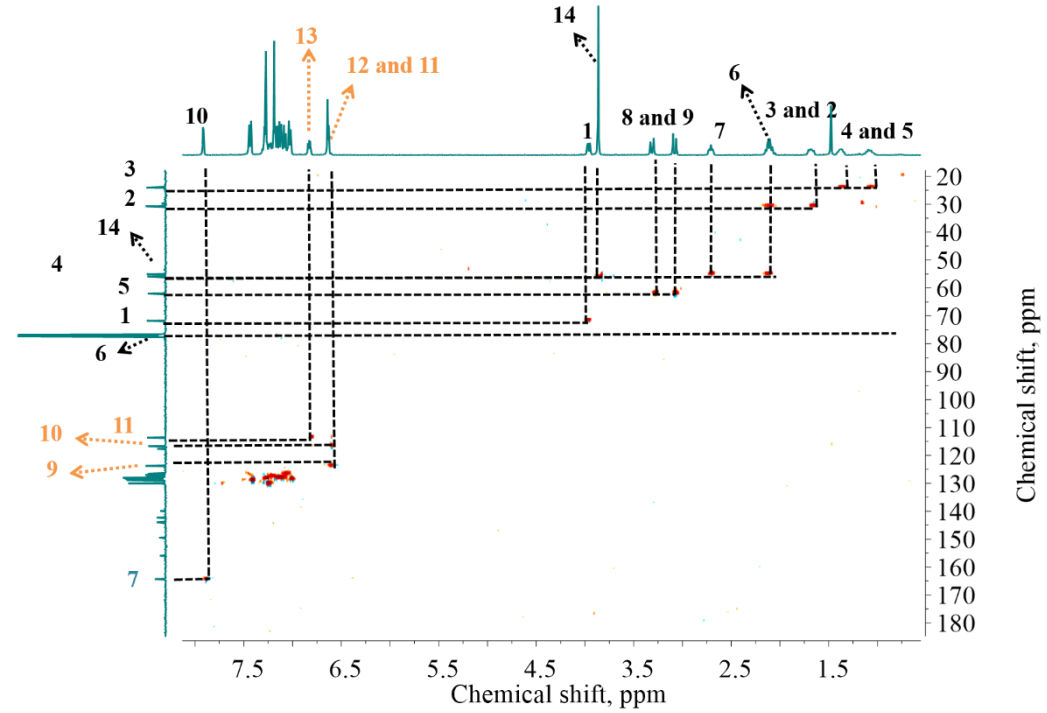

Figura S5.HSQCNMR spectrum of HL2 in $CDCl_3$ at room temperature.

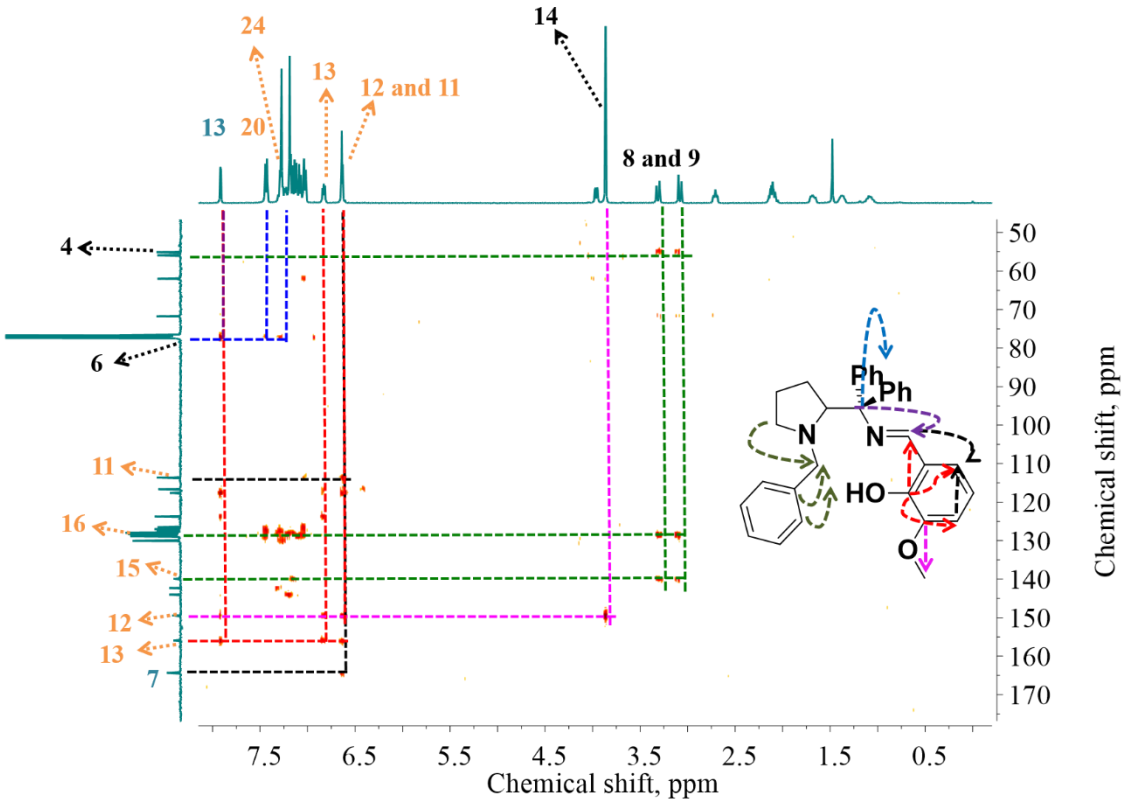

Figura S6.HMBC NMR spectrum of HL2 in $CDCl_3$ at room temperature.

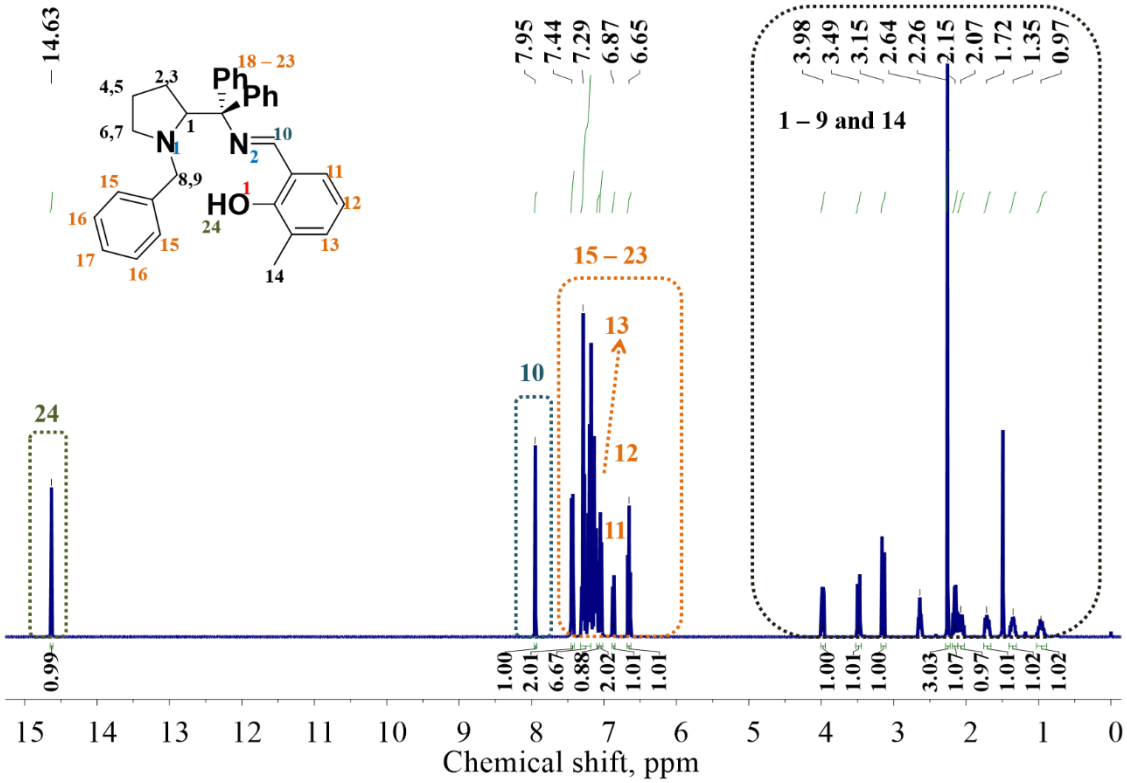

Figura S7. [1]HNMR spectrum of HL3 in $CDCl_3$ at room temperature.

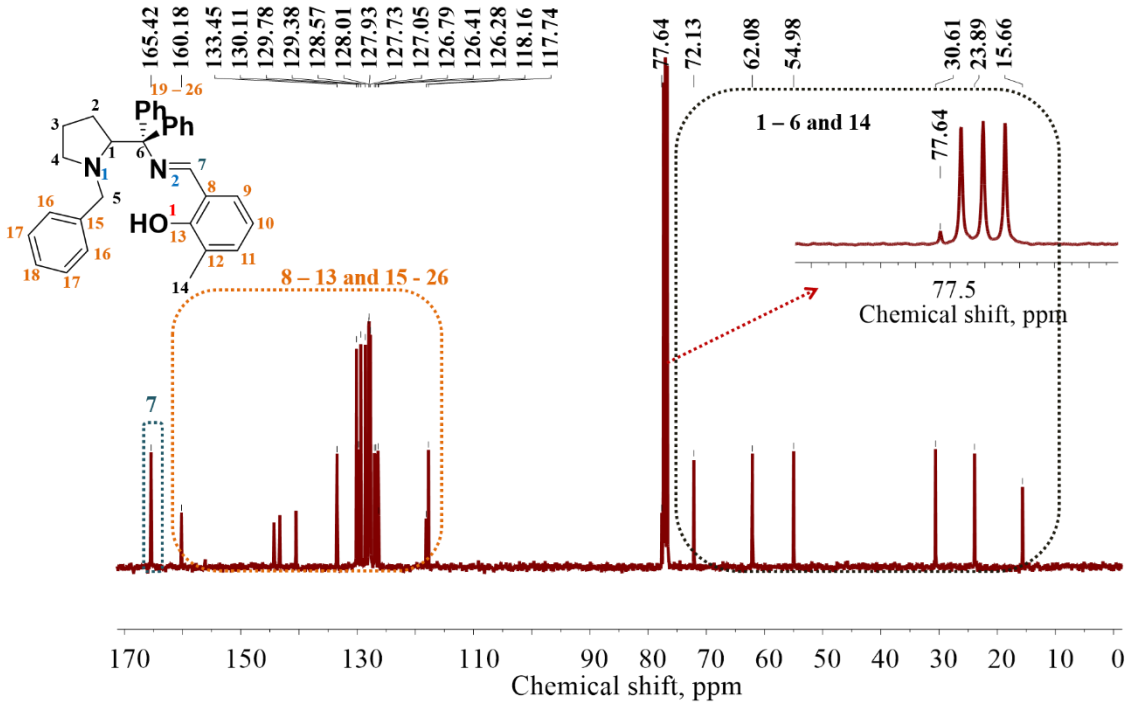

Figura S8. [13]CNMR spectrum of HL3 in $CDCl_3$ at room temperature.

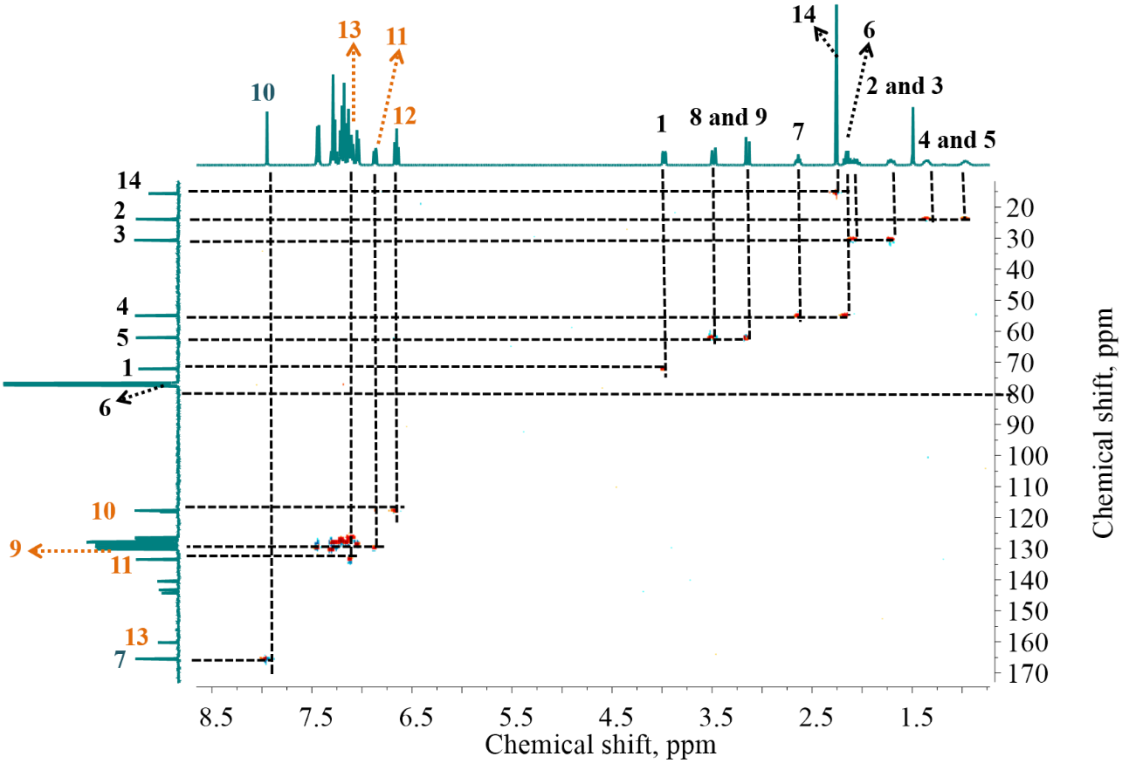

Figura S9.HSQCNMR spectrum of HL3 in $CDCl_3$ at room temperature.

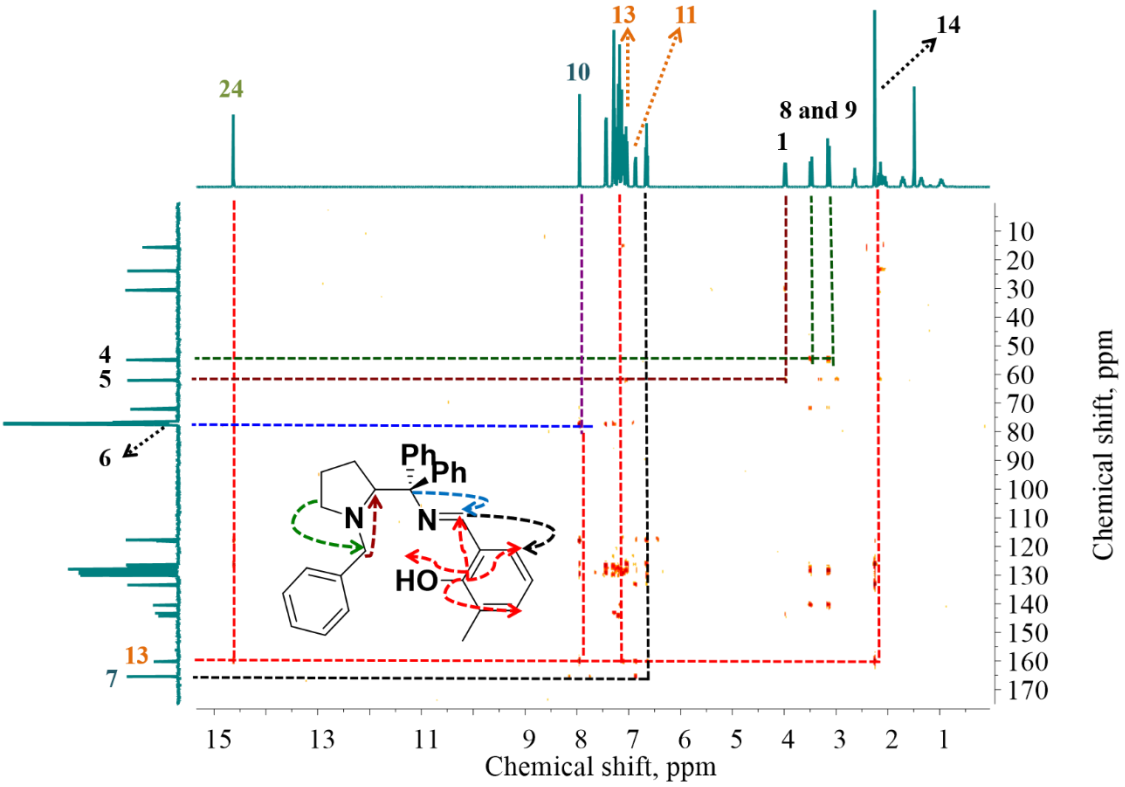

Figura S10.HMBCNMR spectrum of HL3 in $CDCl_3$ at room temperature.

Figura S11. Spectra RMN ^1H of HL4 in $CDCl_3$ at room temperature.

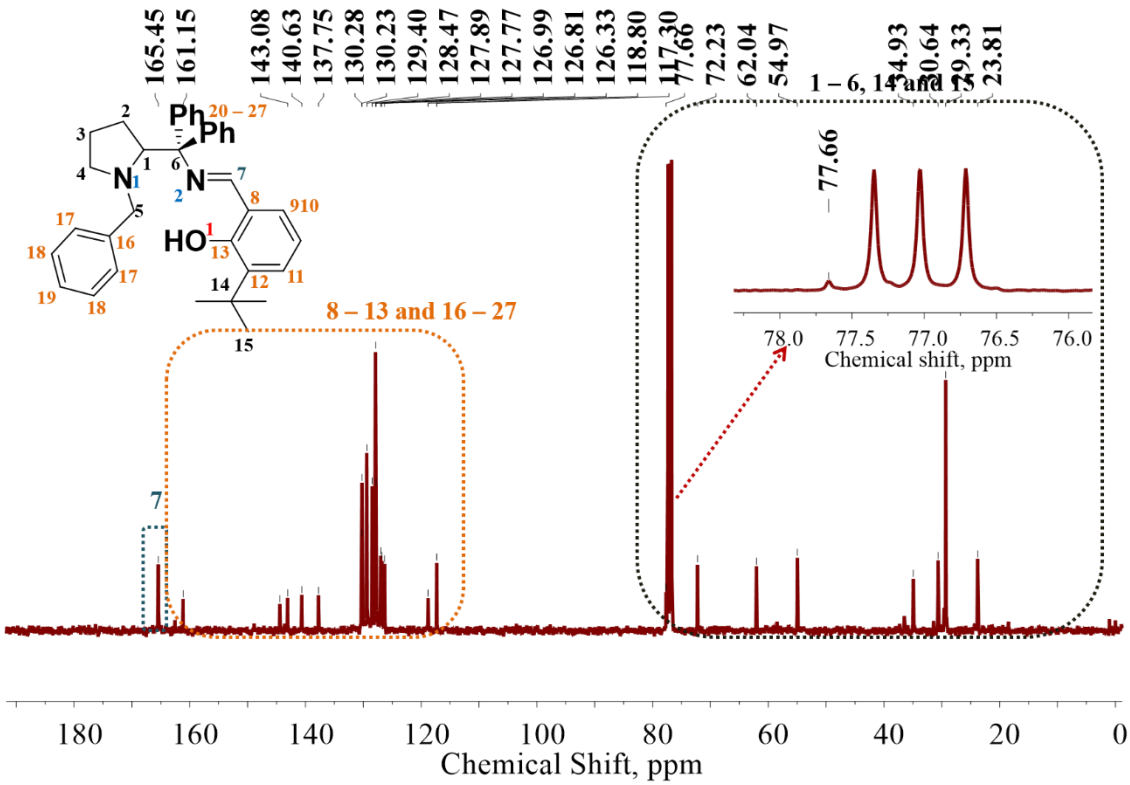

Figura S12. ^{13}C NMR spectrum of HL4 in $CDCl_3$ at room temperature.

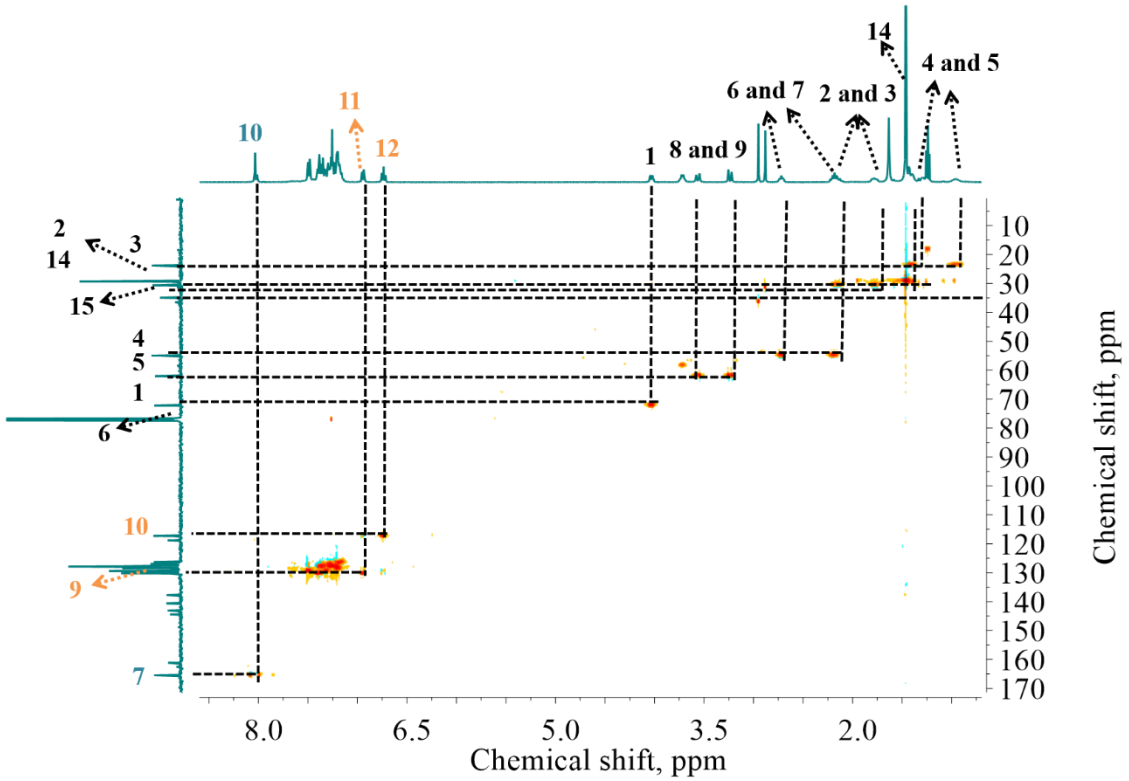

Figura S13.HSQCNMR spectrum of HL4 in $CDCl_3$ at room temperature.

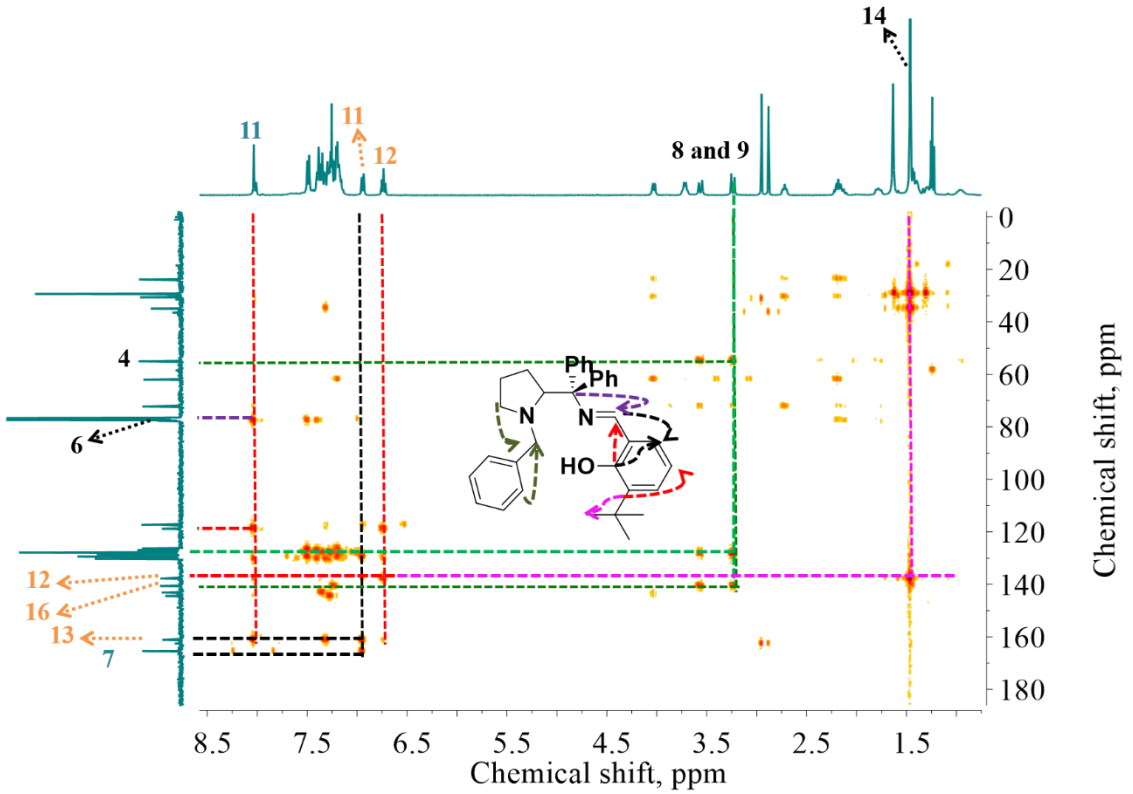

Figura S14.HBMC NMR spectrum of HL4 in $CDCl_3$ at room temperature.

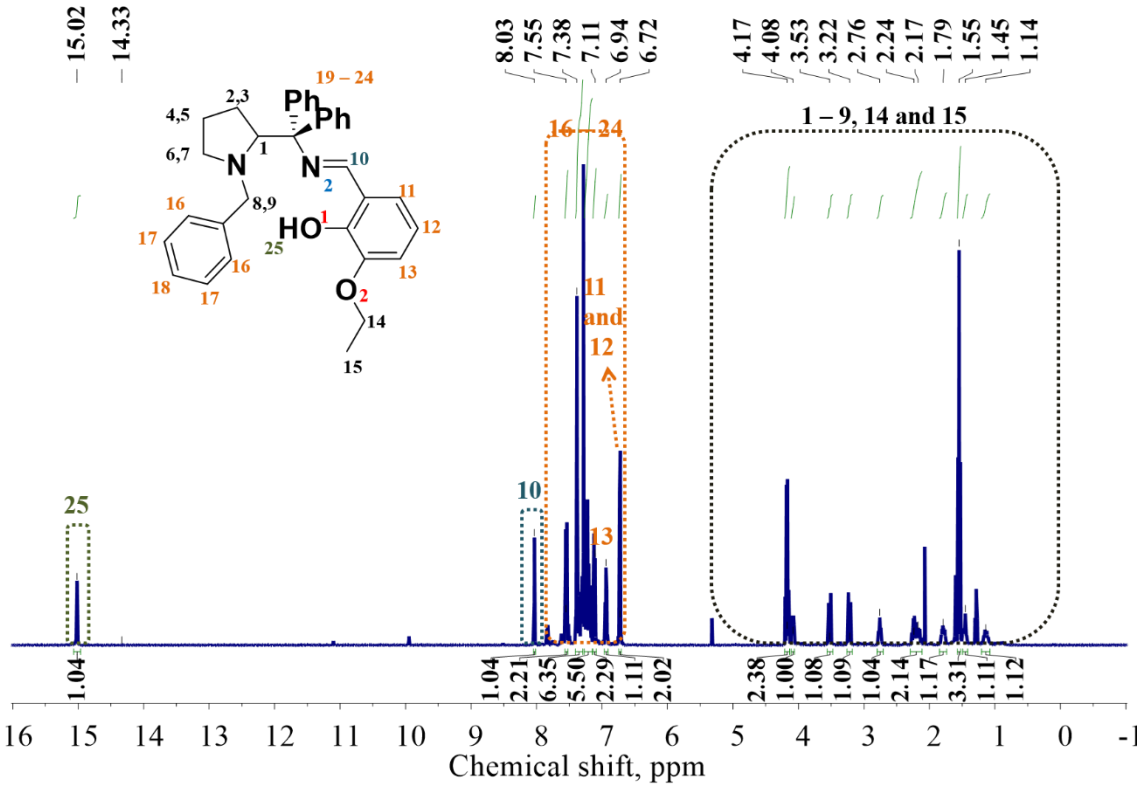

Figura S15.[1]HNMR spectrum of HL5 in $CDCl_3$ at room temperature.

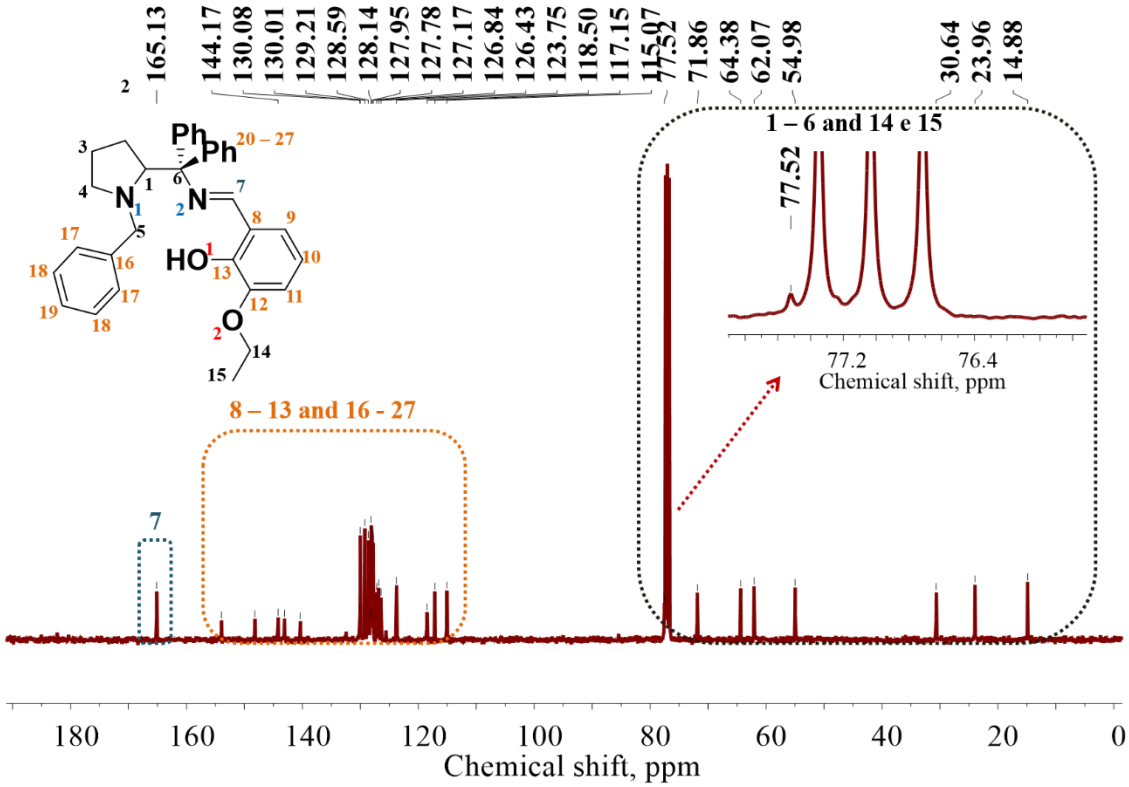

Figura S16. ^{13}C NMR spectrum of HL5 in $CDCl_3$ at room temperature.

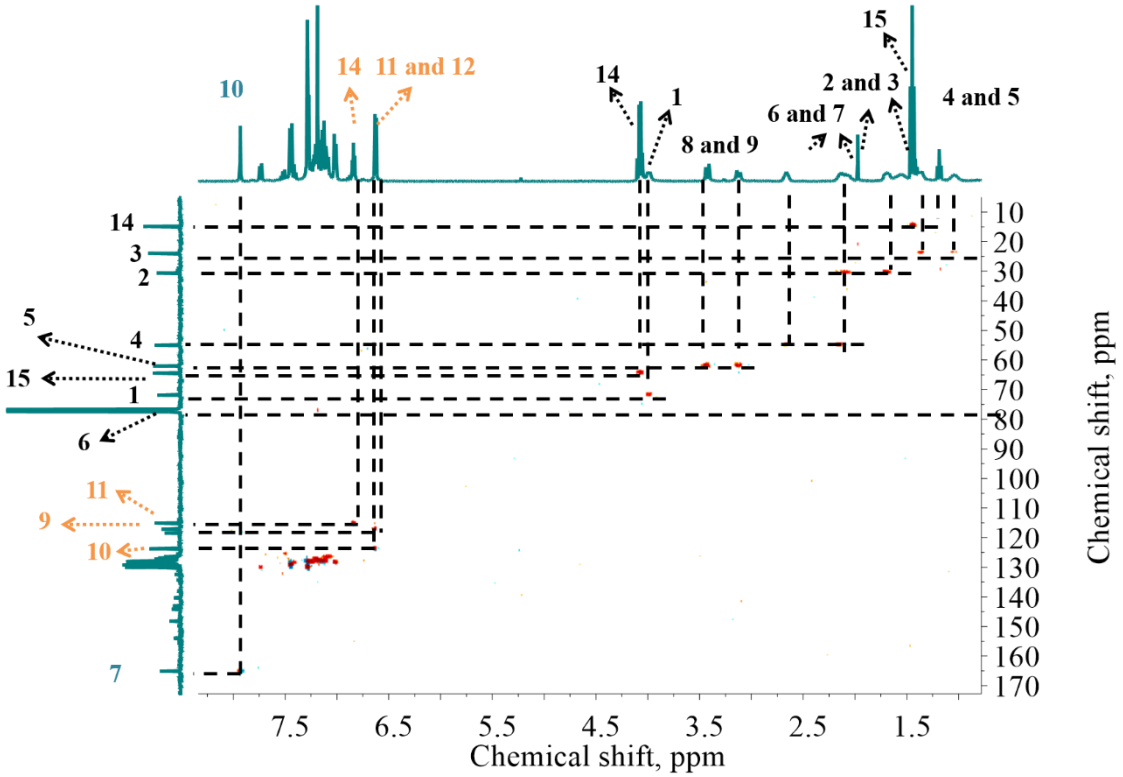

Figura S17.HSQCNMR spectrum of HL5 in $CDCl_3$ at room temperature.

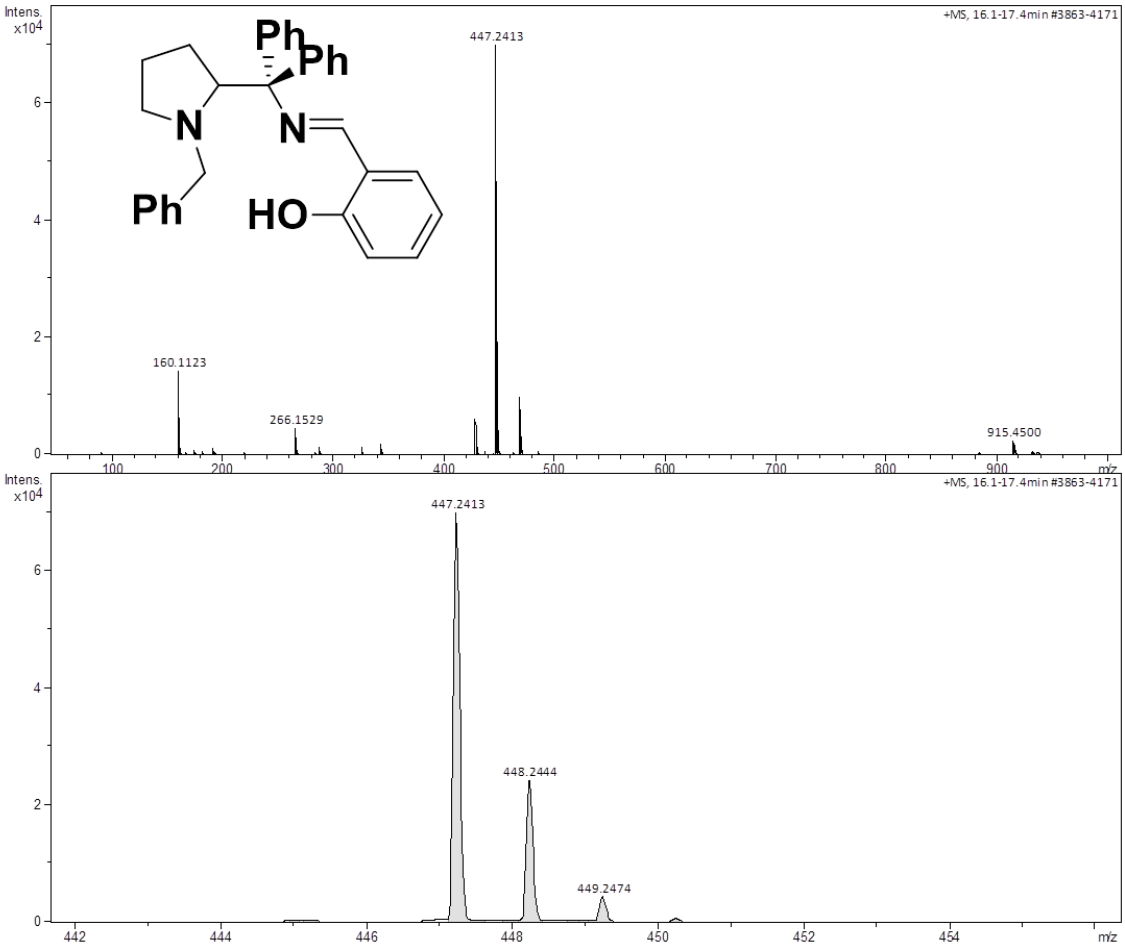

Figura S18. High Resolution Mass Spectra and Isotopic Pattern of HL1 in Ethyl Acetate/Methanol.

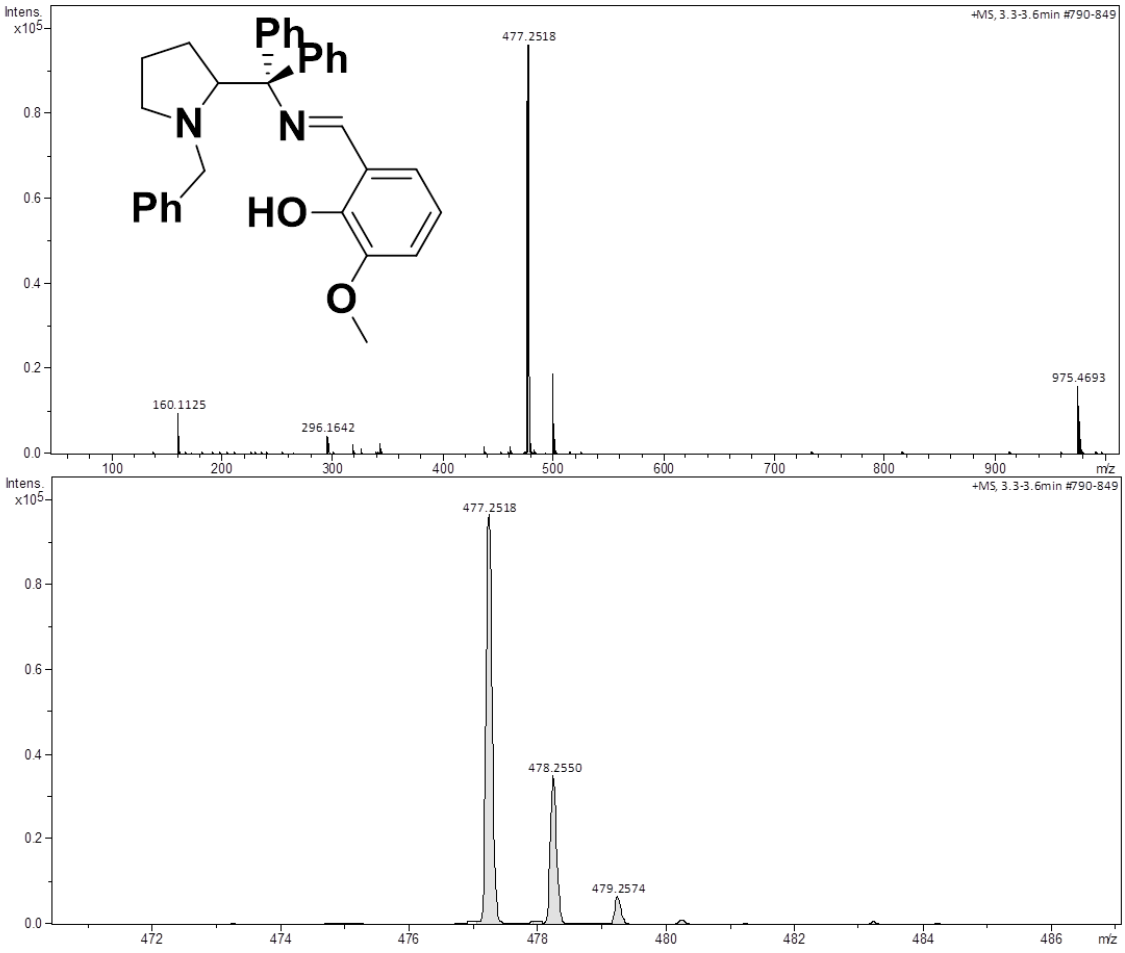

Figura S19. High Resolution Mass Spectra and Isotopic Pattern of HL2 in Ethyl Acetate/Methanol.

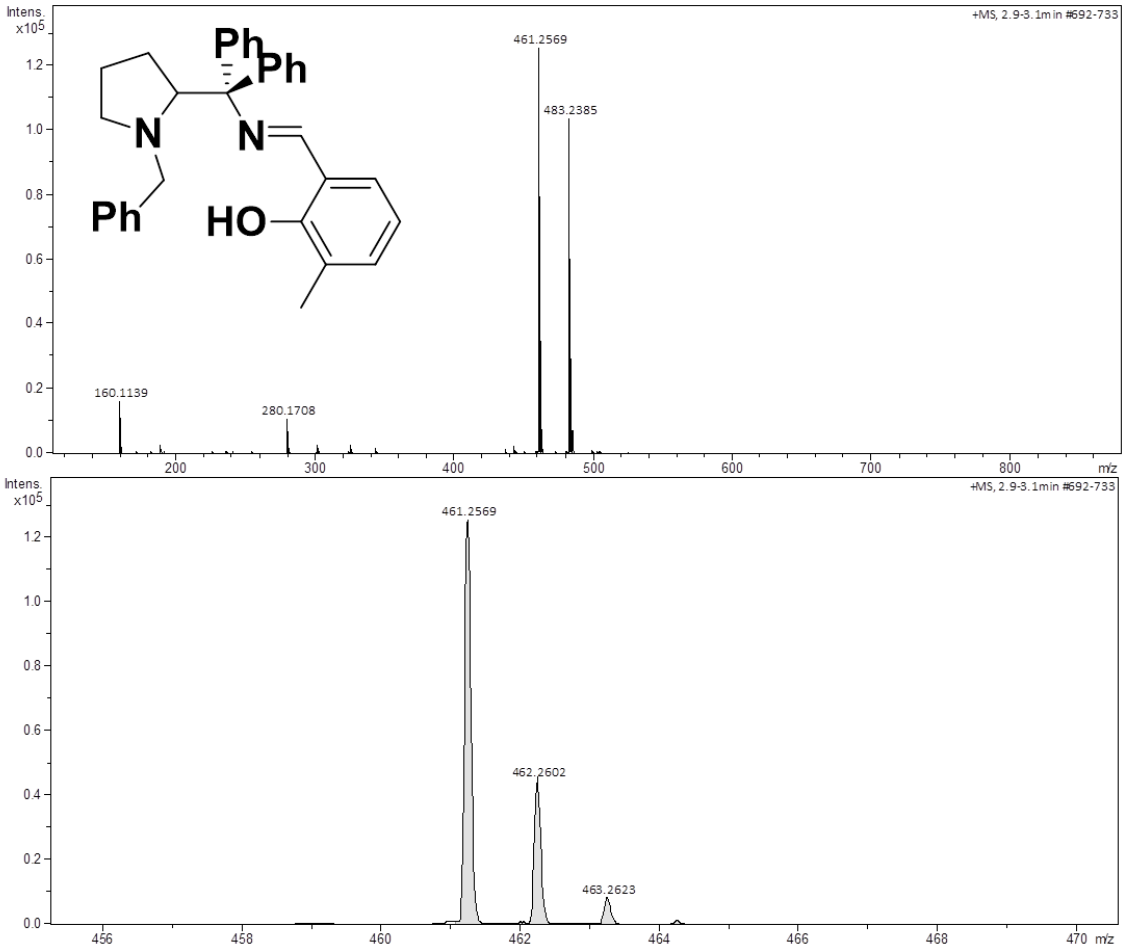

Figura S20. High Resolution Mass Spectra and Isotopic Pattern of HL3 in Ethyl Acetate/Methanol.

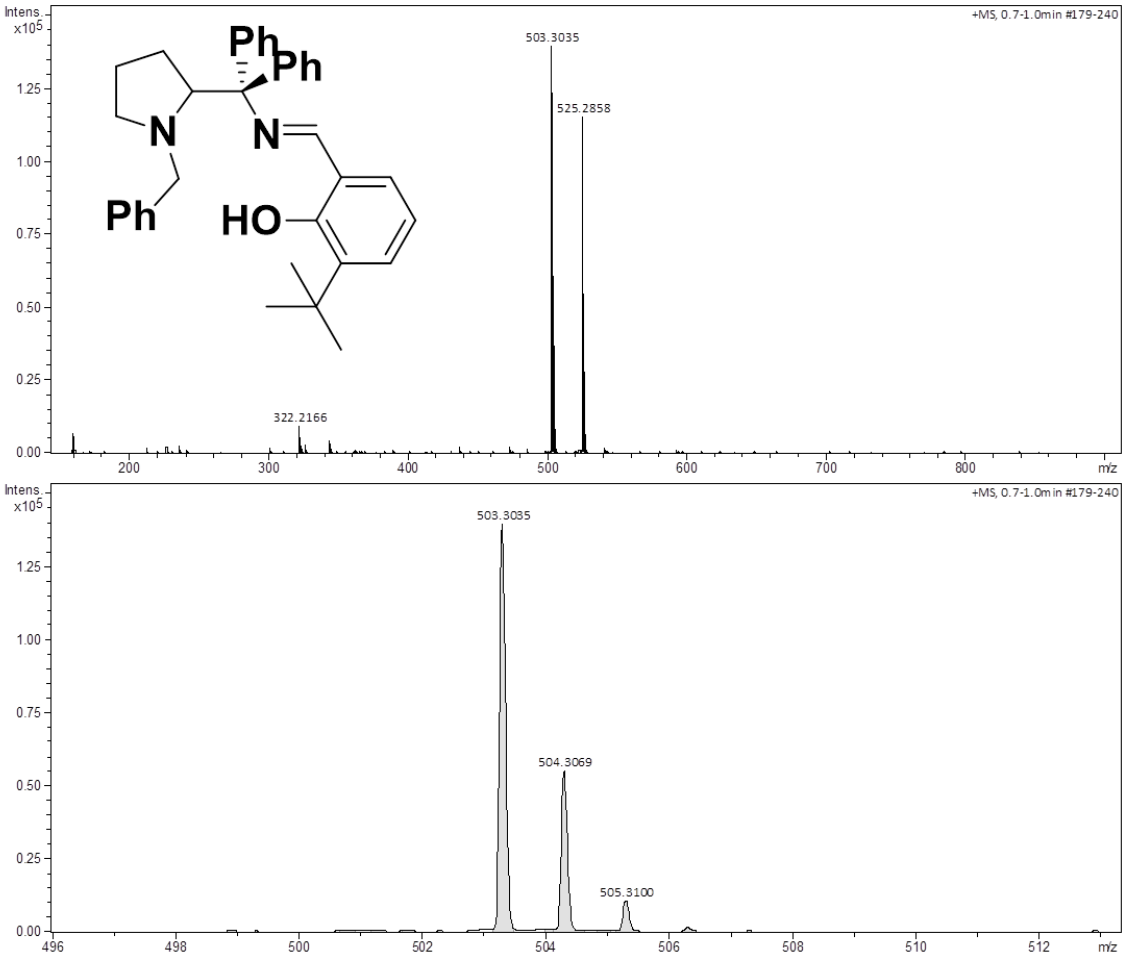

Figura S21. High Resolution Mass Spectra and Isotopic Pattern of HL4 in Ethyl Acetate/Methanol.

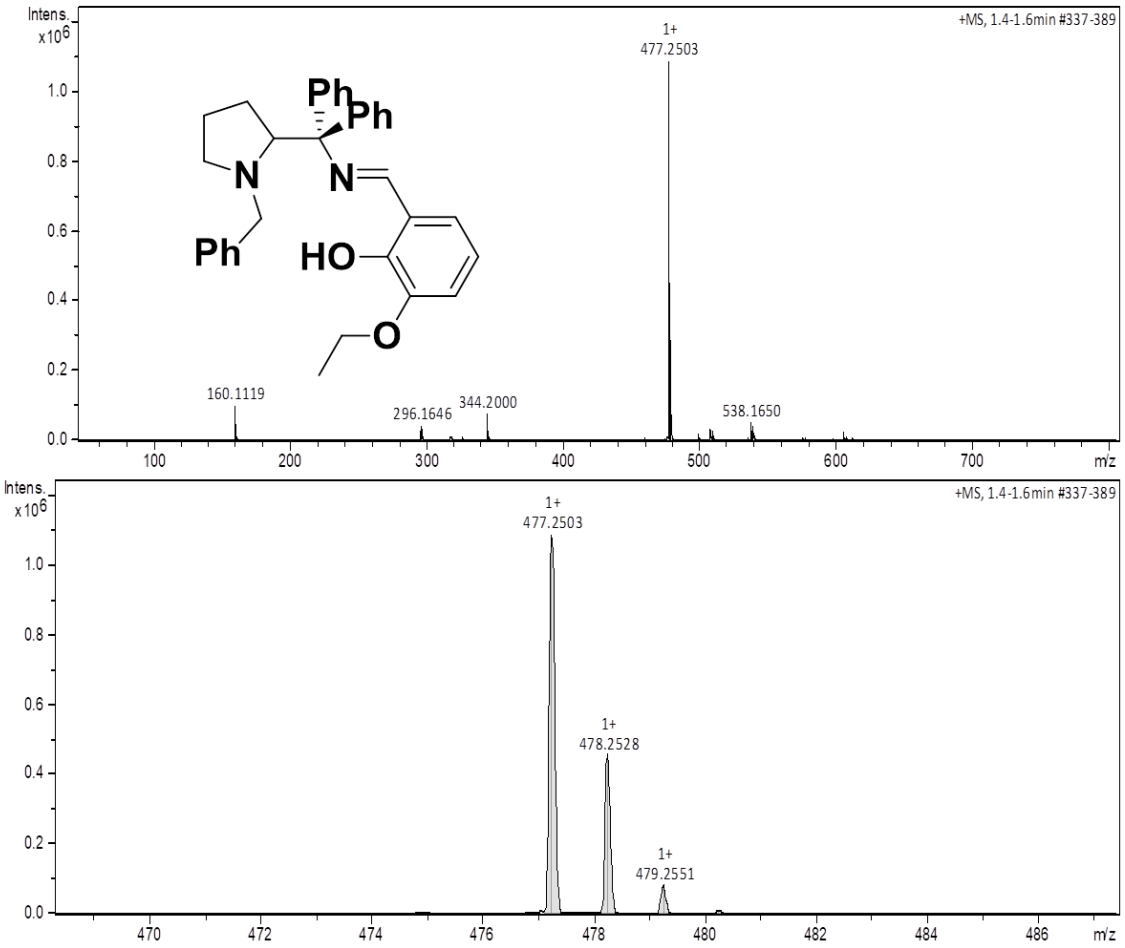

Figura S22. High Resolution Mass Spectra and Isotopic Pattern of HL5 in Ethyl Acetate/Methanol.

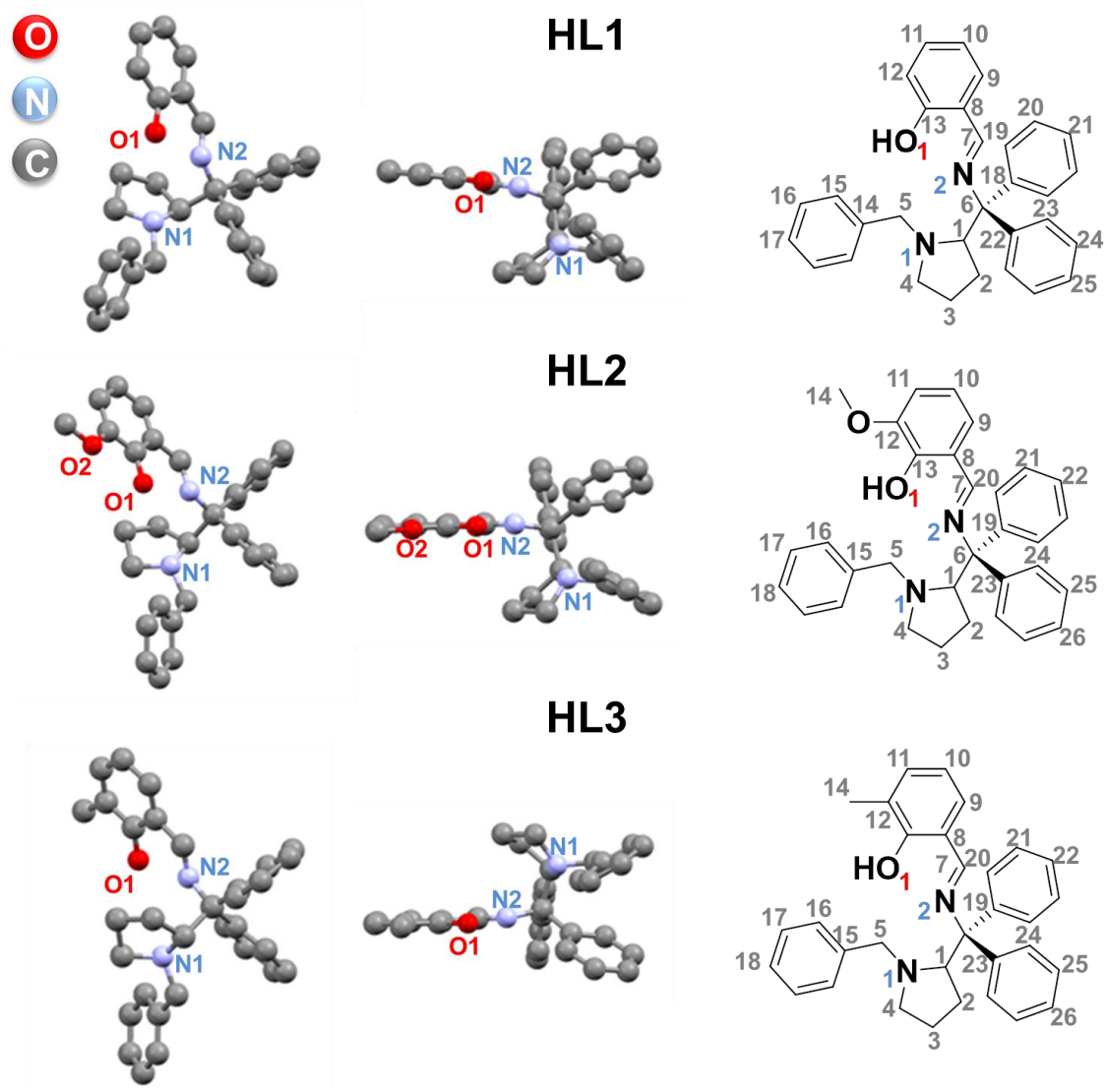

Figura S23. Optimized Crystalline Structure and numeric assignement of HL1, HL2 and HL3.

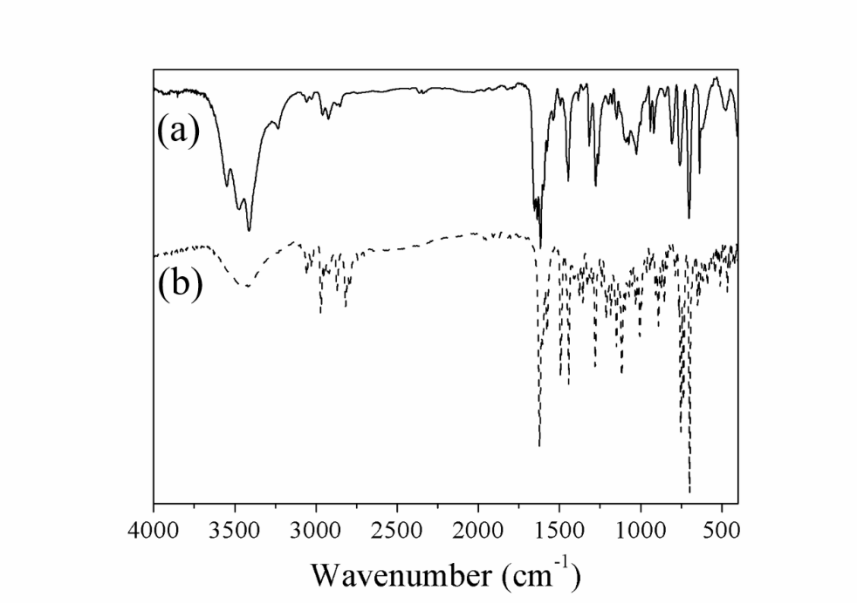

Figure S24. Comparison of FTIR spectra between (a) $Cu^{II}L1$ and (b) HL1.

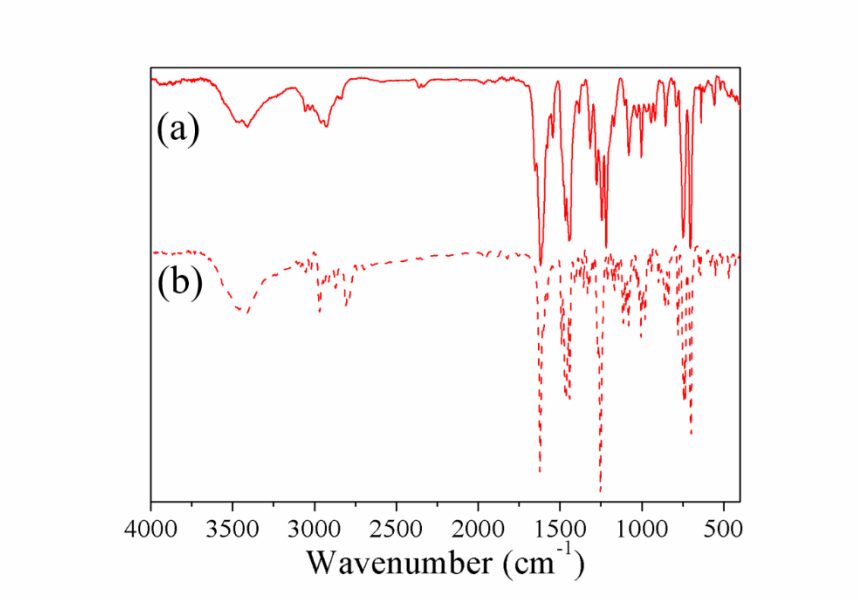

Figure S25. Comparison of FTIR spectra between (a) $Cu^{II}L2$ and (b) HL2.

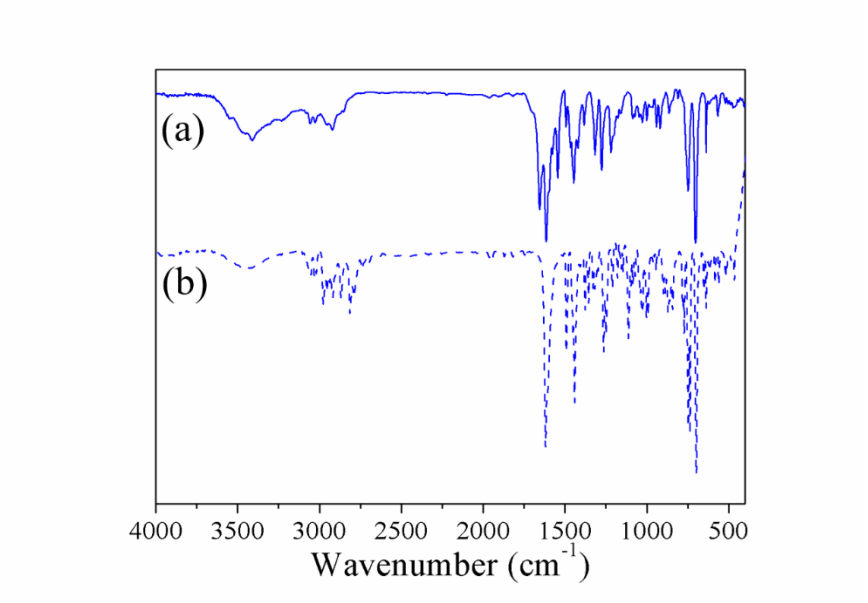

Figure S26. Comparison of FTIR spectra between (a) $Cu^{II}L3$ and (b) HL3.

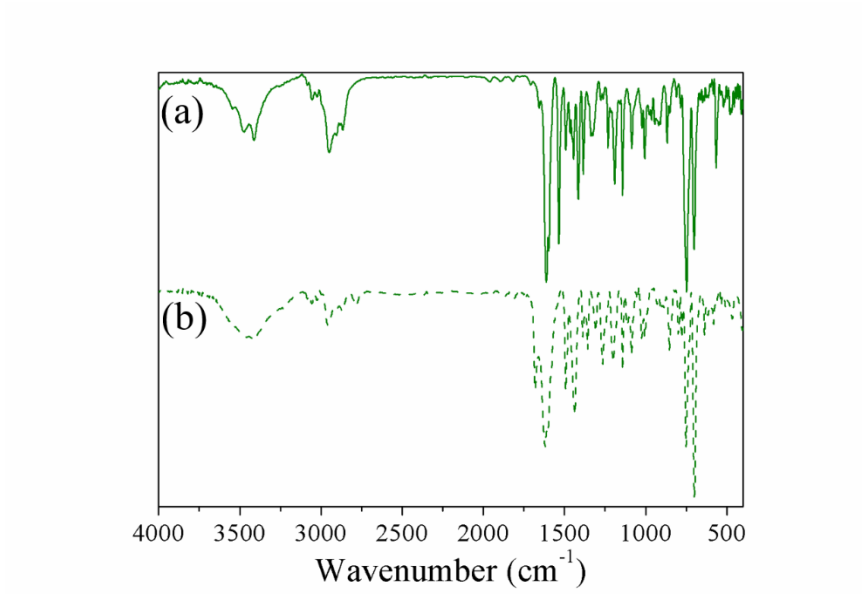

Figure S27. Comparison of FTIR spectra between (a) $Cu^{II}L4$ and (b) HL4.

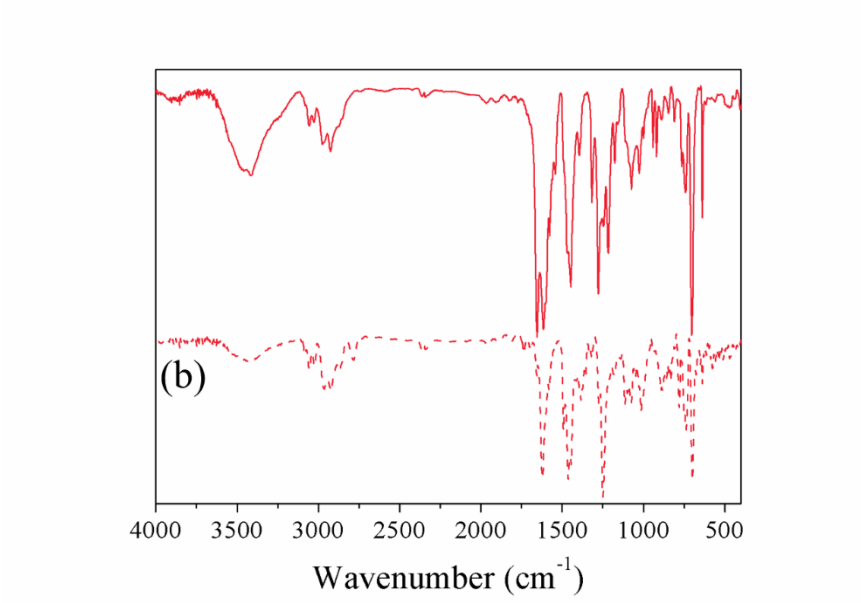

Figure S28. Comparison of FTIR spectra between (a) $Cu^{II}L5$ and (b) HL5 dispersed in KBr.

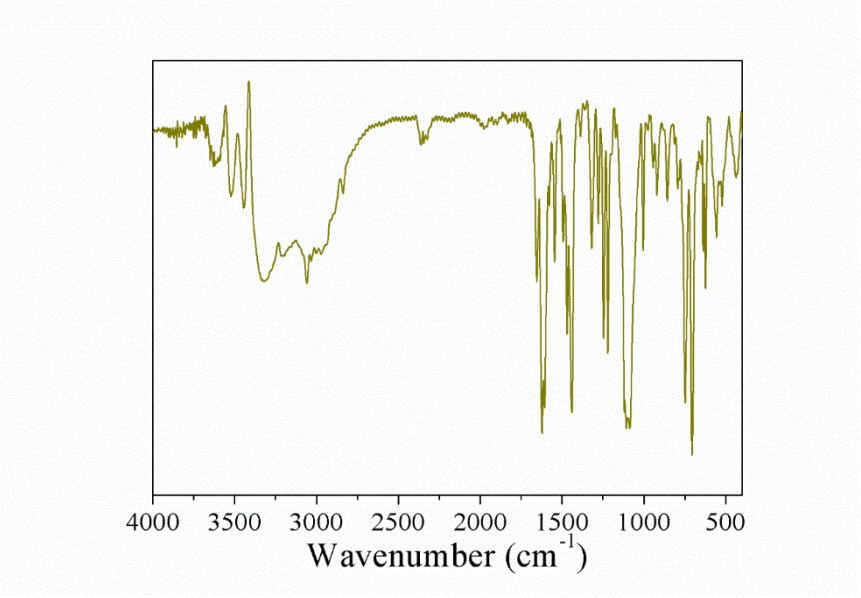

Figure S29. FTIR spectrum of $[Cu^{II}L2(CH_3OH)]ClO_4$ dispersed in KBr.

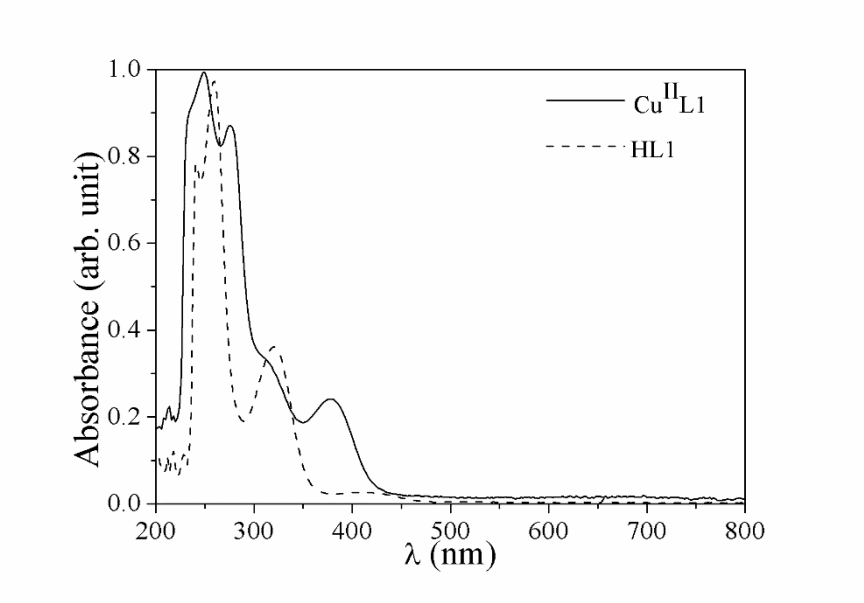

Figure S30. Comparison of UV-Vis spectra between $Cu^{II}L1$ and HL1 in dichloromethane.

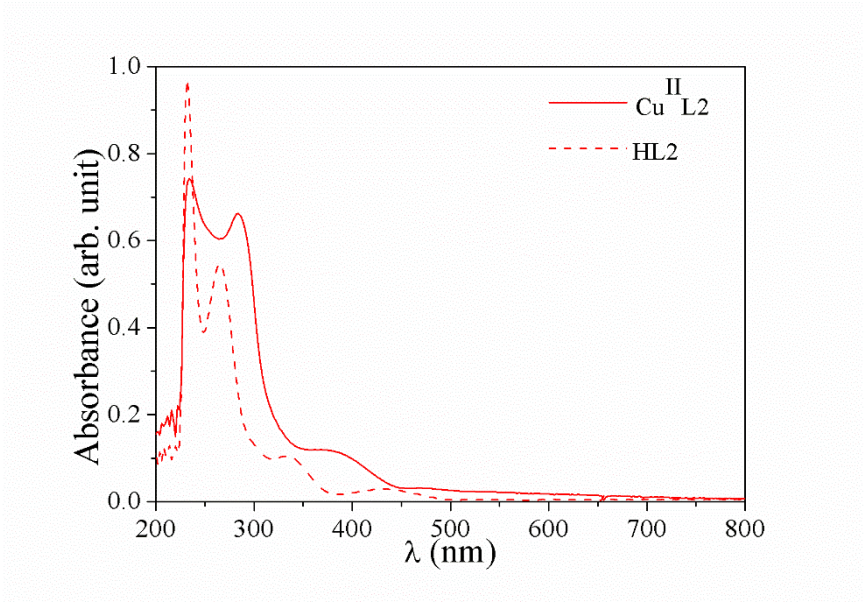

Figure S31. Comparison of UV-Vis spectra between $Cu^{II}L2$ and HL2 in dichloromethane.

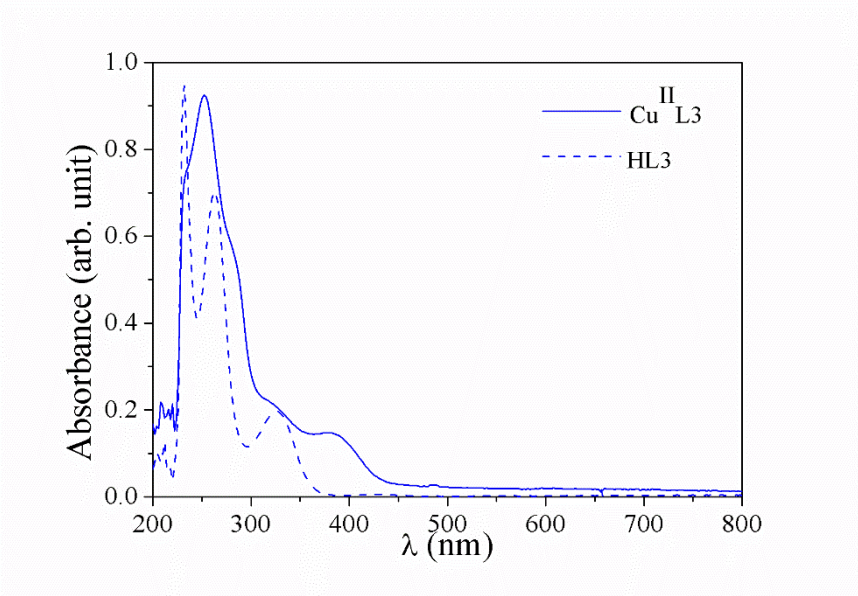

Figure S32. Comparison of UV-Vis spectra between $Cu^{II}L3$ and HL3 in dichloromethane.

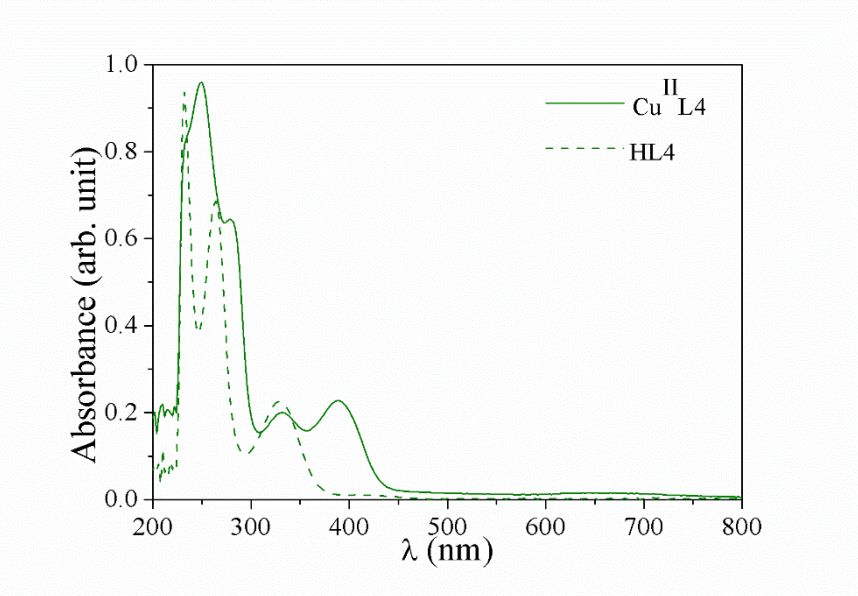

Figure S33. Comparison of UV-Vis spectra between $Cu^{II}L4$ and HL4 dichloromethane.

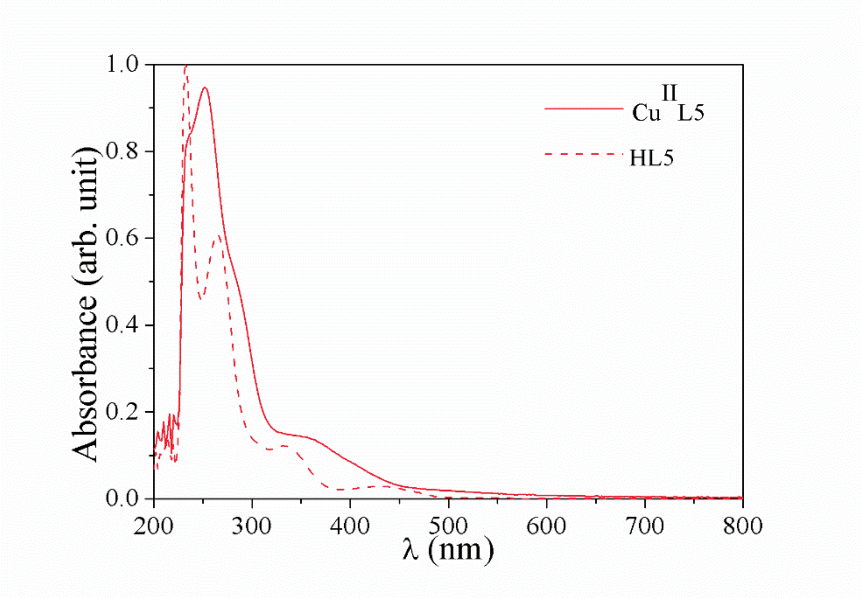

Figure S34. Comparison of UV-Vis spectra between $Cu^{II}L5$ and HL5 in dichloromethane.

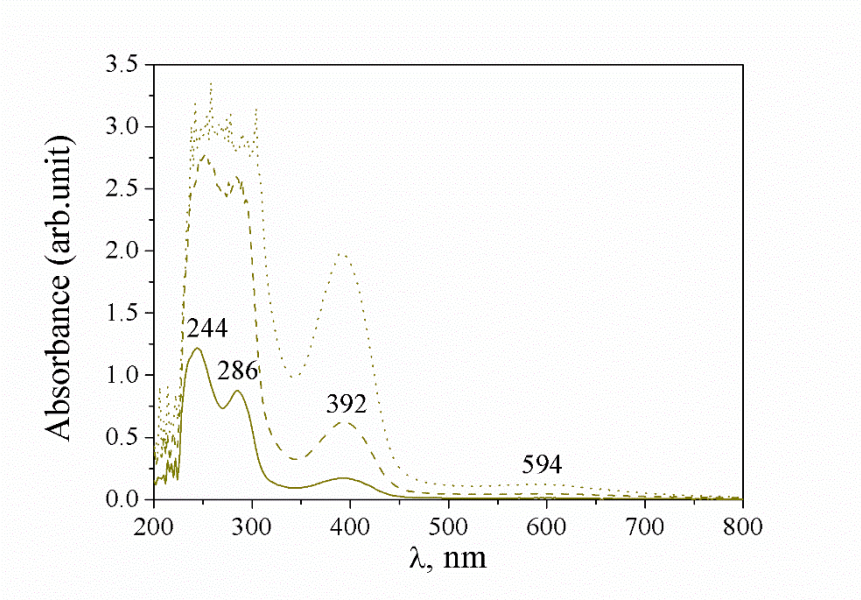

Figure S35. UV-Vis spectrum of $[Cu^{II}L5(CH_3OH)]ClO_4$ in dichloromethane.

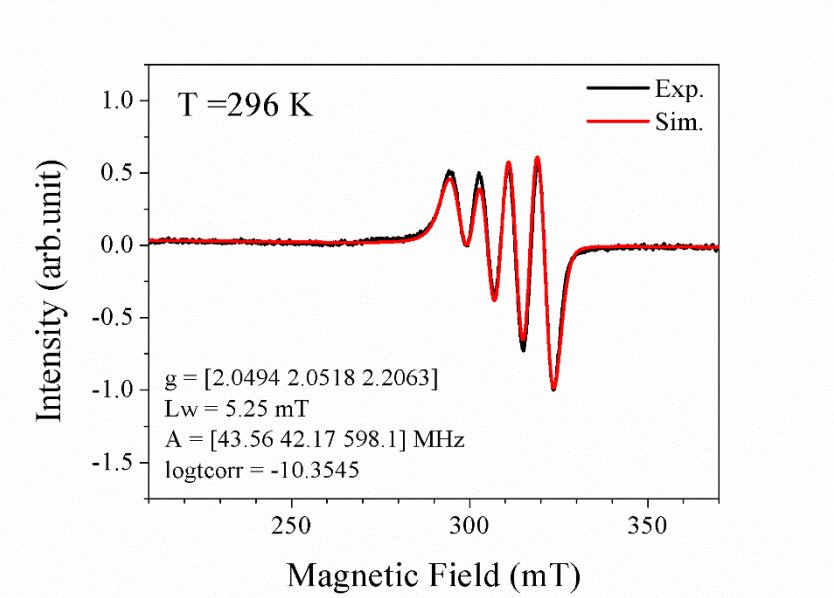

Figure S36. Simulation of EPR spectrum in dichloromethane at 298 K for Cu^{II}L1.

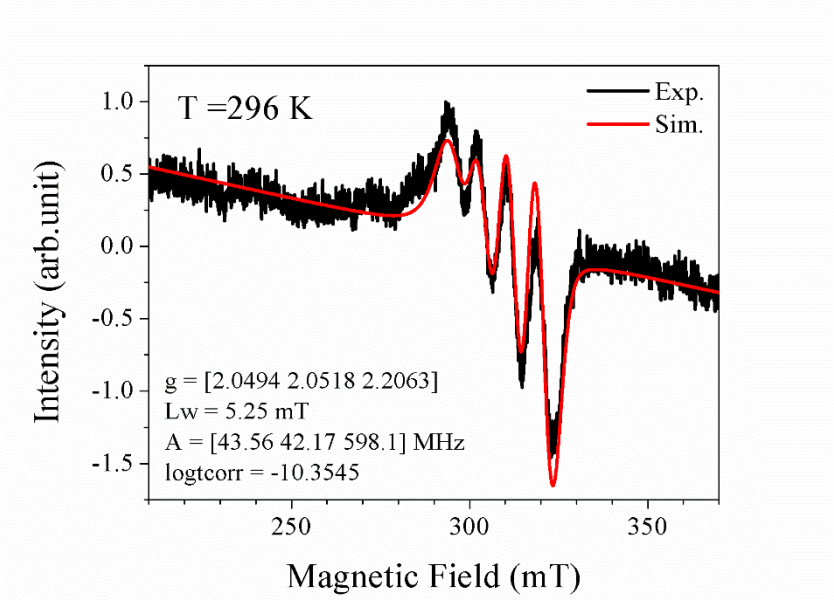

Figure S37. Simulation of EPR spectrum in dichloromethane at 298 K for Cu^{II}L2.

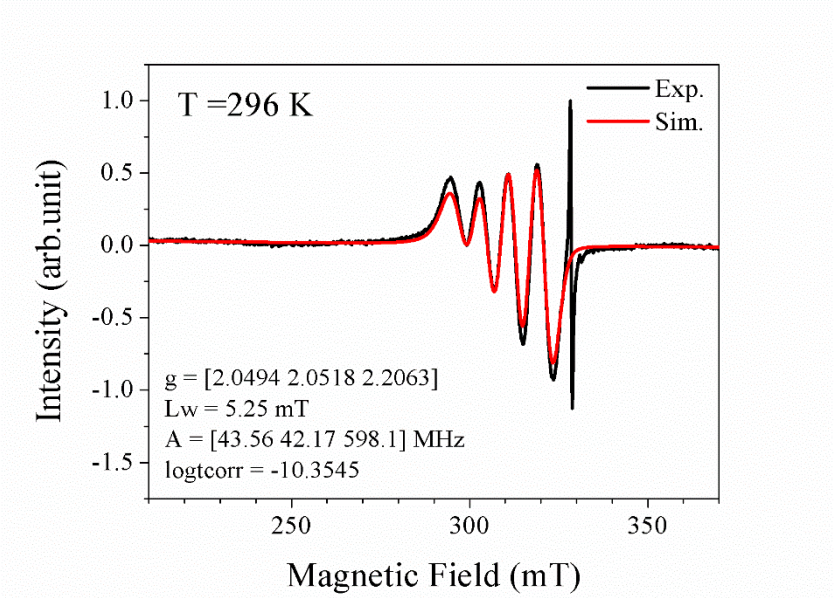

Figure S38. Simulation of EPR spectrum in dichloromethane at 298 K for Cu^{II}L3.

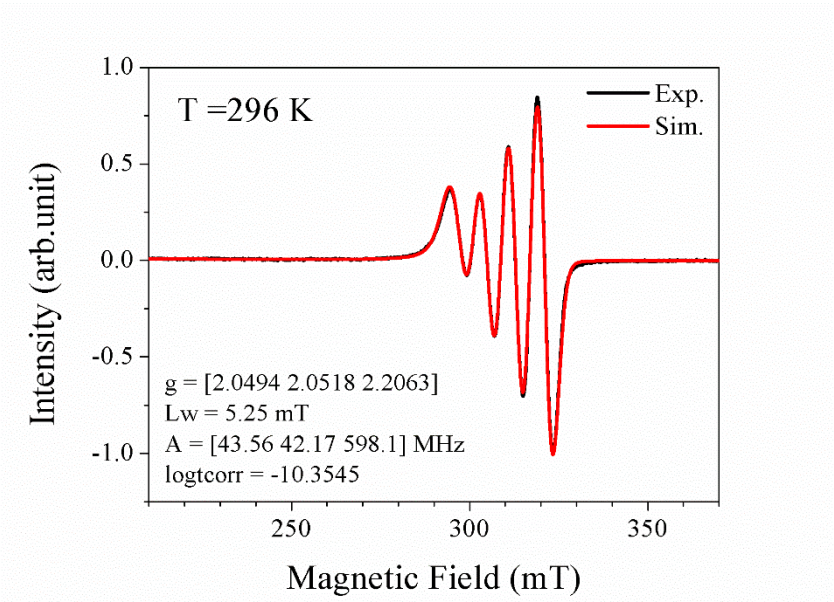

Figure S39. Simulation of EPR spectrum in dichloromethane at 298 K for Cu^{II}L4.

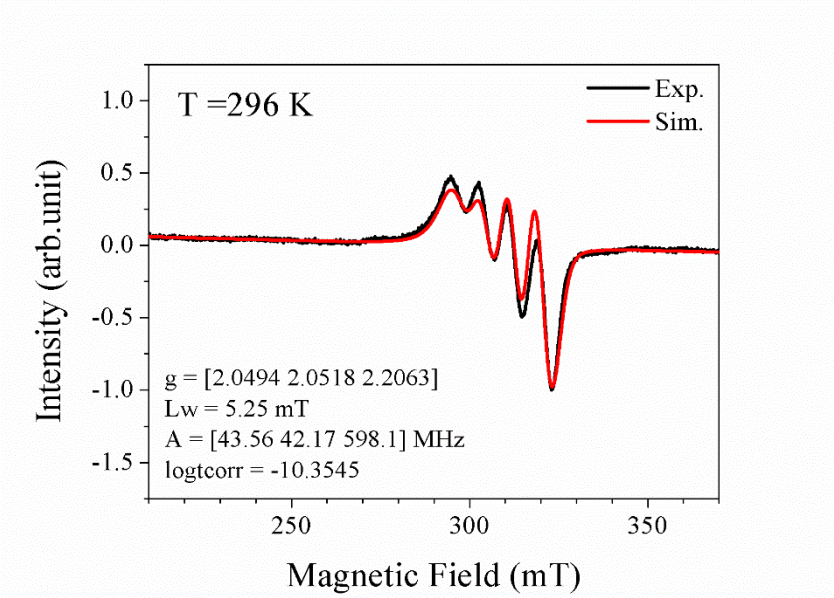

Figure S40. Simulation of EPR spectrum in dichloromethane at 298 K for Cu^{II}L5.

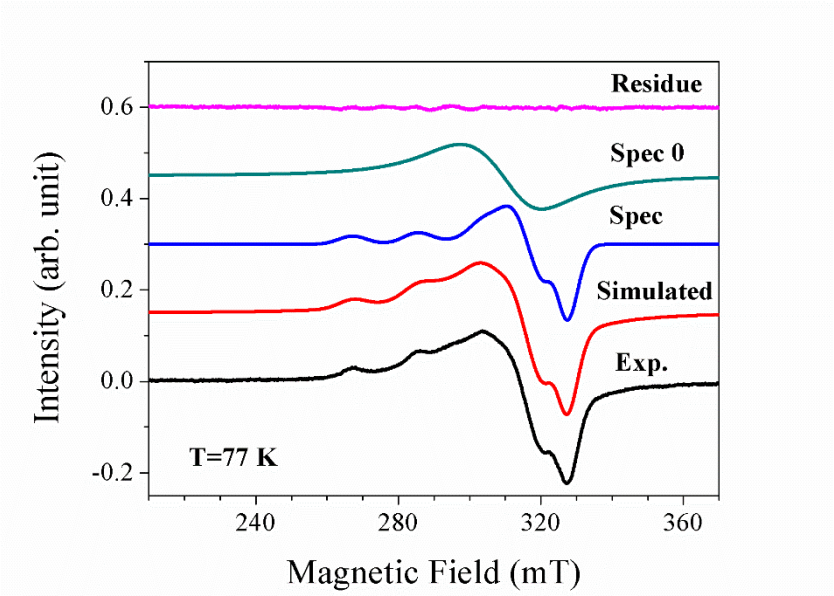

Figure S41.EPRspectral simulation of the Cu^{II}L1 complex at 77 K. “Spec” indicates the spectrum of the monomeric structure and “Spec0” of the dimeric structures.

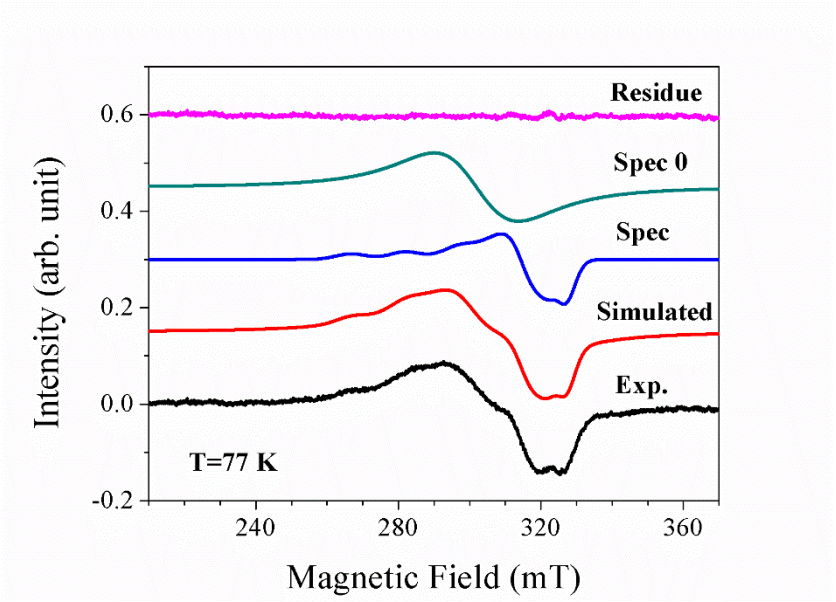

Figure S42.EPRspectral simulation of the $Cu^{II}L2$ complex at 77 K. "Spec" indicates the spectrum of the monomeric structure and "Spec0" of the dimeric structures.

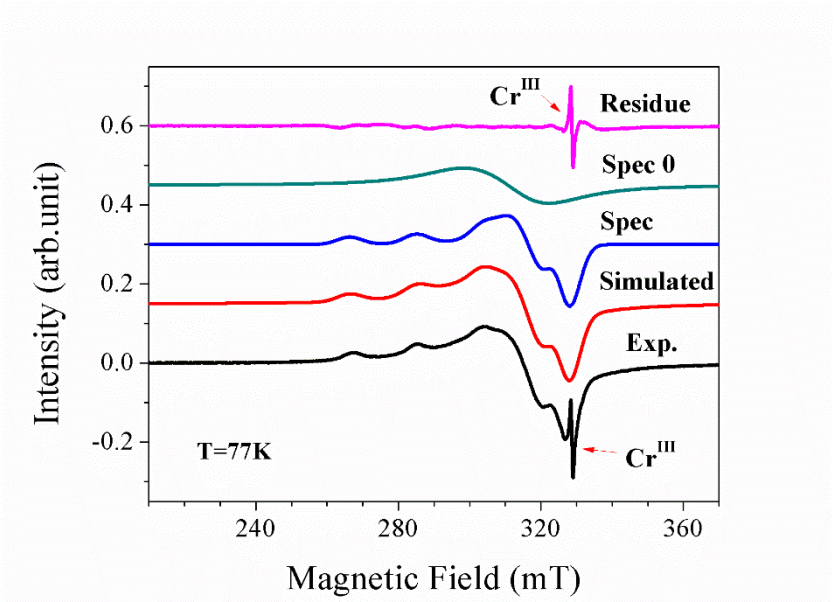

Figure S43. Spectral simulation of the $Cu^{II}L3$ complex at 77 K. "Spec" indicates the spectrum of the monomeric structure and "Spec0" of the dimeric structures.

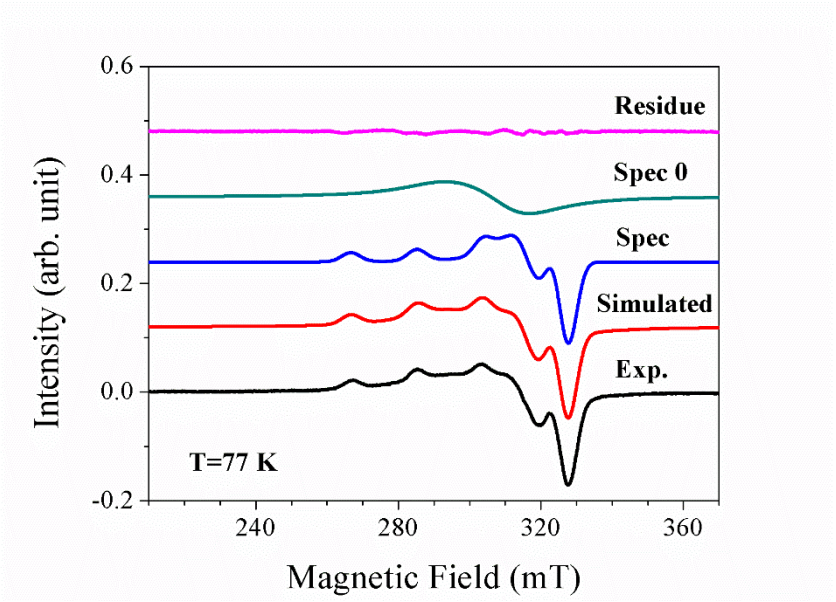

Figure S44.EPRspectral simulation of the Cu^{II}L5 complex at 77 K. "Spec" indicates the spectrum of the monomeric structure and "Spec0" of the dimeric structures.

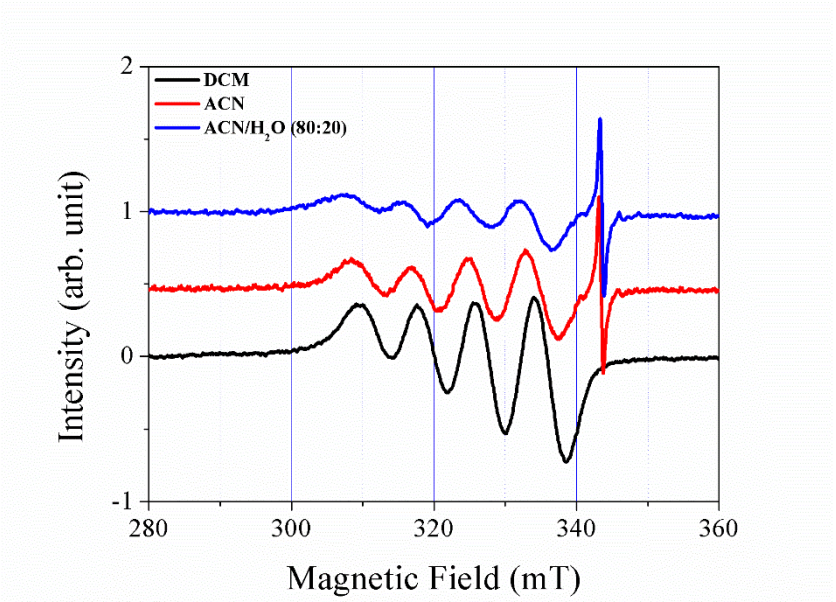

Figure S45. Comparison of the EPR spectra in dichloromethane, acetonitrile and acetonitrile/water (80:20) mixture at 298 K for the Cu^{II}L1 complex.

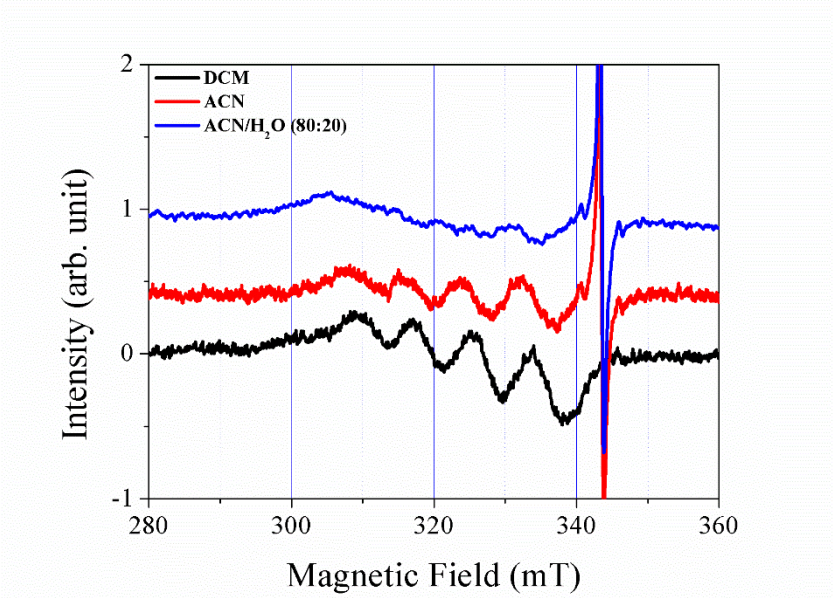

Figure S46. Comparison of the EPR spectra in dichloromethane, acetonitrile and acetonitrile/water (80:20) mixture at 298 K for the Cu^{II}L2 complex.

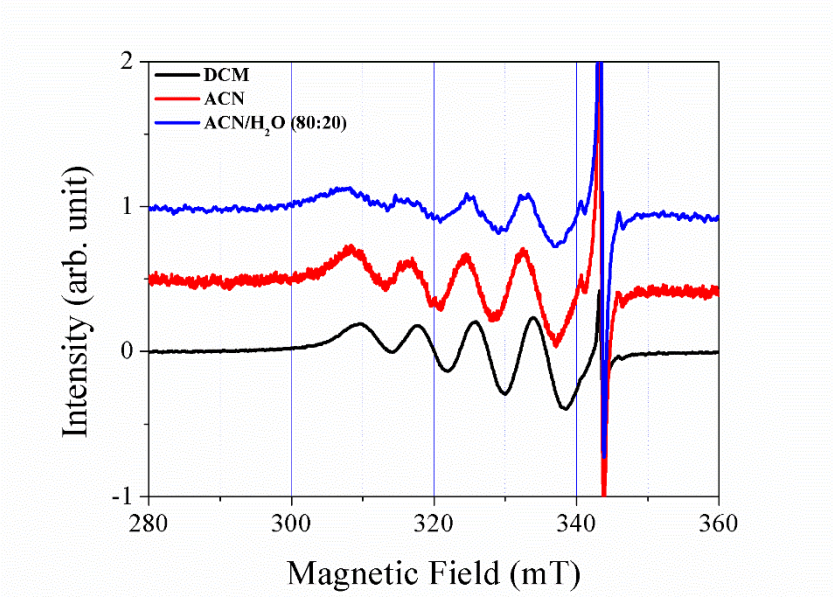

Figure S47. Comparison of the EPR spectra in dichloromethane, acetonitrile and acetonitrile/water (80:20) mixture at 298 K for the Cu^{II}L3 complex.

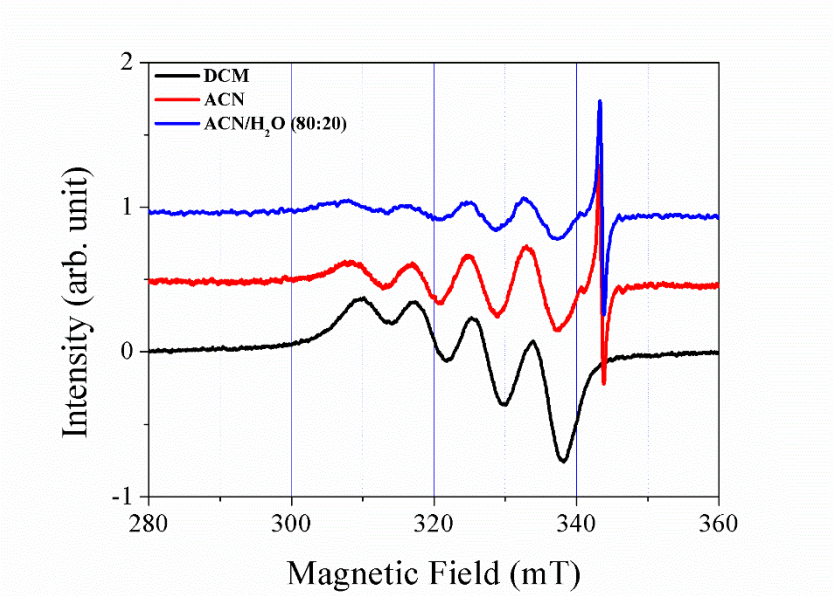

Figure S48. Comparison of the EPR spectra in dichloromethane, acetonitrile and acetonitrile/water (80:20) mixture at 298 K for the Cu^{II}L5 complex.

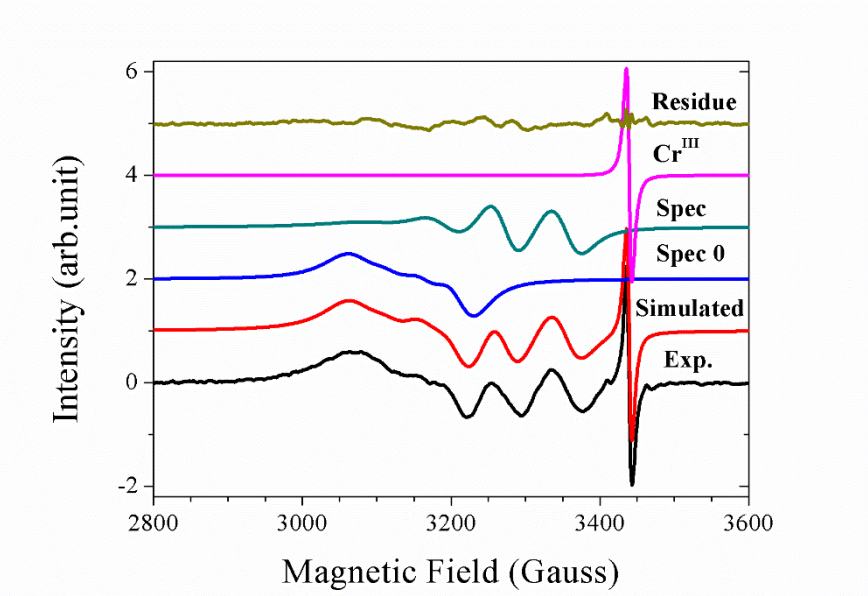

Figure S49.EPRspectral simulation of the Cu^{II}L2 complex at 298 K in methanol. "Spec" indicates the spectrum of the monomeric structure and "Spec0" of the dimeric structures.

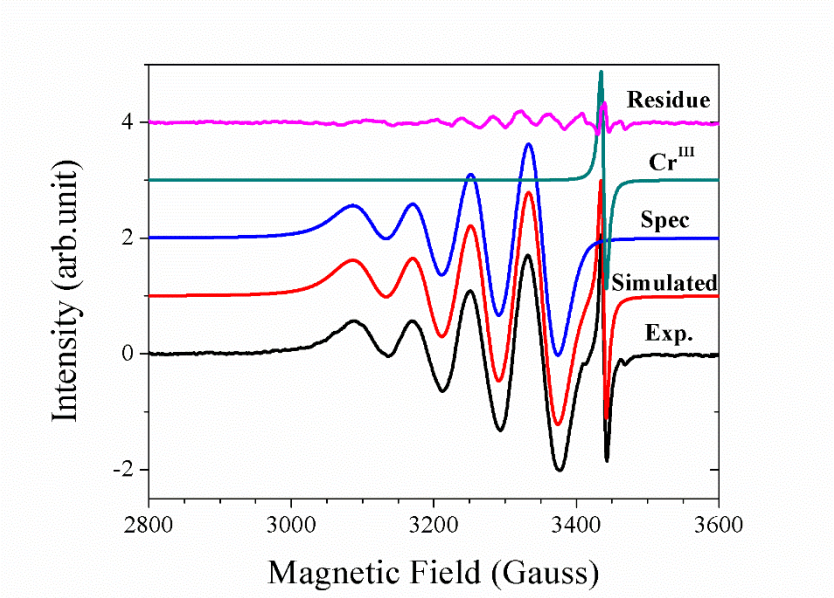

Figure S50.EPRspectral simulation of the [Cu^{II}L2(CH_3OH)]ClO_4 complex at 298 K in methanol. “Spec” indicates the spectrum of the monomeric structure.

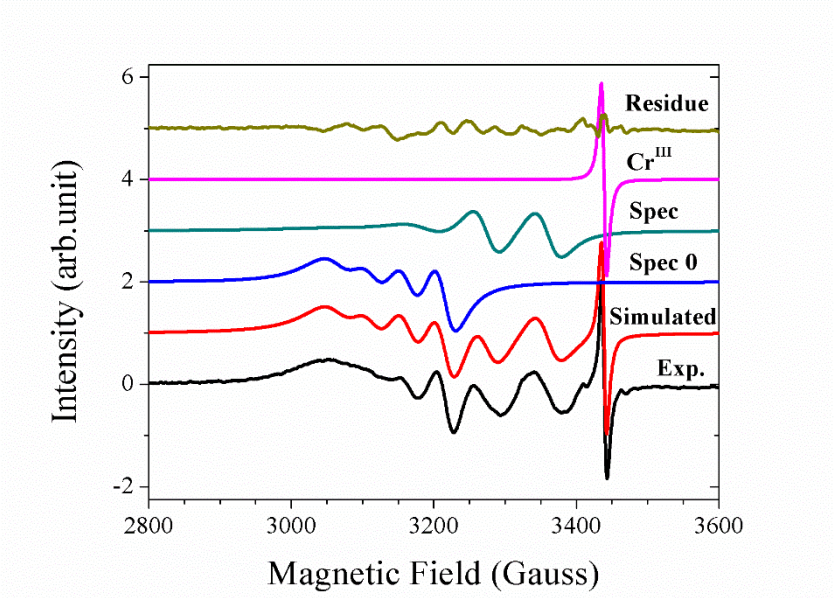

Figure S51.EPRspectral simulation of the Cu^{II}L2 complex at 298 K in methanol/water (80:20). “Spec” indicates the spectrum of the monomeric structure and “Spec0” of the dimeric structures.

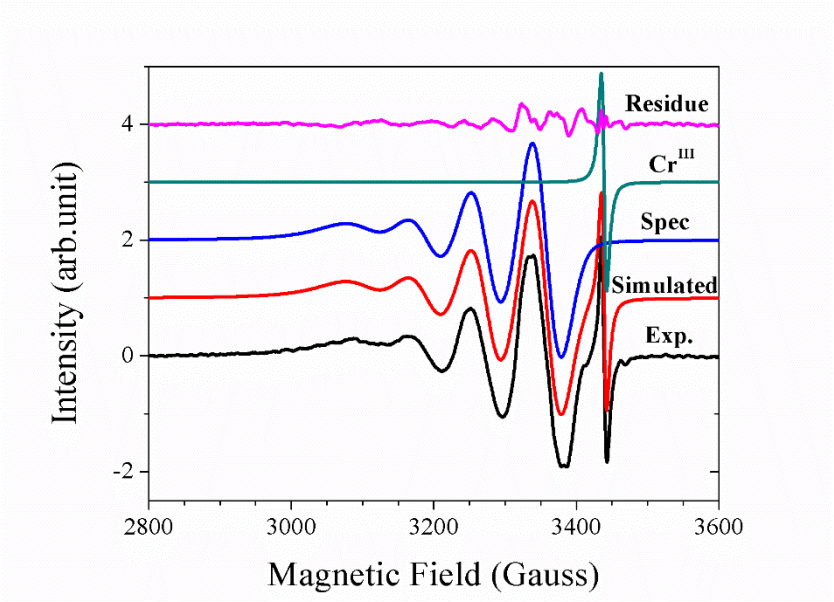

Figure S52.EPRspectral simulation of the [Cu^{II}L2(CH_3OH)]ClO_4 complex at 298 K in methanol/water (80:20). "Spec" indicates the spectrum of the monomeric structure.

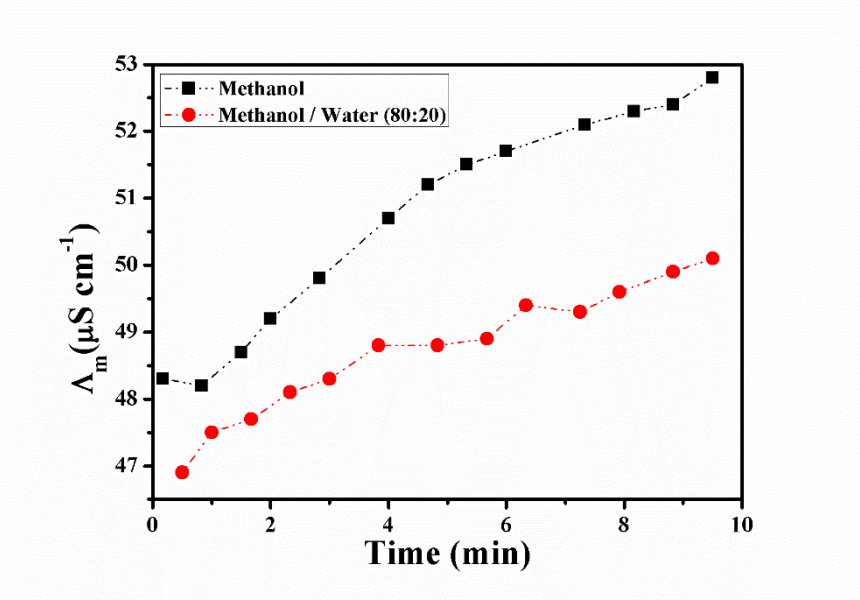

Figure S53. Conductivity measurements over time in (black) methanol and (red) methanol/water mixture for Cu^{II}L2(Cl) complex.

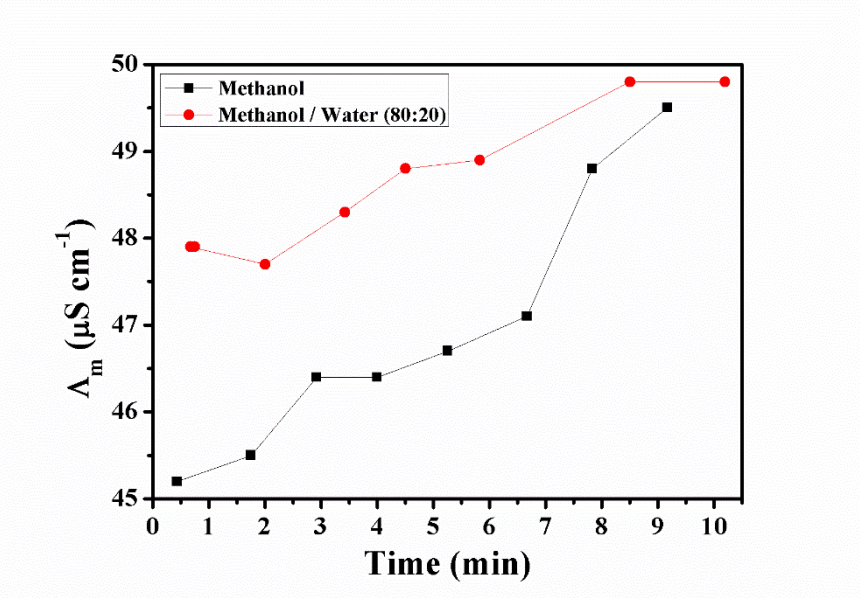

Figure S54. Conductivity measurements over time in (black) methanol and (red) methanol/water mixture for $Cu^{II}L3(Cl)$ complex.

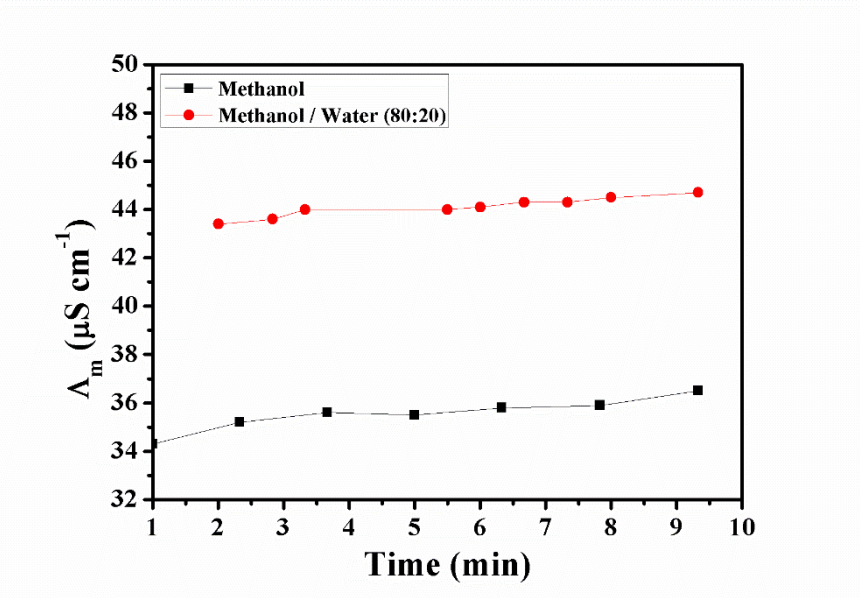

Figure S55. Conductivity measurements over time in (black) methanol and (red) methanol/water mixture for $Cu^{II}L4(Cl)$ complex.

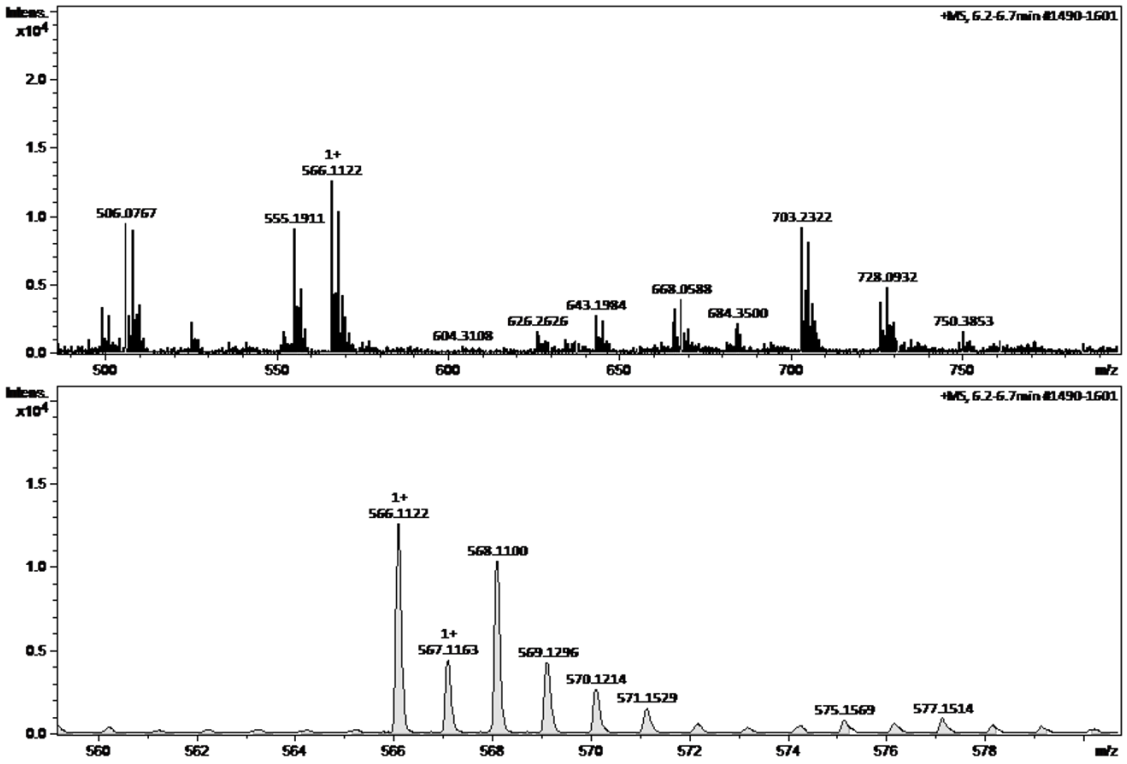

Figura S56. High Resolution Mass Spectra and Isotopic Pattern of $Cu^{II}L1$ from the peak of molecular ion attributed to the illustrated structure with calculated *m/z* 566.1162 $[M + Na^+]^+$.

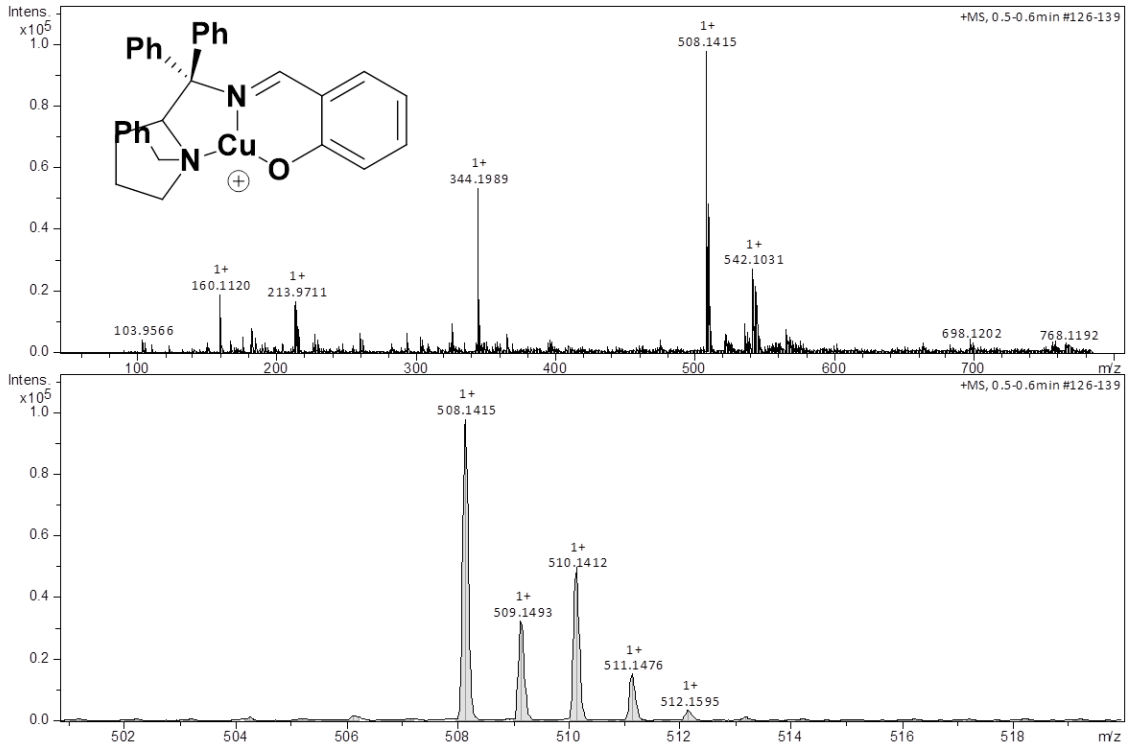

Figura S57. High Resolution Mass Spectra and Isotopic Pattern of $Cu^{II}L2$ from the peak of molecular ion attributed to the illustrated structure with calculated *m/z* 508.1570 $[M - CH_3OH - HCl]^+$. "M" indicates the molecular mass of 574.6080 g mol^{-1}.

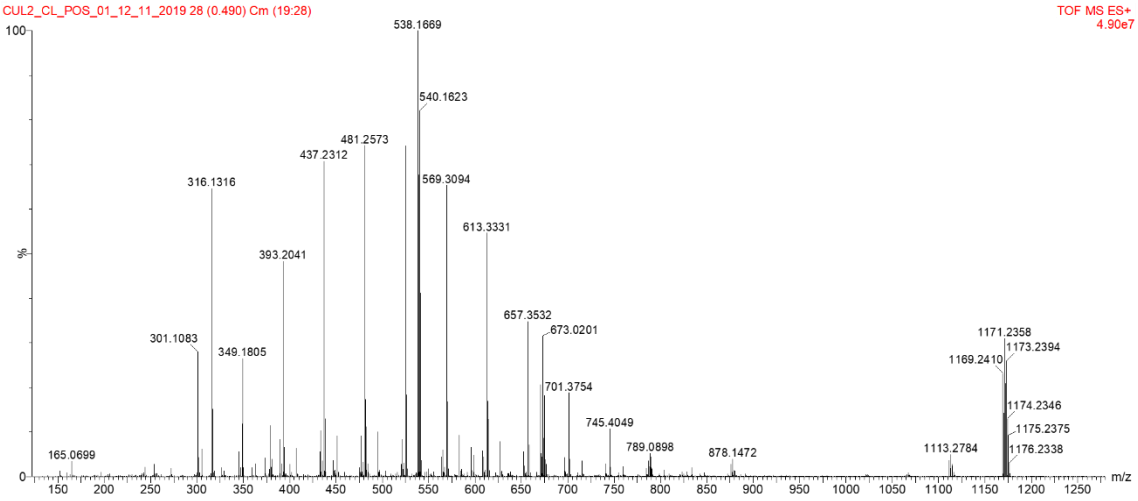

Figura S58. High Resolution Mass Spectra and Isotopic Pattern of $Cu^{II}L2$ from the peak of molecular ion attributed to the illustrated structure with calculated *m/z*538.1682 $[M - HCl]^+$. "M" indicates the molecular mass of 574.6080 g mol^{-1}.

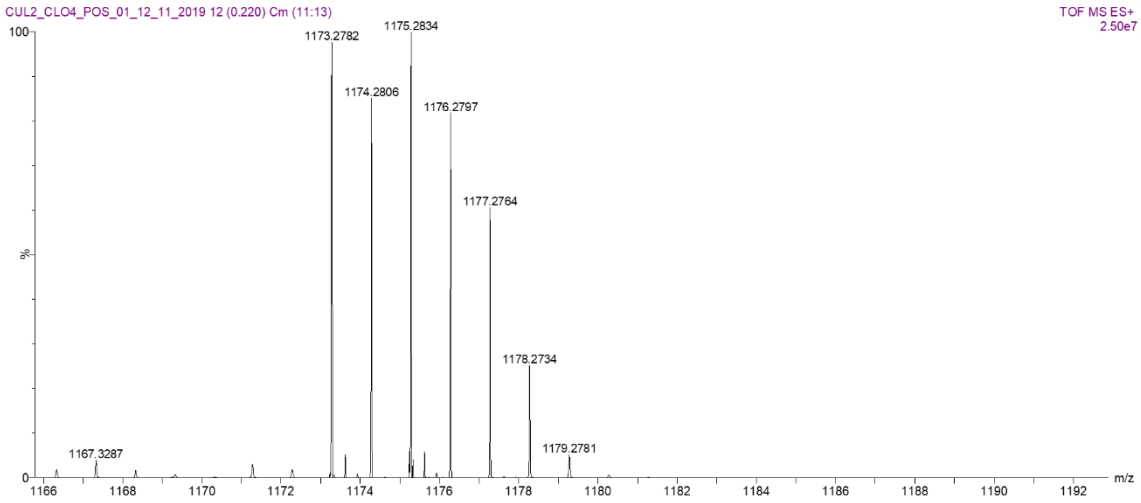

Figura S59. High Resolution Mass Spectra and Isotopic Pattern of $[Cu^{II}L2ClO_4]$ from the peak of molecular ion attributed to the illustrated structure with calculated *m/z* 1175.2834 $[2M - ClO_4]^+$. "M" indicates the molecular mass of 1277.2075 g mol^{-1}.

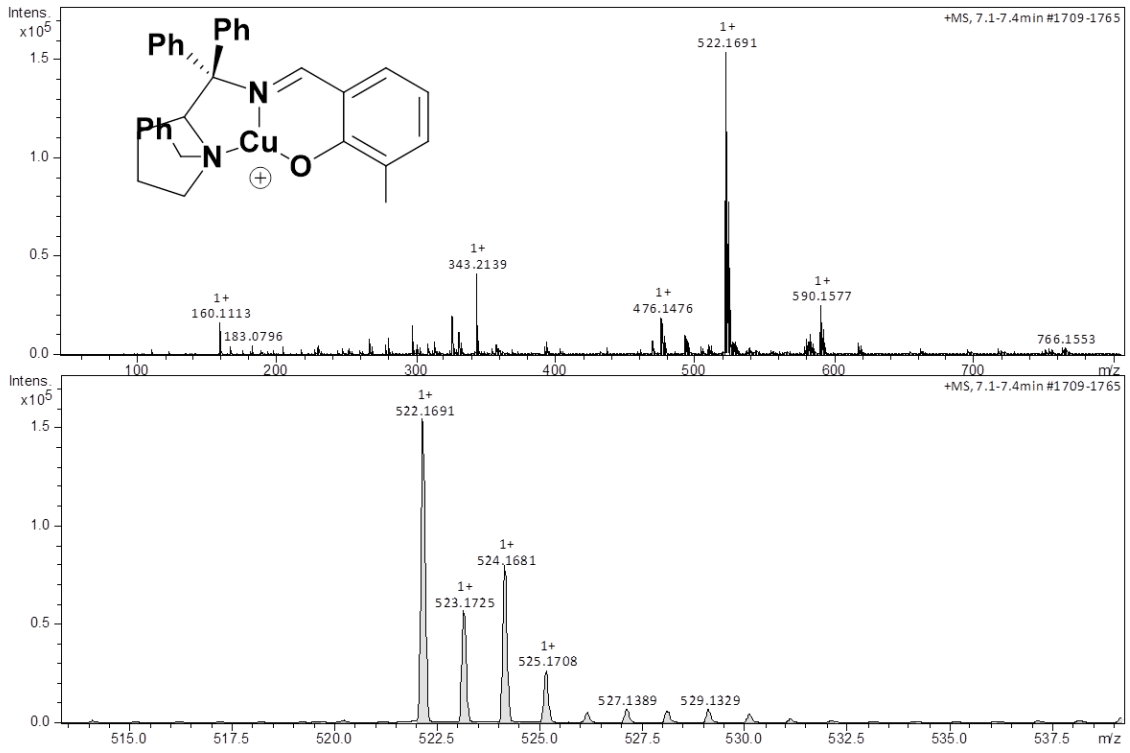

Figura S60. High Resolution Mass Spectra and Isotopic Pattern of $Cu^{II}L3$ from the peak of molecular ion attributed to the illustrated structure with calculated *m/z* 522.1727 $[M - HCl]^+$. "M" indicates the molecular mass of 558.6090 g mol^{-1}.

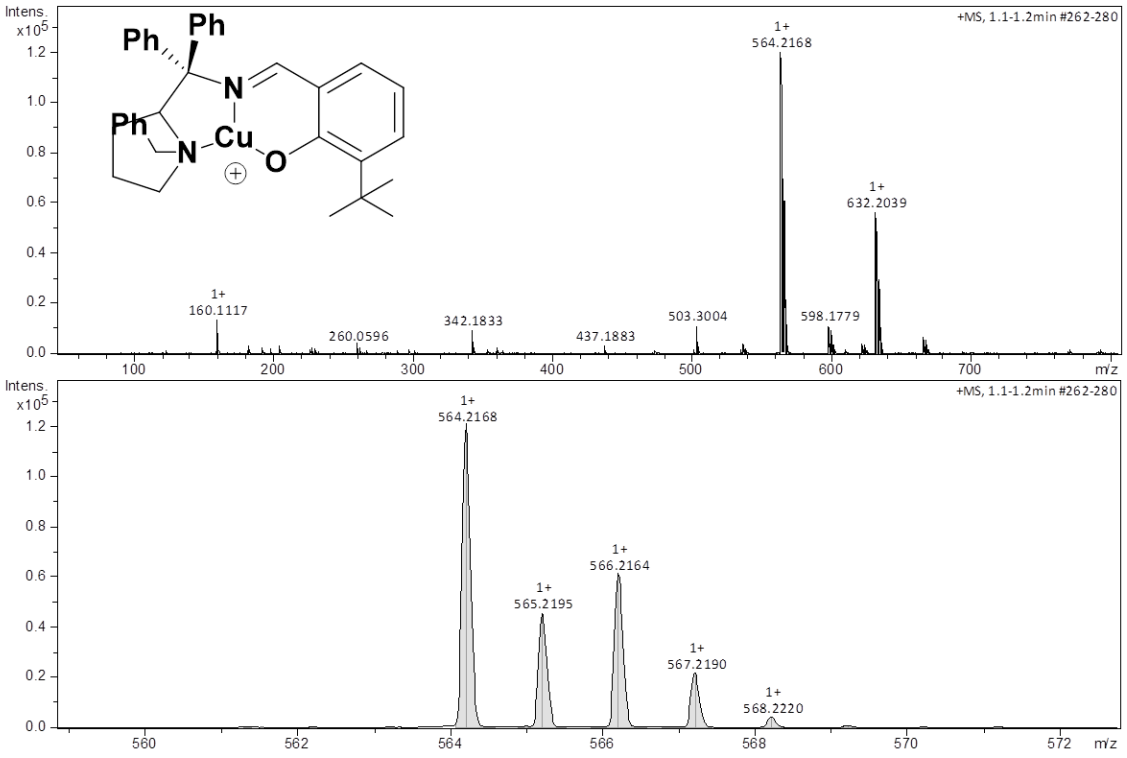

Figura S61. High Resolution Mass Spectra and Isotopic Pattern of $Cu^{II}L4$ from the peak of molecular ion attributed to the illustrated structure with calculated *m/z* 564.2196 $[M - HCl]^+$. "M" indicates the molecular mass of 600.6900 g mol^{-1}.

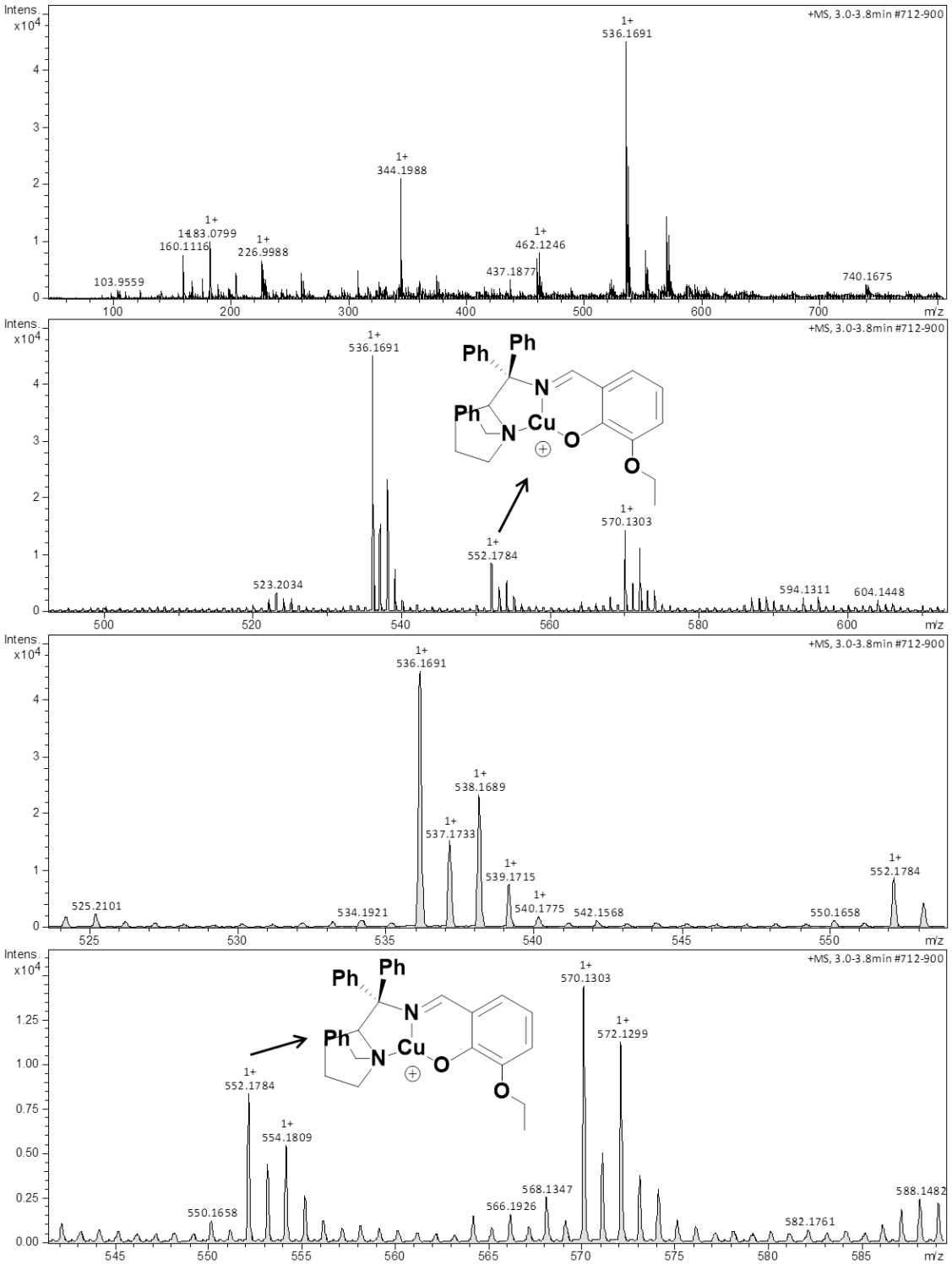

Figure S62. High Resolution Mass Spectra and Isotopic Pattern of Cu^{II}L5 from the peak of molecular ion attributed to the illustrated structure with calculated *m/z*536.1691 $[M - HCl]^+$ to the Cu^{II}L5 by loss of a methane molecule with calculated m/z 552.1833 $[M - CH_4 - HCl]^+$. "M" indicates the molecular mass of 588.6350 g mol^{-1}.

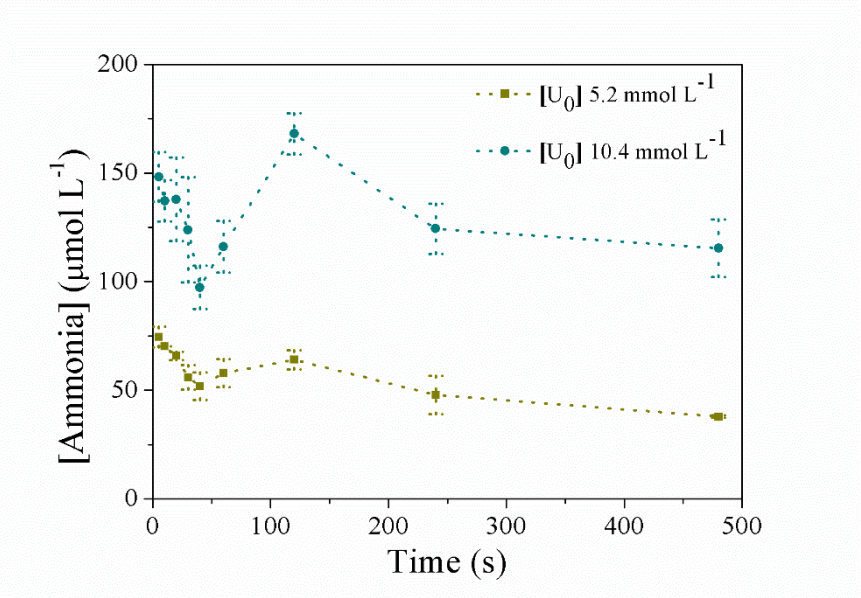

Figure S63. Ammonia quantification produced by Cu^{II}L1 complex in acetonitrile/water and mixture up to 480 at 308 K.

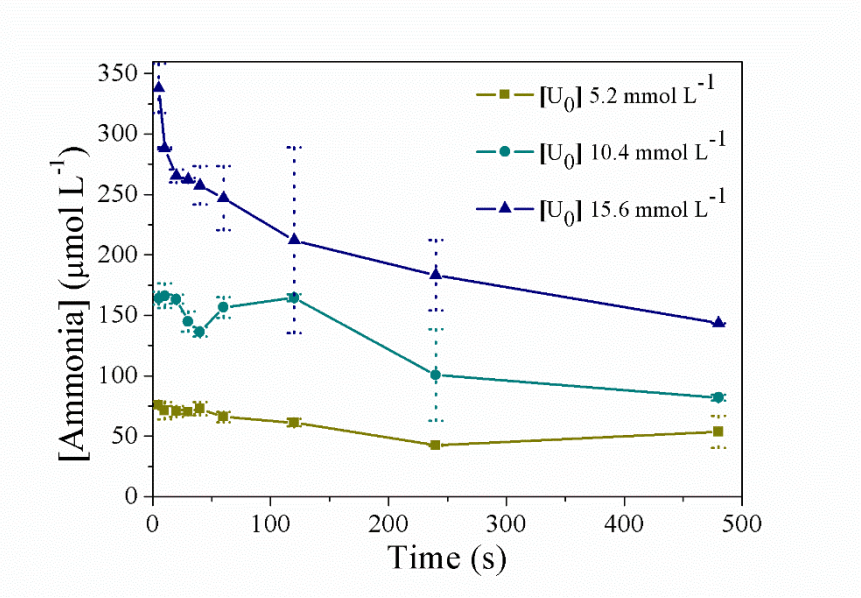

Figure S64. Ammonia quantification produced by Cu^{II}L3 complex in acetonitrile/water and mixture up to 480 at 308 K.

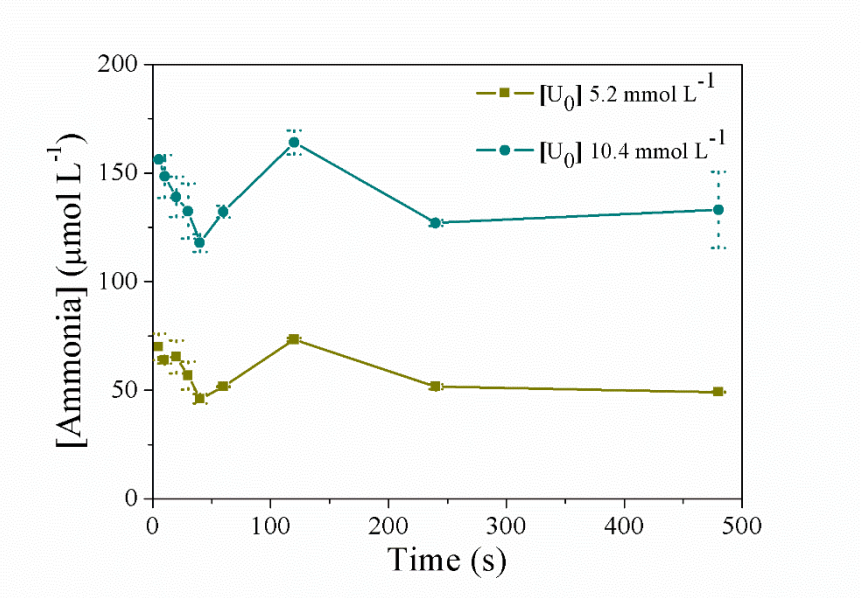

Figure S65. Ammonia quantification produced by Cu^{II}L4 complex in acetonitrile/water and mixture up to 480 at 308 K.

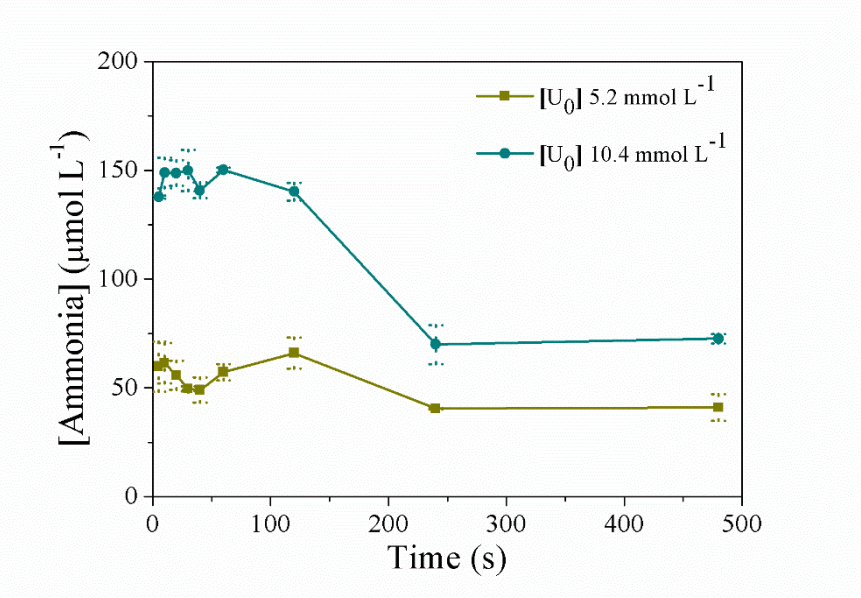

Figure S66. Ammonia quantification produced by Cu^{II}L5 complex in acetonitrile/water and mixture up to 480 at 308 K.

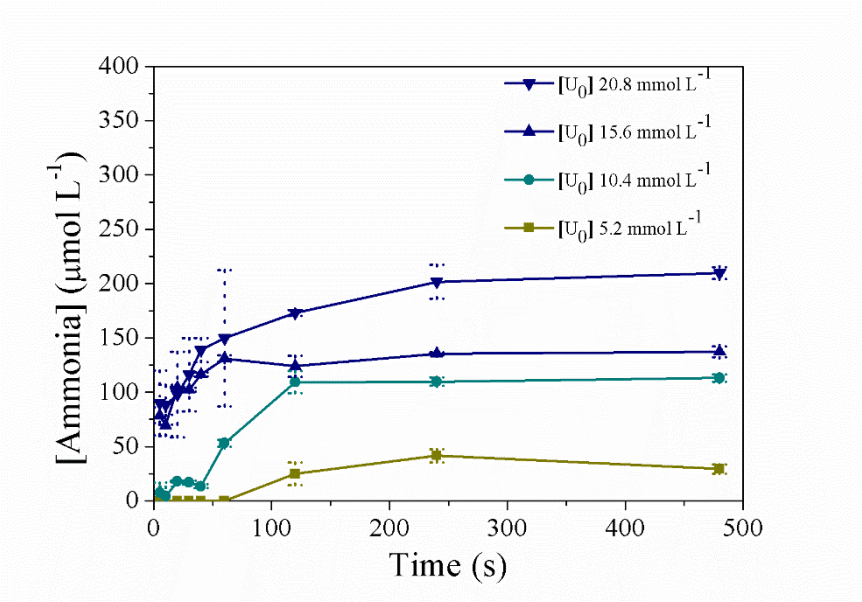

Figure S67. Ammonia quantification produced by $Cu^{II}L4$ complex in methanol/water and mixture up to 480 at 308 K.

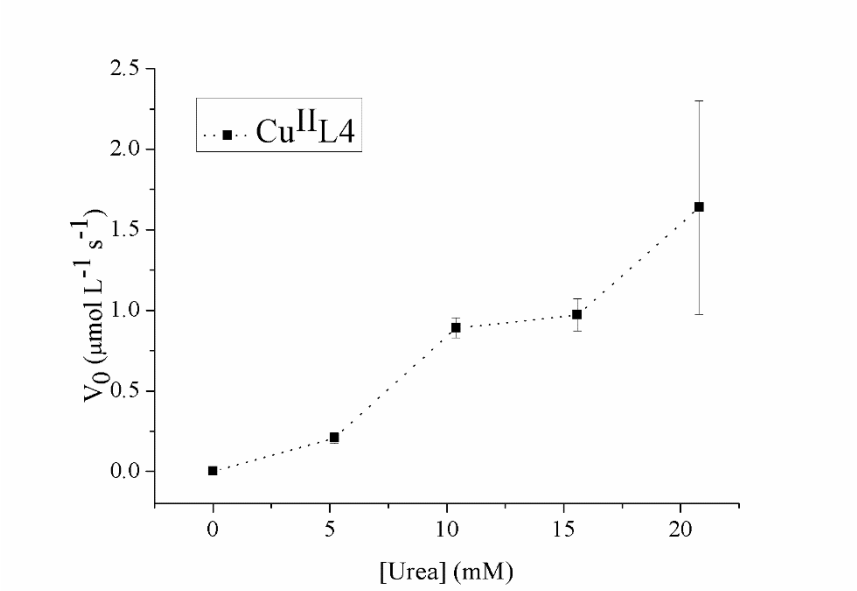

Figure S68. Initial velocity of ammonia production by $Cu^{II}L4$ complex in methanol/water mixture at different urea concentrations.

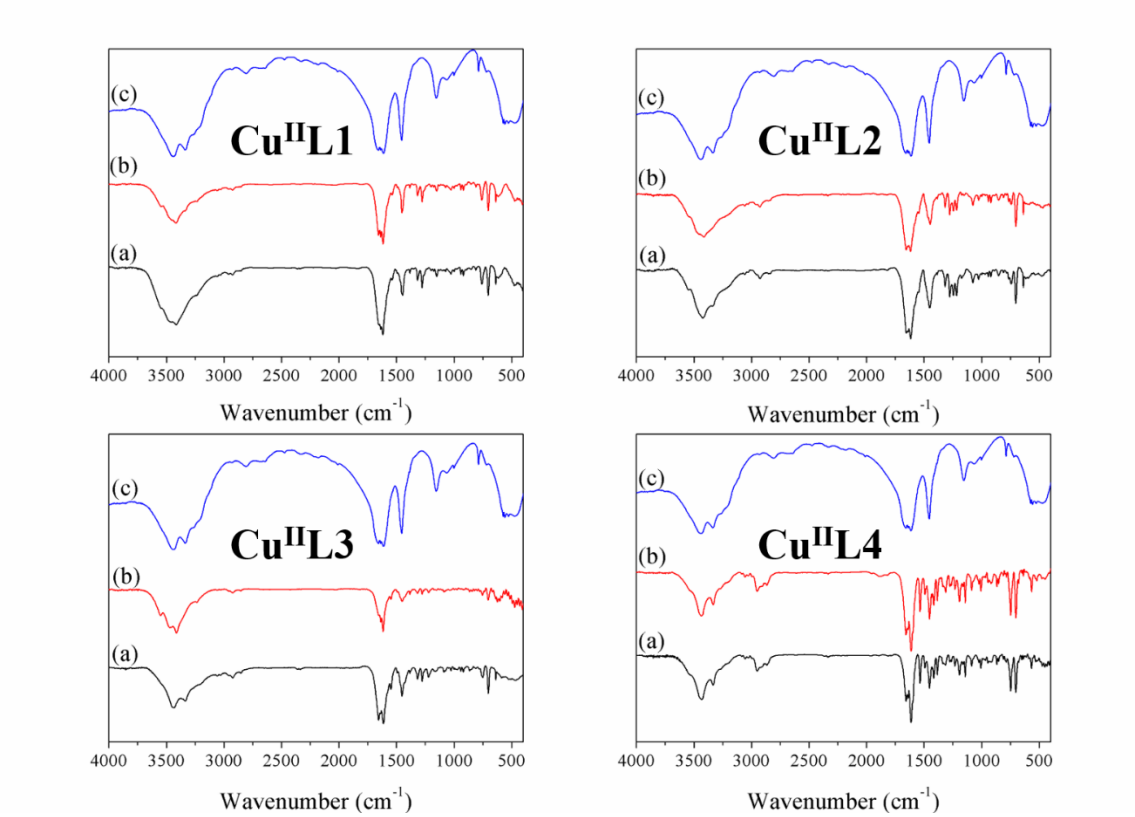

Figure S69. Infrared spectra of reactions of the complexes (a) 30 s, (b) 600 s and with (c) urea.

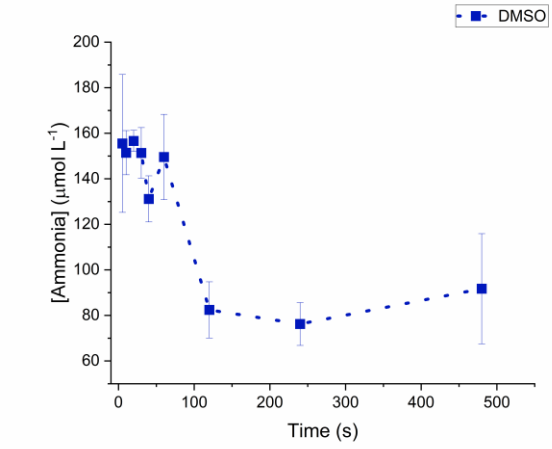

Figure S70. Ammonia quantification produced by [CuIIL3] complex in DMSO/water (20%) 15mmol L^{-1} urea concentration.

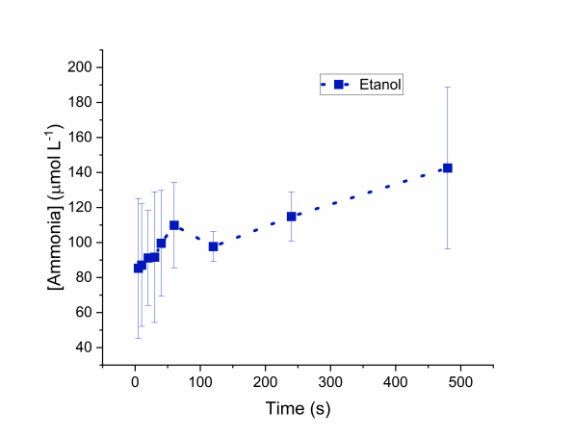

Figure S71. Ammonia quantification produced by [CuIIL3] complex in Ethanol/water (20%) 15mmol L^{-1} urea concentration.

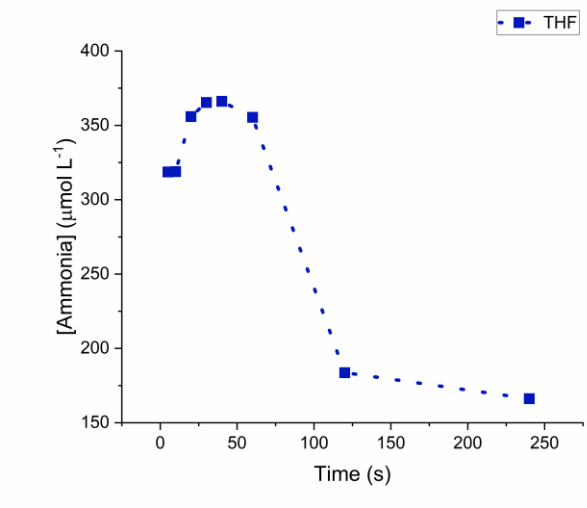

Figure S72. Ammonia quantification produced by [CuIIL3] complex in THF/water (20%) 15mmol L^{-1} urea concentration.

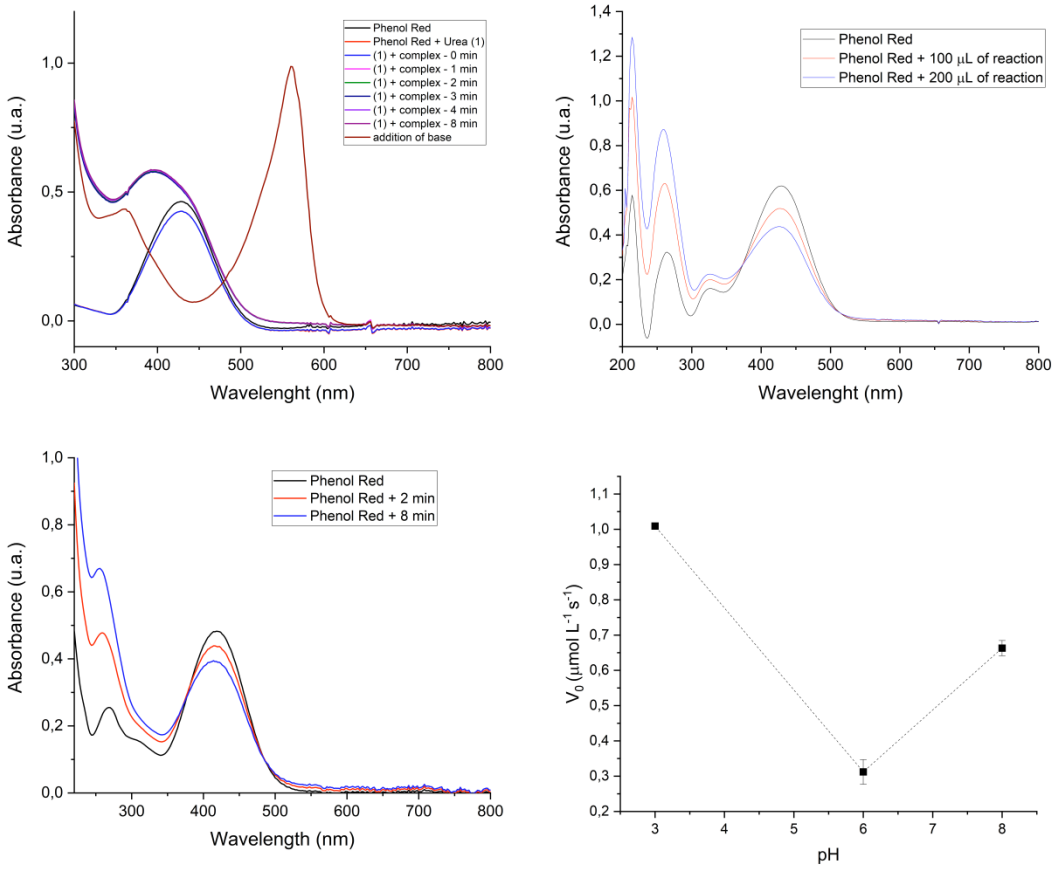

Figure S73. Study of the pH variation during the reaction and the effect of buffered solutions in the reaction rate. Reaction performed in MeOH/H_2O (30%) mixture using [CuIIL3] complex and 15mmol L^{-1} urea concentration, in presence of phenol red (A) and in the absence of phenol red, in which the addition of the reaction mixture was added to a phenol red solution (B).Reaction performed in ACN/H_2O (30%) mixture using [CuIIL3] complex and 15mmol L^{-1} urea concentration. The addition of the reaction mixture was added to a phenol red solution (C). Reaction rates measured from reactions performed in MeOH/H_2O (30%) mixtures using [CuIIL3] complex and buffered solutions (0.1M of phosphate) of 15mmol L^{-1} urea concentration.

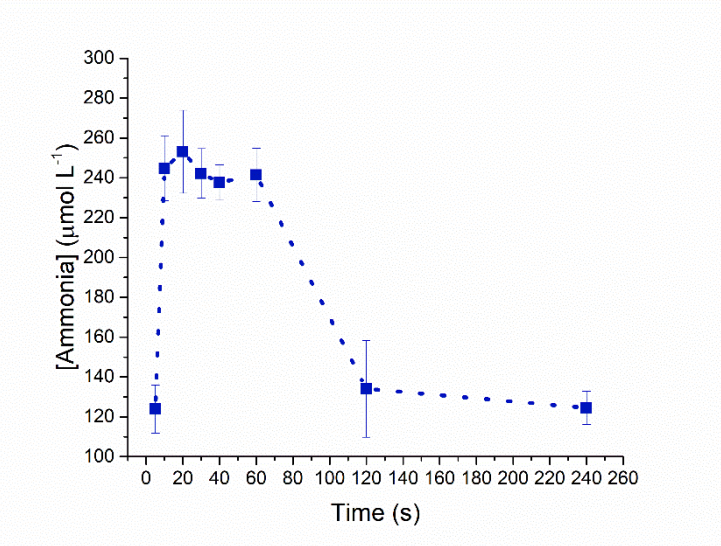

Figure S74. Ammonia quantification produced by CuIIL3 complex in (a) acetonitrile/water mixture (2% v:v) over 240 seconds at 308 K and at 15.6 mmolL^{-1} concentration of urea.

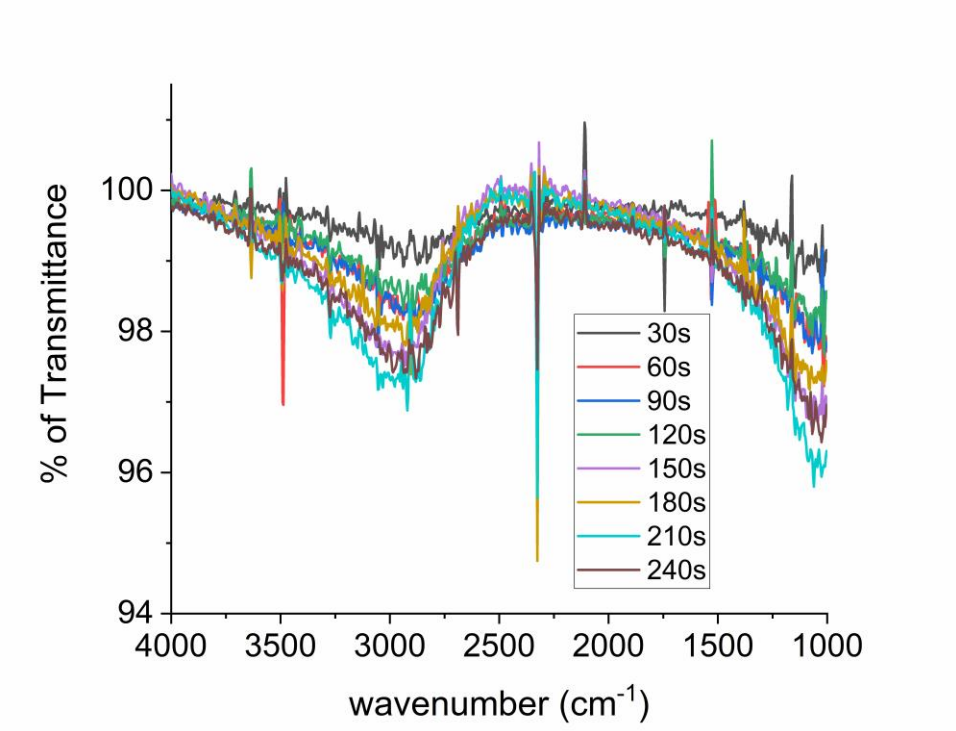

Figure S75.*In situ* FTIR spectra of the reaction in the 4000-1000cm^{-1} region over 240 seconds of reaction, indicating the increase of the band centered at 3000 cm^{-1}. The reaction started with the addition of a 15mM solution of urea, reaching a 10% volume of added water to the methanolic solution of complex CuIIL3.

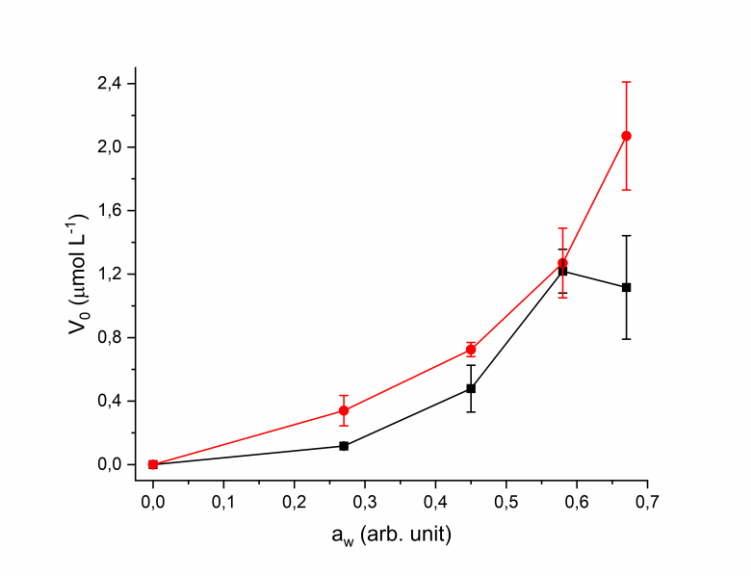

Figure S76. Initial rate of urea hydrolysis reaction versus urea concentration performed by $Cu^{II}L2$*(red line, circles)* and$Cu^{II}L3$ *(black line, squares)* with the increase in water content of the reaction from 0 to 40%

Table S1. Crystal data and structure refinement of L_1 – L_3.

	L_1	**L_2**	**L_3**
Empirical formula	$C_{15.5}H_{15}NO_{0.5}$	$C_{32}H_{32}N_2O_2$	$C_{32}H_{32}N_2O$
Formula weight	223.28	476.59	460.59
Colour, shapes	Yellowish green	Bright yellow	Yellowish green
Temperature/K	298	298	298
Crystal system	orthorhombic	Orthorhombic	orthorhombic
Space group	$P2_12_12_1$	$P2_12_12_1$	$P2_12_12_1$
a/Å	11.1917(6)	11.5740(15)	11.4294(5)
b/Å	14.7510(8)	14.9910(8)	14.6241(7)
c/Å	14.8637(8)	15.1410(13)	15.2779(7)
α/°	90	90	90
β/°	90	90	90

γ/°	90	90	90
Volume/Å^3	2453.8(2)	2627.1(4)	2553.6(2)
Z	8	4	4
ρ_{calc}g/cm^3	1.209	1.205	1.198
μ/mm^{-1}	0.073	0.075	0.072
F(000)	952.0	1016.0	984.0
Crystal size/mm^3	0.25 × 0.23 × 0.2	0.25 × 0.2 × 0.18	0.4 × 0.32 × 0.3
Radiation	MoKα (λ = 0.71073)	MoKα (λ = 0.71073)	MoKα (λ = 0.71073)
2Θ range for data collection/°	5.328 to 56.542	6.064 to 52.744	5.25 to 68.828
Index ranges	-10 ≤ h ≤ 14, -19 ≤ k ≤ 19, -15 ≤ l ≤ 19	? ≤ h ≤ ?, ? ≤ k ≤ ?, ? ≤ l ≤ ?	-17 ≤ h ≤ 13, -21 ≤ k ≤ 20, -10 ≤ l ≤ 24
Reflections collected	16738	5370	21809
Independent reflections	6054 [R_{int} = 0.0238, R_{sigma} = 0.0287]	5370 [R_{int} = ?, R_{sigma} = 0.0541]	9811 [R_{int} = 0.0205, R_{sigma} = 0.0339]
Data/restraints/parameters	6054/0/311	5370/48/331	9811/0/318
Goodness-of-fit on F^2	1.069	1.027	1.034
Final R indexes [I>=2σ (I)]	R_1 = 0.0414, wR_2 = 0.0902	R_1 = 0.0704, wR_2 = 0.1683	R_1 = 0.0527, wR_2 = 0.1109
Final R indexes [all data]	R_1 = 0.0632, wR_2 = 0.1024	R_1 = 0.1182, wR_2 = 0.2054	R_1 = 0.1026, wR_2 = 0.1386
Largest diff. peak/hole / e Å^{-3}	0.12/-0.18	0.18/-0.24	0.14/-0.21
Flack parameter	-0.9(6)	-1.4(10)	0.4(6)

Table S2. Bond lengthfor L_1 – L_3.

L_1					
Atom	**Atom**	**Length/ Å**	**Atom**	**Atom**	**Length/ Å**
$N^{(2)}$	$C^{(7)}$	1.270(3)		$C^{(18)}$	$C^{(19A)}$
$N^{(2)}$	$C^{(6)}$	1.469(3)		$C^{(18)}$	$C^{(19)}$
$N^{(1)}$	$C^{(1)}$	1.475(3)		$C^{(3)}$	$C^{(4)}$
$N^{(1)}$	$C^{(5)}$	1.453(3)		$C^{(24)}$	$C^{(23)}$
$N^{(1)}$	$C^{(4)}$	1.459(3)		$C^{(24)}$	$C^{(25)}$
$O^{(1)}$	$C^{(13)}$	1.344(3)		$C^{(20)}$	$C^{(19)}$
$C^{(14)}$	$C^{(5)}$	1.505(3)		$C^{(20)}$	$C^{(21)}$
$C^{(14)}$	$C^{(15)}$	1.383(3)		$C^{(23A)}$	$C^{(24A)}$
$C^{(14)}$	$C^{(15A)}$	1.377(3)		$C^{(13)}$	$C^{(12)}$
$C^{(7)}$	$C^{(8)}$	1.454(3)		$C^{(19A)}$	$C^{(20A)}$
$C^{(22)}$	$C^{(23)}$	1.394(3)		$C^{(25)}$	$C^{(24A)}$
$C^{(22)}$	$C^{(6)}$	1.531(3)		$C^{(9)}$	$C^{(10)}$
$C^{(22)}$	$C^{(23A)}$	1.383(3)		$C^{(20A)}$	$C^{(21)}$

$C^{(2)}$	$C^{(1)}$	1.540(3)	$C^{(15)}$	$C^{(16)}$	
$C^{(2)}$	$C^{(3)}$	1.518(3)	$C^{(15A)}$	$C^{(16A)}$	
$C^{(8)}$	$C^{(13)}$	1.397(3)	$C^{(16A)}$	$C^{(17)}$	
$C^{(8)}$	$C^{(9)}$	1.395(3)	$C^{(11)}$	$C^{(10)}$	
$C^{(1)}$	$C^{(6)}$	1.574(3)	$C^{(11)}$	$C^{(12)}$	
$C^{(18)}$	$C^{(6)}$	1.528(3)	$C^{(17)}$	$C^{(16)}$	

L_2

Atom	**Atom**	**Length/ Å**	**Atom**	**Atom**	**Length/ Å**
$N^{(2)}$	$C^{(7)}$	1.278(6)	$C^{(6)}$	$C^{(23)}$	1.526(7)
$N^{(2)}$	$C^{(6)}$	1.478(6)	$C^{(6)}$	$C^{(1)}$	1.581(6)
$O^{(1)}$	$C^{(13)}$	1.347(6)	$C^{(23)}$	$C^{(24A)}$	1.393(7)
$C^{(7)}$	$C^{(8)}$	1.457(7)	$C^{(15)}$	$C^{(16A)}$	1.381(11)
$O^{(2)}$	$C^{(12)}$	1.367(6)	$C^{(15)}$	$C^{(16)}$	1.357(10)
$O^{(2)}$	$C^{(14)}$	1.421(8)	$C^{(9)}$	$C^{(10)}$	1.364(9)
$C^{(20A)}$	$C^{(19)}$	1.395(8)	$C^{(1)}$	$C^{(2)}$	1.544(7)
$C^{(20A)}$	$C^{(21A)}$	1.366(7)	$C^{(21A)}$	$C^{(22)}$	1.364(8)
$C^{(8)}$	$C^{(13)}$	1.395(7)	$C^{(11)}$	$C^{(10)}$	1.387(9)
$C^{(8)}$	$C^{(9)}$	1.396(7)	$C^{(2)}$	$C^{(3)}$	1.525(9)
$N^{(1)}$	$C^{(5)}$	1.462(7)	$C^{(22)}$	$C^{(21)}$	1.377(9)
$N^{(1)}$	$C^{(1)}$	1.474(6)	$C^{(24A)}$	$C^{(25A)}$	1.372(8)
$N^{(1)}$	$C^{(4)}$	1.470(8)	$C^{(20)}$	$C^{(21)}$	1.380(8)
$C^{(19)}$	$C^{(6)}$	1.530(7)	$C^{(4)}$	$C^{(3)}$	1.506(8)
$C^{(19)}$	$C^{(20)}$	1.374(7)	$C^{(16A)}$	$C^{(17A)}$	1.347(13)
$C^{(5)}$	$C^{(15)}$	1.505(8)	$C^{(25A)}$	$C^{(26)}$	1.381(10)
$C^{(13)}$	$C^{(12)}$	1.408(7)	$C^{(25)}$	$C^{(26)}$	1.365(10)
$C^{(12)}$	$C^{(11)}$	1.363(7)	$C^{(16)}$	$C^{(17)}$	1.410(10)
$C^{(24)}$	$C^{(23)}$	1.406(7)	$C^{(17A)}$	$C^{(18)}$	1.340(16)
$C^{(24)}$	$C^{(25)}$	1.375(8)	$C^{(17)}$	$C^{(18)}$	1.379(16)

L_3

Atom	**Atom**	**Length/ Å**	**Atom**	**Atom**	**Length/ Å**
$O^{(34)}$	$C^{(6)}$	1.346(3)	$C^{(22)}$	$C^{(27)}$	1.370(3)
$N^{(8)}$	$C^{(7)}$	1.272(3)	$C^{(15)}$	$C^{(14)}$	1.375(3)
$N^{(8)}$	$C^{(9)}$	1.474(2)	$C^{(33)}$	$C^{(32)}$	1.377(3)
$N^{(20)}$	$C^{(16)}$	1.474(3)	$C^{(14)}$	$C^{(13)}$	1.365(3)
$N^{(20)}$	$C^{(21)}$	1.454(3)	$C^{(11)}$	$C^{(12)}$	1.377(3)
$N^{(20)}$	$C^{(19)}$	1.461(3)	$C^{(5)}$	$C^{(4)}$	1.368(4)
$C^{(7)}$	$C^{(1)}$	1.454(3)	$C^{(5)}$	$C^{(35)}$	1.500(4)
$C^{(10)}$	$C^{(9)}$	1.528(3)	$C^{(17)}$	$C^{(18)}$	1.518(3)
$C^{(10)}$	$C^{(15)}$	1.390(3)	$C^{(13)}$	$C^{(12)}$	1.374(4)
$C^{(10)}$	$C^{(11)}$	1.386(3)	$C^{(29)}$	$C^{(30)}$	1.386(4)
$C^{(1)}$	$C^{(6)}$	1.400(3)	$C^{(19)}$	$C^{(18)}$	1.507(3)
$C^{(1)}$	$C^{(2)}$	1.390(3)	$C^{(32)}$	$C^{(31)}$	1.370(4)
$C^{(16)}$	$C^{(9)}$	1.575(3)	$C^{(23)}$	$C^{(24)}$	1.378(4)
$C^{(16)}$	$C^{(17)}$	1.542(3)	$C^{(27)}$	$C^{(26)}$	1.403(4)
$C^{(28)}$	$C^{(9)}$	1.528(3)	$C^{(4)}$	$C^{(3)}$	1.374(4)
$C^{(28)}$	$C^{(33)}$	1.393(3)	$C^{(2)}$	$C^{(3)}$	1.375(4)
$C^{(28)}$	$C^{(29)}$	1.387(3)	$C^{(31)}$	$C^{(30)}$	1.368(5)

$C^{(6)}$	$C^{(5)}$	1.396(3)	$C^{(26)}$	$C^{(25)}$	1.385(5)
$C^{(22)}$	$C^{(21)}$	1.511(3)	$C^{(25)}$	$C^{(24)}$	1.348(5)
$C^{(22)}$	$C^{(23)}$	1.387(3)			

Table S3. Bond angles for L_1 – L_3.

L_1							
Atom	**Atom**	**Atom**	**Length/ Å**	**Atom**	**Atom**	**Atom**	**Length/ Å**
$C^{(7)}$	$N^{(2)}$	$C^{(6)}$	123.37(18)	$N^{(2)}$	$C^{(6)}$	$C^{(22)}$	113.37(16)
$C^{(5)}$	$N^{(1)}$	$C^{(1)}$	114.34(17)	$N^{(2)}$	$C^{(6)}$	$C^{(1)}$	104.95(16)
$C^{(5)}$	$N^{(1)}$	$C^{(4)}$	112.83(18)	$N^{(2)}$	$C^{(6)}$	$C^{(18)}$	109.24(16)
$C^{(4)}$	$N^{(1)}$	$C^{(1)}$	108.85(17)	$C^{(22)}$	$C^{(6)}$	$C^{(1)}$	112.57(15)
$C^{(15)}$	$C^{(14)}$	$C^{(5)}$	118.9(2)	$C^{(18)}$	$C^{(6)}$	$C^{(22)}$	108.44(17)
$C^{(15A)}$	$C^{(14)}$	$C^{(5)}$	122.2(2)	$C^{(18)}$	$C^{(6)}$	$C^{(1)}$	108.10(16)
$C^{(15A)}$	$C^{(14)}$	$C^{(15)}$	118.8(2)	$C^{(24A)}$	$C^{(23A)}$	$C^{(22)}$	120.8(2)
$N^{(2)}$	$C^{(7)}$	$C^{(8)}$	121.1(2)	$O^{(1)}$	$C^{(13)}$	$C^{(8)}$	121.4(2)
$C^{(23)}$	$C^{(22)}$	$C^{(6)}$	117.91(18)	$O^{(1)}$	$C^{(13)}$	$C^{(12)}$	119.1(3)
$C^{(23A)}$	$C^{(22)}$	$C^{(23)}$	117.5(2)	$C^{(12)}$	$C^{(13)}$	$C^{(8)}$	119.5(3)
$C^{(23A)}$	$C^{(22)}$	$C^{(6)}$	124.55(19)	$C^{(20A)}$	$C^{(19A)}$	$C^{(18)}$	120.8(2)
$C^{(3)}$	$C^{(2)}$	$C^{(1)}$	104.79(17)	$C^{(24)}$	$C^{(25)}$	$C^{(24A)}$	119.8(2)
$C^{(13)}$	$C^{(8)}$	$C^{(7)}$	120.9(2)	$C^{(20)}$	$C^{(19)}$	$C^{(18)}$	121.0(2)
$C^{(9)}$	$C^{(8)}$	$C^{(7)}$	120.1(2)	$C^{(10)}$	$C^{(9)}$	$C^{(8)}$	120.7(3)
$C^{(9)}$	$C^{(8)}$	$C^{(13)}$	118.8(2)	$C^{(21)}$	$C^{(20A)}$	$C^{(19A)}$	120.9(2)
$N^{(1)}$	$C^{(1)}$	$C^{(2)}$	105.32(17)	$N^{(1)}$	$C^{(4)}$	$C^{(3)}$	104.89(19)
$N^{(1)}$	$C^{(1)}$	$C^{(6)}$	111.00(16)	$C^{(25)}$	$C^{(24A)}$	$C^{(23A)}$	120.5(2)
$C^{(2)}$	$C^{(1)}$	$C^{(6)}$	113.70(17)	$C^{(20)}$	$C^{(21)}$	$C^{(20A)}$	118.9(2)
$C^{(19A)}$	$C^{(18)}$	$C^{(6)}$	123.1(2)	$C^{(16)}$	$C^{(15)}$	$C^{(14)}$	121.2(3)
$C^{(19A)}$	$C^{(18)}$	$C^{(19)}$	117.8(2)	$C^{(14)}$	$C^{(15A)}$	$C^{(16A)}$	120.0(3)
$C^{(19)}$	$C^{(18)}$	$C^{(6)}$	118.81(19)	$C^{(17)}$	$C^{(16A)}$	$C^{(15A)}$	119.8(3)
$N^{(1)}$	$C^{(5)}$	$C^{(14)}$	113.78(19)	$C^{(12)}$	$C^{(11)}$	$C^{(10)}$	121.4(3)
$C^{(4)}$	$C^{(3)}$	$C^{(2)}$	102.81(19)	$C^{(11)}$	$C^{(10)}$	$C^{(9)}$	119.4(3)
$C^{(25)}$	$C^{(24)}$	$C^{(23)}$	119.9(2)	$C^{(11)}$	$C^{(12)}$	$C^{(13)}$	120.2(3)
$C^{(24)}$	$C^{(23)}$	$C^{(22)}$	121.6(2)	$C^{(16)}$	$C^{(17)}$	$C^{(16A)}$	120.3(3)
$C^{(21)}$	$C^{(20)}$	$C^{(19)}$	120.6(2)	$C^{(17)}$	$C^{(16)}$	$C^{(15)}$	120.0(3)
				L_2			
Atom	**Atom**	**Atom**	**Length/ Å**	**Atom**	**Atom**	**Atom**	**Length/ Å**
$C^{(7)}$	$N^{(2)}$	$C^{(6)}$	121.2(4)	$C^{(24A)}$	$C^{(23)}$	$C^{(24)}$	117.3(5)
$N^{(2)}$	$C^{(7)}$	$C^{(8)}$	121.9(4)	$C^{(24A)}$	$C^{(23)}$	$C^{(6)}$	125.1(5)
$C^{(12)}$	$O^{(2)}$	$C^{(14)}$	116.1(5)	$C^{(16A)}$	$C^{(15)}$	$C^{(5)}$	120.0(8)
$C^{(21A)}$	$C^{(20A)}$	$C^{(19)}$	121.3(5)	$C^{(16)}$	$C^{(15)}$	$C^{(5)}$	123.5(6)
$C^{(13)}$	$C^{(8)}$	$C^{(7)}$	121.0(4)	$C^{(16)}$	$C^{(15)}$	$C^{(16A)}$	116.5(7)
$C^{(13)}$	$C^{(8)}$	$C^{(9)}$	119.3(5)	$C^{(10)}$	$C^{(9)}$	$C^{(8)}$	120.5(5)
$C^{(9)}$	$C^{(8)}$	$C^{(7)}$	119.7(5)	$N^{(1)}$	$C^{(1)}$	$C^{(6)}$	111.7(3)

$C^{(5)}$	$N^{(1)}$	$C^{(1)}$	113.9(4)	$N^{(1)}$	$C^{(1)}$	$C^{(2)}$	105.1(4)
$C^{(5)}$	$N^{(1)}$	$C^{(4)}$	112.9(4)	$C^{(2)}$	$C^{(1)}$	$C^{(6)}$	114.1(4)
$C^{(4)}$	$N^{(1)}$	$C^{(1)}$	108.1(4)	$C^{(22)}$	$C^{(21A)}$	$C^{(20A)}$	121.0(5)
$C^{(20A)}$	$C^{(19)}$	$C^{(6)}$	118.6(4)	$C^{(12)}$	$C^{(11)}$	$C^{(10)}$	121.6(6)
$C^{(20)}$	$C^{(19)}$	$C^{(20A)}$	117.2(5)	$C^{(3)}$	$C^{(2)}$	$C^{(1)}$	104.4(4)
$C^{(20)}$	$C^{(19)}$	$C^{(6)}$	124.1(5)	$C^{(21A)}$	$C^{(22)}$	$C^{(21)}$	118.7(5)
$N^{(1)}$	$C^{(5)}$	$C^{(15)}$	113.1(5)	$C^{(25A)}$	$C^{(24A)}$	$C^{(23)}$	120.9(6)
$O^{(1)}$	$C^{(13)}$	$C^{(8)}$	122.3(5)	$C^{(19)}$	$C^{(20)}$	$C^{(21)}$	121.4(5)
$O^{(1)}$	$C^{(13)}$	$C^{(12)}$	117.9(4)	$N^{(1)}$	$C^{(4)}$	$C^{(3)}$	104.6(4)
$C^{(8)}$	$C^{(13)}$	$C^{(12)}$	119.7(4)	$C^{(22)}$	$C^{(21)}$	$C^{(20)}$	120.5(5)
$O^{(2)}$	$C^{(12)}$	$C^{(13)}$	115.7(4)	$C^{(17A)}$	$C^{(16A)}$	$C^{(15)}$	123.7(12)
$C^{(11)}$	$C^{(12)}$	$O^{(2)}$	125.3(5)	$C^{(9)}$	$C^{(10)}$	$C^{(11)}$	119.7(5)
$C^{(11)}$	$C^{(12)}$	$C^{(13)}$	119.0(5)	$C^{(24A)}$	$C^{(25A)}$	$C^{(26)}$	120.4(6)
$C^{(25)}$	$C^{(24)}$	$C^{(23)}$	121.3(5)	$C^{(26)}$	$C^{(25)}$	$C^{(24)}$	119.9(6)
$N^{(2)}$	$C^{(6)}$	$C^{(19)}$	108.9(4)	$C^{(4)}$	$C^{(3)}$	$C^{(2)}$	101.2(5)
$N^{(2)}$	$C^{(6)}$	$C^{(23)}$	113.2(4)	$C^{(25)}$	$C^{(26)}$	$C^{(25A)}$	120.1(6)
$N^{(2)}$	$C^{(6)}$	$C^{(1)}$	104.9(4)	$C^{(15)}$	$C^{(16)}$	$C^{(17)}$	121.2(9)
$C^{(19)}$	$C^{(6)}$	$C^{(1)}$	107.8(3)	$C^{(18)}$	$C^{(17A)}$	$C^{(16A)}$	119.4(11)
$C^{(23)}$	$C^{(6)}$	$C^{(19)}$	109.0(4)	$C^{(18)}$	$C^{(17)}$	$C^{(16)}$	118.5(11)
$C^{(23)}$	$C^{(6)}$	$C^{(1)}$	112.8(4)	$C^{(17A)}$	$C^{(18)}$	$C^{(17)}$	120.6(9)
$C^{(24)}$	$C^{(23)}$	$C^{(6)}$	117.6(4)				

L_3

Atom	**Atom**	**Atom**	**Length/ Å**	**Atom**	**Atom**	**Atom**	**Length/ Å**
$C^{(7)}$	$N^{(8)}$	$C^{(9)}$	121.90(16)	$C^{(27)}$	$C^{(22)}$	$C^{(21)}$	122.8(2)
$C^{(21)}$	$N^{(20)}$	$C^{(16)}$	113.40(16)	$C^{(27)}$	$C^{(22)}$	$C^{(23)}$	119.2(2)
$C^{(21)}$	$N^{(20)}$	$C^{(19)}$	112.86(18)	$C^{(14)}$	$C^{(15)}$	$C^{(10)}$	121.4(2)
$C^{(19)}$	$N^{(20)}$	$C^{(16)}$	108.49(17)	$C^{(32)}$	$C^{(33)}$	$C^{(28)}$	121.6(2)
$N^{(8)}$	$C^{(7)}$	$C^{(1)}$	121.71(19)	$C^{(13)}$	$C^{(14)}$	$C^{(15)}$	120.4(2)
$C^{(15)}$	$C^{(10)}$	$C^{(9)}$	119.32(18)	$C^{(12)}$	$C^{(11)}$	$C^{(10)}$	120.7(2)
$C^{(11)}$	$C^{(10)}$	$C^{(9)}$	122.90(18)	$C^{(6)}$	$C^{(5)}$	$C^{(35)}$	119.9(3)
$C^{(11)}$	$C^{(10)}$	$C^{(15)}$	117.5(2)	$C^{(4)}$	$C^{(5)}$	$C^{(6)}$	118.0(2)
$C^{(6)}$	$C^{(1)}$	$C^{(7)}$	121.25(19)	$C^{(4)}$	$C^{(5)}$	$C^{(35)}$	122.0(2)
$C^{(2)}$	$C^{(1)}$	$C^{(7)}$	119.6(2)	$N^{(20)}$	$C^{(21)}$	$C^{(22)}$	114.29(18)
$C^{(2)}$	$C^{(1)}$	$C^{(6)}$	119.1(2)	$C^{(18)}$	$C^{(17)}$	$C^{(16)}$	104.42(17)
$N^{(20)}$	$C^{(16)}$	$C^{(9)}$	111.84(15)	$C^{(14)}$	$C^{(13)}$	$C^{(12)}$	119.1(2)
$N^{(20)}$	$C^{(16)}$	$C^{(17)}$	105.04(16)	$C^{(30)}$	$C^{(29)}$	$C^{(28)}$	120.7(3)
$C^{(17)}$	$C^{(16)}$	$C^{(9)}$	113.99(17)	$N^{(20)}$	$C^{(19)}$	$C^{(18)}$	104.49(18)
$C^{(33)}$	$C^{(28)}$	$C^{(9)}$	117.81(18)	$C^{(13)}$	$C^{(12)}$	$C^{(11)}$	120.9(2)
$C^{(29)}$	$C^{(28)}$	$C^{(9)}$	124.9(2)	$C^{(31)}$	$C^{(32)}$	$C^{(33)}$	120.1(3)
$C^{(29)}$	$C^{(28)}$	$C^{(33)}$	117.3(2)	$C^{(19)}$	$C^{(18)}$	$C^{(17)}$	101.79(19)
$N^{(8)}$	$C^{(9)}$	$C^{(10)}$	109.08(15)	$C^{(24)}$	$C^{(23)}$	$C^{(22)}$	120.8(3)
$N^{(8)}$	$C^{(9)}$	$C^{(16)}$	105.39(15)	$C^{(22)}$	$C^{(27)}$	$C^{(26)}$	119.7(3)
$N^{(8)}$	$C^{(9)}$	$C^{(28)}$	112.45(16)	$C^{(5)}$	$C^{(4)}$	$C^{(3)}$	122.5(2)
$C^{(10)}$	$C^{(9)}$	$C^{(16)}$	107.89(15)	$C^{(3)}$	$C^{(2)}$	$C^{(1)}$	120.2(3)
$C^{(10)}$	$C^{(9)}$	$C^{(28)}$	109.74(16)	$C^{(30)}$	$C^{(31)}$	$C^{(32)}$	119.6(2)
$C^{(28)}$	$C^{(9)}$	$C^{(16)}$	112.10(15)	$C^{(25)}$	$C^{(26)}$	$C^{(27)}$	119.5(3)
$O^{(34)}$	$C^{(6)}$	$C^{(1)}$	121.36(19)	$C^{(31)}$	$C^{(30)}$	$C^{(29)}$	120.7(3)

$O^{(34)}$	$C^{(6)}$	$C^{(5)}$	118.1(2)	$C^{(24)}$	$C^{(25)}$	$C^{(26)}$	120.6(3)
$C^{(5)}$	$C^{(6)}$	$C^{(1)}$	120.6(2)	$C^{(4)}$	$C^{(3)}$	$C^{(2)}$	119.5(3)
$C^{(23)}$	$C^{(22)}$	$C^{(21)}$	117.9(2)	$C^{(25)}$	$C^{(24)}$	$C^{(23)}$	120.0(3)

Table S4. Comparision of the main infrared bands between ligands and complexes.

Compostos	**ν C=N**	**ν C – O**	**ν C – N**	**ν Cu – O**	**ν Cu – O**
HL1	1623	1280	1116, 1097	-	-
Cu^{II}L1	1654, 1637, 1617	1317, 1276, 1261	1089, 1074, 1028	638	474
HL2	1623	1269	1114, 1097	-	-
Cu^{II}L2	1619	1316, 1276	1081, 1004	638	557
HL3	1619	1265	1112, 1099	-	-
Cu^{II}L3	1654	1317, 1276	638	638	567
HL4	1617	1264	1143, 1114	-	-
Cu^{II}L4	1611	1336, 1326	1143, 1085	-	567
HL5	1621	1272	1114, 1015	-	-
Cu^{II}L5	1654, 1615	1317, 1278	1073, 1028	638	-

Table S5. Comparision of transitions in the ultravioleta and visible region between ligands and complexes.

Compostos	**π → π* C=C λ nm (εmax mol^{-1} cm^{-1} L)**	**π → π* C=C λ nm (εmax mol^{-1} cm^{-1} L)**	**π→π* C=N λ nm (εmax mol^{-1} cm^{-1} L)**	**n →π* C=C λ nm (εmax mol^{-1} cm^{-1} L)**	**d – d λ nm (εmax mol^{-1} cm^{-1} L)**
HL1	240 (8140)	260 (9513)	320 (3729)	414 (450)	-
Cu^{II}L1	248 (18246)	276 (16002)	380 (4383)	-	636 (265)
HL2	232 (27271)	262 (15775)	324 (3046)	432 (871)	-
Cu^{II}L2	234 (15660)	284 (13953)	362 (2479)	-	600<
HL3	232 (24009)	262 (18426)	326 (5085)	420 (358)	-
Cu^{II}L3	252 (19765)	280 (12308)	378 (3053)	-	600 – 700
HL4	232 (22025)	264 (16192)	330 (5320)	400 (269)	-
Cu^{II}L4	250 (18922)	278 (12694)	332 (3959) e 388 (4499)	-	650 (294)
HL5	232 (15984)	264 (9288)	332 (2716)	430 (622)	-
Cu^{II}L5	236 (10803)	252 (15770)	356 (2348)	-	600<

Table S6. Comparision of oxidation and reduction potentials due to the cyclic voltammetry of ligands and complexes.

Compounds	**E, V**			
	$E_{pa}1$	$E_{pa}2$	E_{pa} 3	$E_{pc}1$
HL1	0.992	1.531	-	-
Cu^{II}L1	0.776	1.375	-	0,723
HL2	0.816	1.284	1.492	-
Cu^{II}L2	0.781	1.285	-	0.842
HL3	0.928	1.424	-	-
Cu^{II}L3	0.821	1.220	-	0.814
HL4	0.930	1.410	-	
Cu^{II}L4				
HL5	0.800	1.260	1.426	-
Cu^{II}L5				

Table S7. ESR parameters of aggregates and monomeric species of the Cu^{II} complexes of this work in dichloromethane at77 K.

Compounds	**g***			**g0***			**A, cm^{-1} ($x10^{-4}$)**		
	g_x	g_y	g_z	g_x0	g_y0	g_z0	A_x	A_y	A_z
Cu^{II}L1	2.0364	2.0752	2.2115	2.073(	2.0699	2.180[illegible]	10.3	12.9	187.6
Cu^{II}L2	2.0292	2.0926	2.2498	2.154[illegible]	2.1066	2.207[illegible]	33.1	1.3	158.0
Cu^{II}L3	2.0339	2.0733	2.2111	2.080[illegible]	2.1771	2.037(	0.6	9.6	193.0
Cu^{II}L4	2.0322	2.0779	2.2064	2.051[illegible]	2.1838	2.040[illegible]	0.5	15.6	185.4

$Cu^{II}L5$	2.0317	2.0709	2.2105	2.093	2.0878	2.222	0.3	18.8	190.9

g indicates the g factor for monomeric species and g0for aggregates species.

Table S8. ESR parameters for the Cu^{II} complexes of this work in acetonitrile at 298 K.

Compounds	**g**			**t_{corr}, ps**	**A, cm^{-1} ($x10^{-4}$)**		
	g_x	g_y	g_z		A_x	A_y	A_z
$Cu^{II}L1$	2.0535	2.0531	2.2063	25.9	14.53	14.06	198.7
$Cu^{II}L2$	2.0695	2.0932	2.1653	47.6	14.53	14.06	191.9
$Cu^{II}L3$	2.0569	2.0566	2.2055	36.2	14.53	14.06	193.8
$Cu^{II}L4$	2.0512	2.0518	2.2063	36.2	14.53	14.06	201.0
$Cu^{II}L5$	2.0537	2.0537	2.2063	35.9	14.53	14.06	201.4

Table S9. ESR parameters for the Cu^{II} complexes of this work in acetonitrile/water (80/20) mixture at 298 K.

Compounds	**g**			**t_{corr}, ps**	**A, cm^{-1} ($x10^{-4}$)**		
	g_x	g_y	g_z		A_x	A_y	A_z
$Cu^{II}L1$	2.0695	2.0789	2.1842	45.6	14.53	11.51	197.8
$Cu^{II}L2$	2.0695	2.0932	2.2022	39.7	11.88	11.51	192.8
$Cu^{II}L3$	2.0555	2.0555	2.2022	38.5	13.62	13.62	192.8
$Cu^{II}L4$	2.0494	2.0518	2.2063	44.2	14.53	14.06	200.1
$Cu^{II}L5$	2.0542	2.0537	2.2063	48.6	14.53	14.06	197.0

Table S10.ESR parameters for the $Cu^{II}L2$ and $[Cu^{II}L2(CH_3OH)]ClO_4$ of this work in methanol and methanol/water (80/20) mixture at 298 K.

Complexes	**Methanol**				**Methanol/Water (80:20)**			
	g_x	g_y	g_z	t_{corr}, (ps)	g_x	g_y	g_z	t_{corr}, (ps)
$Cu^{II}L2$ – 0[a]	2.0082	2.0604	2.4230	18.8	2.0388	2.1059	2.3560	32.8

$Cu^{II}L2$	2.0802	2.0783	2.1536	23.7	2.0758	2.0847	2.1513	44.9
$[Cu^{II}L2(CH_3OH]ClO_4$ – 0[a]	-	-	-	-	-	-	-	-
$[Cu^{II}L2(CH_3OH]ClO_4$	2.0627	2.0514	2.1969	66.0	2.0494	2.0419	2.2189	94.4

[a]Todimeric species.

Table S11. Maximum amount of ammonia formed by the complexes of this work under the conditions of acetonitrile/water and metanol/water mixture at 308 K.

Compounds	**Urea concentration (mmol L^{-1}) Acetonitrile/water**			**Urea concentration (mmol L^{-1}) Acetonitrile/water**			
	5.2	10.4	15.6	5.2	10.4	15.6	20.8
	$[Ammonia]_{max}$ (µmol L^{-1})						
$Cu^{II}L1$	74.54^{a} ± 4.72	168.06^{e} ± 9.58	-	-	-	-	-
$Cu^{II}L2$	70.68^{b} ± 9.61	185.73^{c} ± 6.51	270.90^{a} ± 9.76	42.88^{g} ± 7.75	111.16^{g} ± 3.32	129.95^{e} ± 3.31	203.28^{g} ± 3.51
$Cu^{II}L3$	75.70^{a} ± 2.79	166.28^{b} ± 10.11	337.81^{a} ± 20.38	-	-	-	-
$Cu^{II}L4$	69.99^{a} ± 6.08	156.05^{a} ± 0.49	-	41.56^{f} ± 6.04	113.09^{g} ± 3.26	137.32^{g} ± 4.82	209.67^{g} ± 5.37
$Cu^{II}L5$	61.35^{b} ± 9.25	150.15^{d} ± 1.18	-	-	-	-	-

[a]5s. [b]10s. [c]20s. [d] 60s. [e] 120s. [f]240s. [g] 480s.

Theoretical simulations

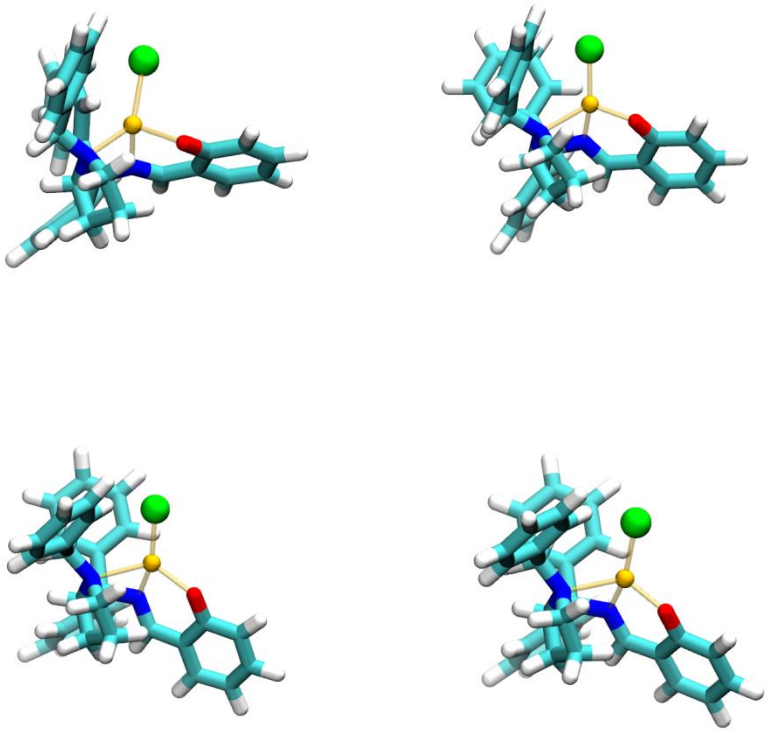

Figure S77 – Structures of the $Cu^{II}L1$ monomer complex: initial structure (top left); structure obtained after first geometry optimization (top right); structure obtained after a 10 ps molecular dynamics run (bottom left) and structure obtained after final geometry optimization (bottom right). All calculations were performed considering the doublet multiplicity.

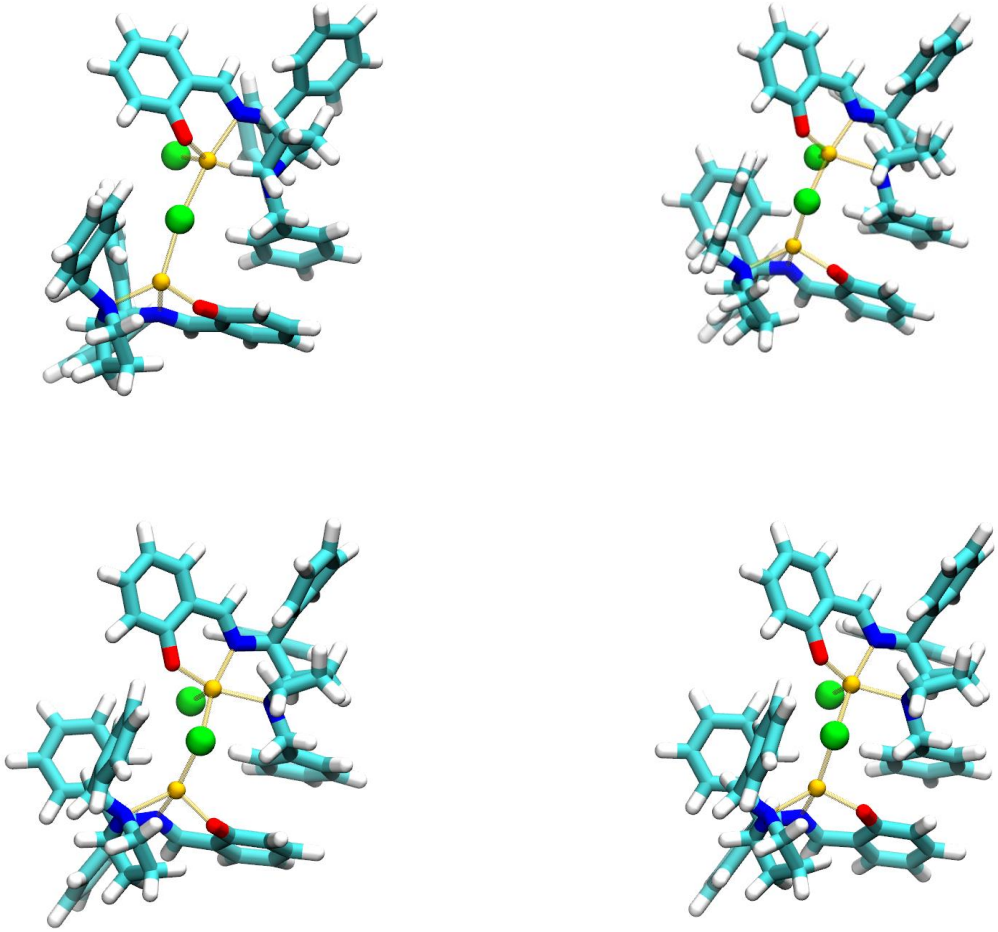

Figure S78 – Structures of the $Cu^{II}L1$ dimer complex: initial structure (top left); structure obtained after first geometry optimization (top right); structure obtained after a 10 ps molecular dynamics run (bottom left) and structure obtained after final geometry optimization (bottom right). All calculations were performed considering the singlet multiplicity.

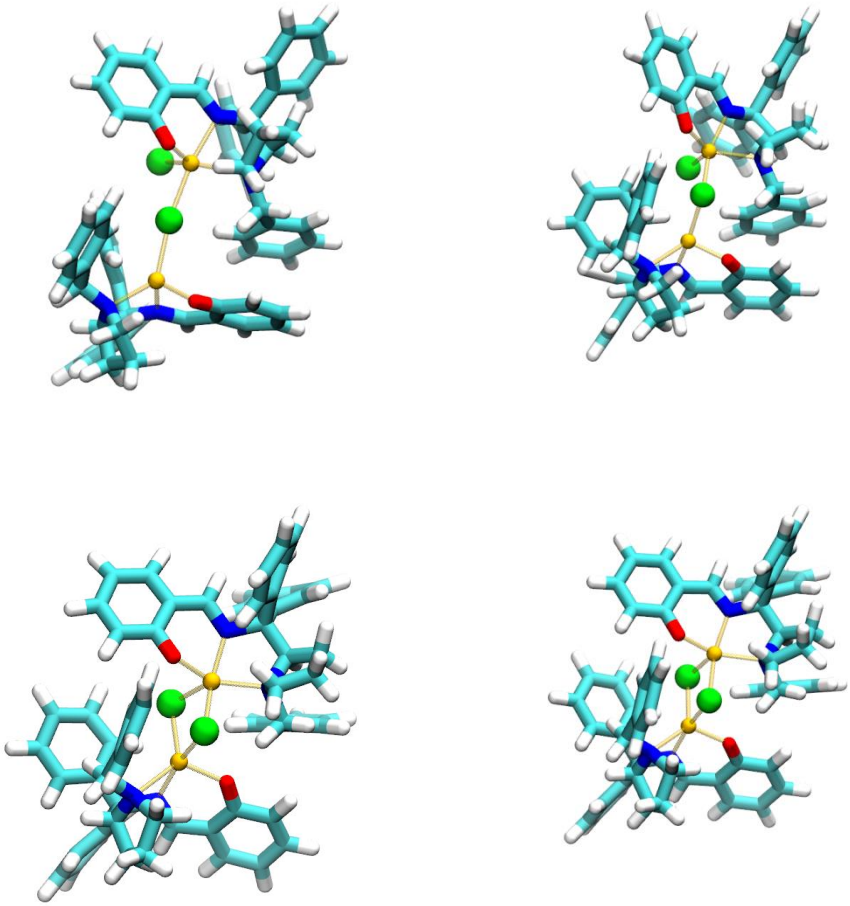

Figure S79 – Structures of the Cu^{II}L1 dimer complex: initial structure (top left); structure obtained after first geometry optimization (top right); structure obtained after a 10 ps molecular dynamics run (bottom left) and structure obtained after final geometry optimization (bottom right). All calculations were performed considering the triplet multiplicity.

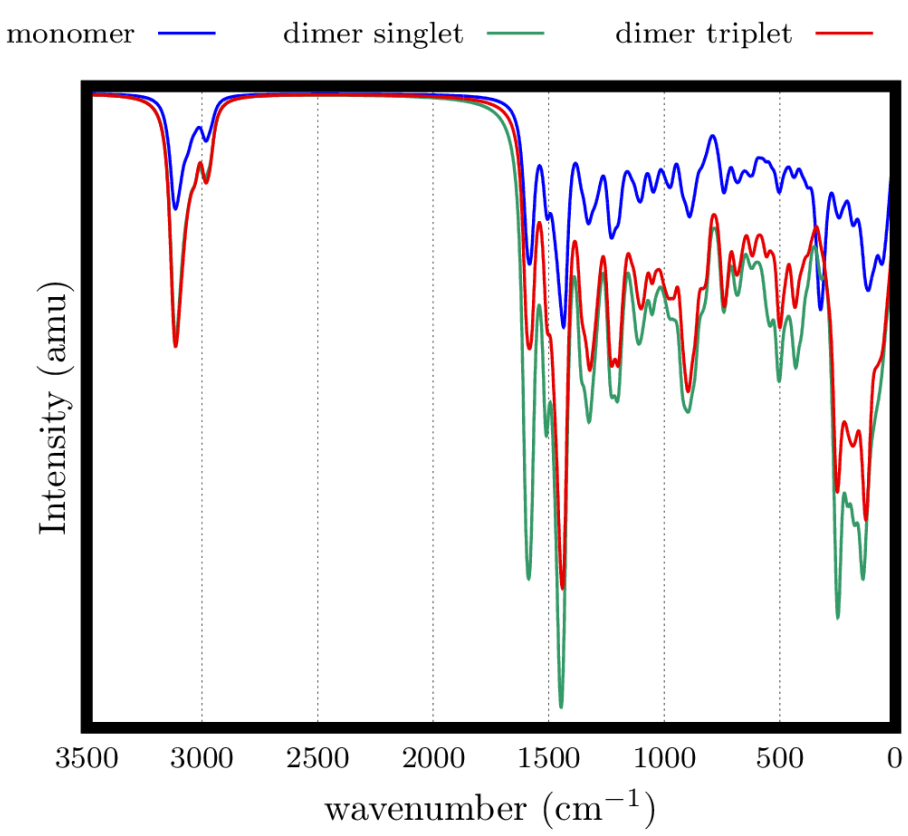

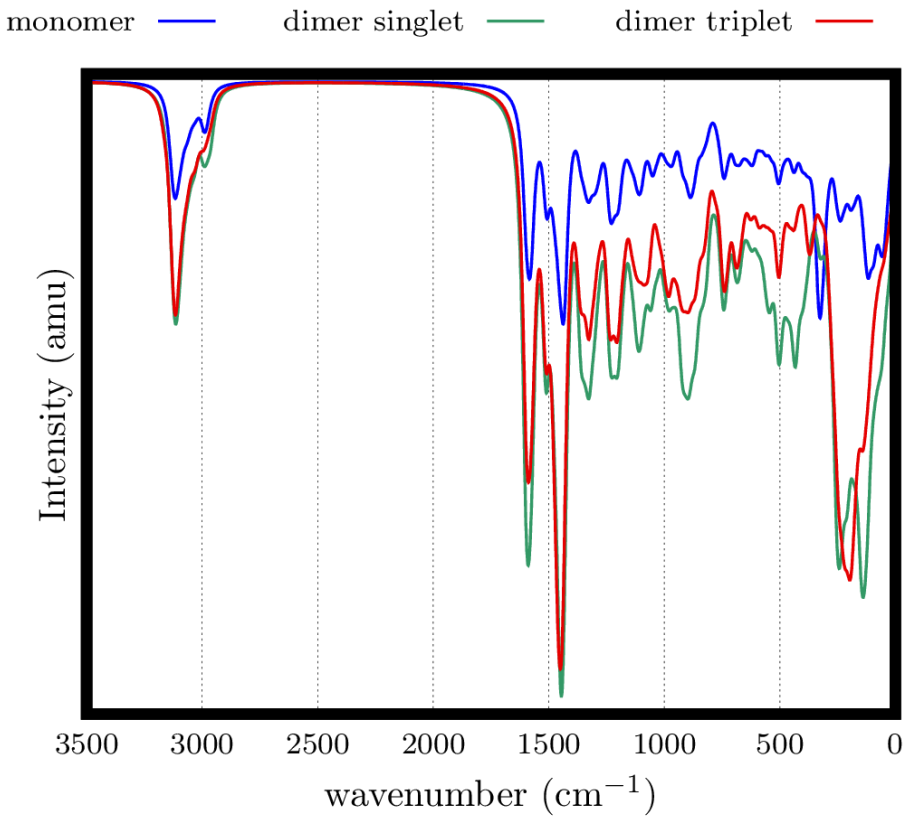

Figure 4 – Vibrational infrared spectra of the $Cu^{II}L1$ monomer and dimer (singlet and triplet) structures obtained after initial geometry optimization (top) and final geometry optimization

(bottom).

Association thermodynamics of different solvent molecules into these complexes were studied by means of a configurational phase space sampling using Themis software as follows:

i) complex structures optimized as described before were used as the reference molecule;

ii) a translation grid was build around the solvent-acessible-surface (SAS) area of these structures considering the vdw radii of each atom plus a 1.2 A probing radius.

iii) since previous calculations considering the grid around the whole molecule resulted in hot spots near the metallic center, only points within 5.0 A of Cu^{2+} and Cl^{-} were considered;

iv) a reference atom of the second molecule (Tref) was placed in each grid point in turn;

v) a second reference atom of the second molecule (Rref) originates its rotation axis: this axis will perform Nrot1 rotations around the grid point and the whole molecule will perform Nrot2 rotations around such axis;

vi) this succession of moves resulted in Ntrans x Nrot1 x Nrot2 = Nconf independent structures of solvent molecule around the complex;

vii) in order to reduce the number of structures, configurations that presented intermolecular distances below 1.6 A are considered invalid: a highly repulsive interaction energy value (10^6 kJ/mol) is assigned to such structure;

viii) cartesian coordinates of all valid structures were written in ordered files;

ix) a total of Nsp single-point calculations at the GFN1-xTB level were then performed considering the same convergence criteria described below (SCC and WF convergence, electronic temperature);

x) interaction energy for each *i*-th microstate was obtained by

$$E_{inter} = E_i - E_{far}$$

where Ei corresponds to the total energy of the *i*-th microstate and Efar corresponds to the total energy of the given solvent molecule nearly 100 A apart of the complex.

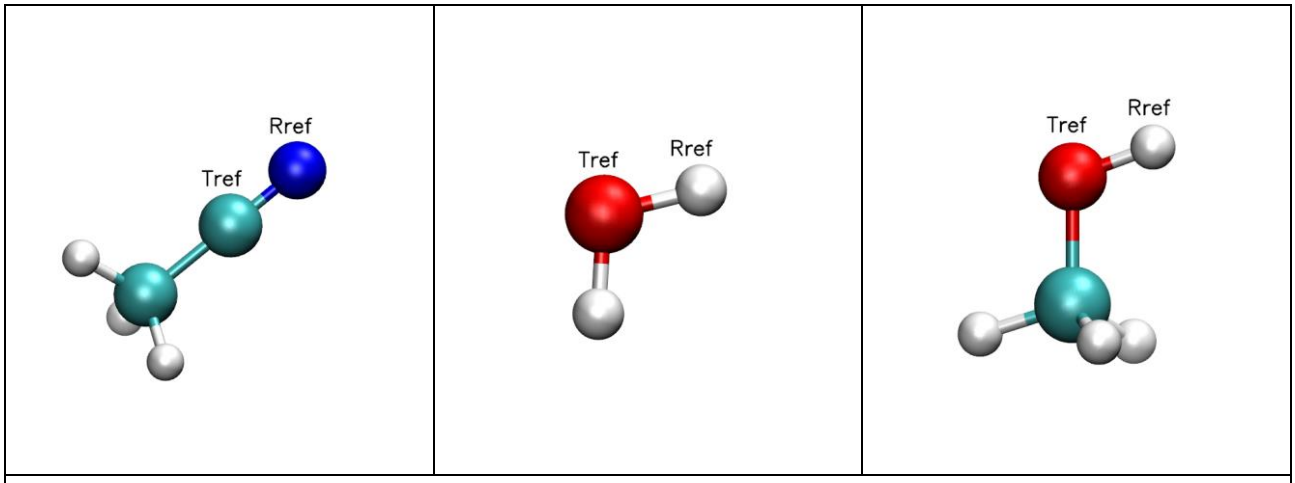

Figure S79 – Equilibrium structures of solvent molecules used in the configurational phase space sampling around the complex structures. Acetonitrile (AcN, left); water (H2O, center) and methanol (MeOH, right). Reference atoms for translation (Tref) and rotation (Rref) moves are presented for each structure.

Complex	Molecule	multiplicity	Ntrans	Nrot1	Nrot2	Nconf	Nsp
monomer	AcN	doublet	145	42	12	73080	39469
	H_2O	doublet	145	42	36	219240	199968
	MeOH	doublet	145	42	36	219240	125285
dimer	AcN	singlet	153	42	12	77112	35180
	H_2O	singlet	153	42	36	231336	202726
	MeOH	singlet	153	42	36	231336	115162
	AcN	triplet	154	42	12	77616	32147
	H_2O	triplet	154	42	36	232848	198939
	MeOH	triplet	154	42	36	232848	104412
Total number						1594656	1053288

Although the manuscript describing the Themis program is still under submission[67], this methodology was effectively used to sample the surface of a CdTe nanoparticle functionalized with cysteine molecules and find the preferential binding sites of the four DNA nucleobases using the PM7 Hamiltonian implemented in MOPAC 2016 software[68]. More recently, it was shown that free energy surfaces of first coordination shell of ion pairs of ionic liquids obtained at DFT level produces results in excellent agreement with the ones obtained from liquid phase MD simulations [69,70] demonstrating that even in some complex cases, Themis is able to probe the structure of condensed phases. It was also possible to study the interaction of carbon nitride sheets in order to build a multilayer structure and its further interaction with different cations to build a single-cation catalyst[71] using quantum chemistry energies from the GFN1-xTB Hamiltonian implemented in xTB 6.2 software.

Results for Monomer/molecules

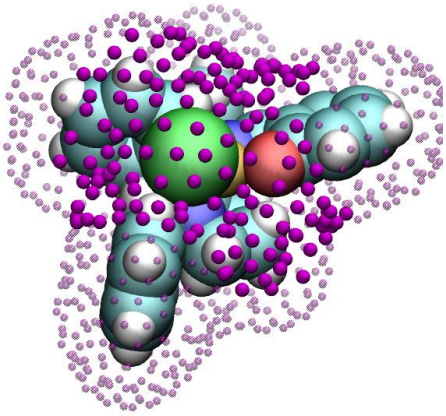

translation grid points near Cu^{2+} and Cl^{-} ions

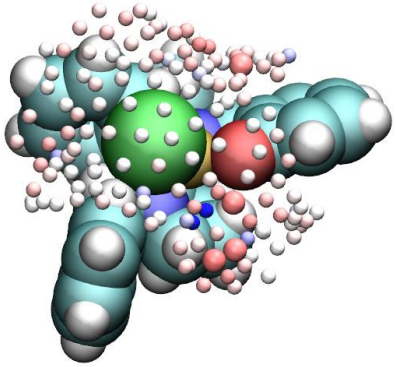

free energy landscape for AcN

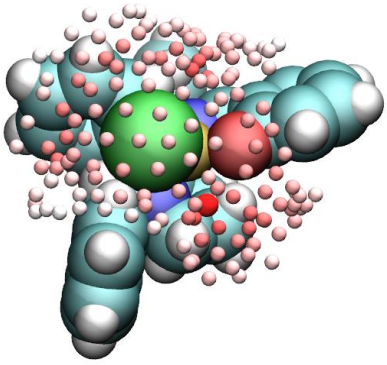

free energy landscape for H2O

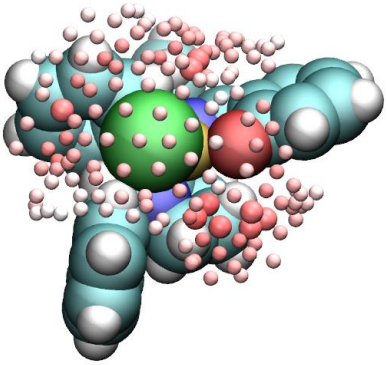

free energy landscape for MeOH

Figure S80 – Translation grid along surface accessible area (SAS) of the monomeric complex (transparent purple spheres). Points within 5.0 A of Cu^{2+} or Cl^{-} ions are highlighted (opaque purple spheres) and were used to sample the surface (top left). Free energy landscapes obtained at the GFN1-xTB level: AcN molecule (top right); H2O molecule (bottom left) and MeOH molecule (bottom right). Colorscale for the landscapes correspond to free energy values ranging from –32 kJ/mol (dark red) to +32 kJ/mol (dark blue). While color correspond to 0 kJ/mol.

As one can observe, each solvent molecule binds preferentially to different region of the complex. Free energy landscapes indicate the hot spots where such adsorption is preferential. In these representations, we highlight the grid points that correspond to a cumulative probability of approximately 50 % (bigger grid spheres). Thus, free energy landscape for ACN presented 4 translation points that amount to a 51.57 % probability, with free energy values ranging from –19.90 kJ/mol (p = 19.39 %) to –17.51 kJ/mol (p = 7.44 %). While the landscape for H2O molecule the most

probable translation point amounts to a 68.62 % probability alone (with a free energy value of –31.18 kJ/mol), MeOH landscape presented a more spread probability in which the 9 most probable translation points amounted to a 52.31 % probability, with free energy values ranging from –23.06 kJ/mol (p = 12.28 %) to –19.55 kJ/mol (p = 2.99 %).

After the full thermodynamic sampling and analysis performed by Themis, the most probable complex/molecule structures within the ensemble are written out for further analysis. At this point it is interesting to notice that although thousands of structures were sampled, only a few presented noticeable probabilities. For instance, the 50 most probable monomer/AcN structures amounted to a cumulative probability of 38.95 %, with interaction energies ranging from –29.79 kJ/mol (p = 2.03 %) to –25.89 kJ/mol (p = 0.42 %). Similarly, considering monomer/H2O structures, the 18 most probable structures amounted to a cumulative probability of 50.95 %, with interaction energy values ranging from –43.99 kJ/mol (p = 7.73 %) to –38.96 kJ/mol (p = 1.03 %). On the other hand, considering monomer/MeOH structures, even taking the 50 most probable structures amount to “only” 26.49 %, with interaction energies ranging from –36.99 kJ/mol (p = 2.15 %) to –31.07 % (p = 0.20 %).

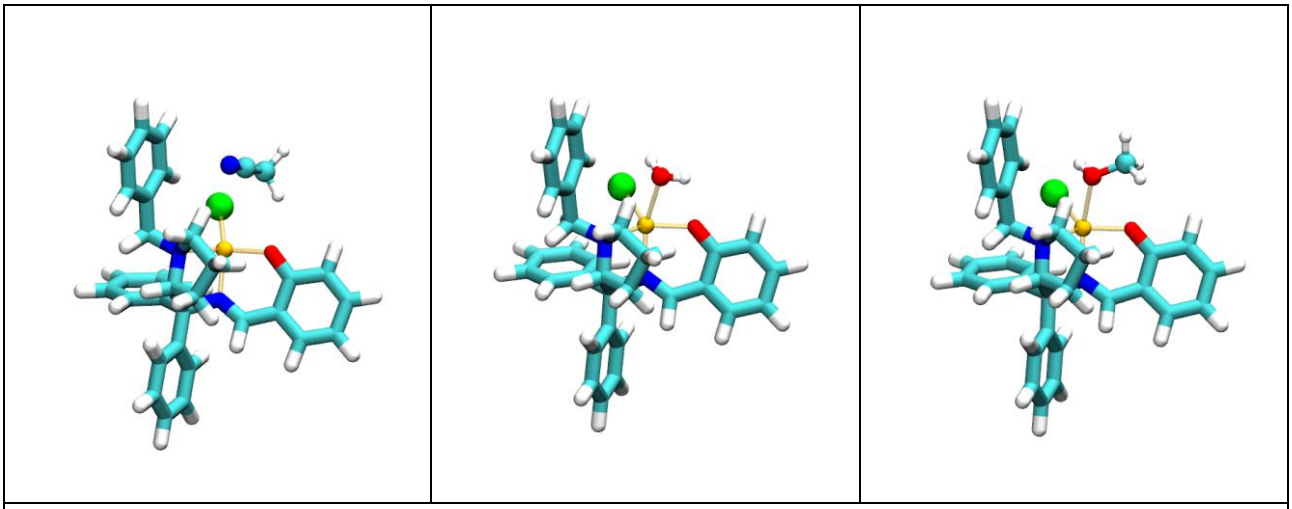

Figure 81 – Most probable complex/molecule structures after Themis search followed by a full geometry optimization: monomer/AcN (left); monomer/H2O (center) and monomer/MeOH (right).

Results for Dimer (singlet)/molecules

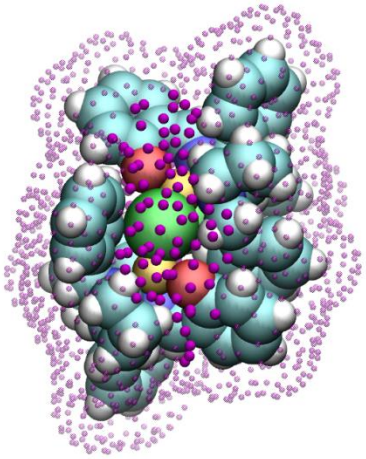

translation grid points near Cu^{2+} and Cl^{-} ions

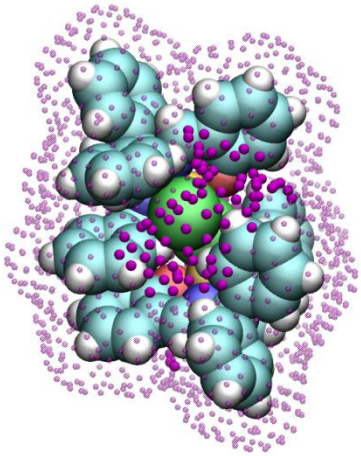

translation grid points near Cu^{2+} and Cl^{-} ions

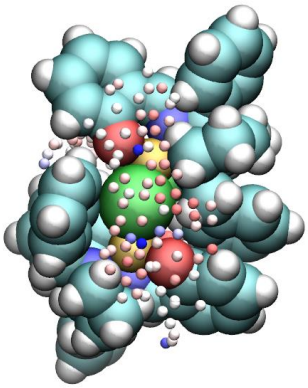

free energy landscape for CAN

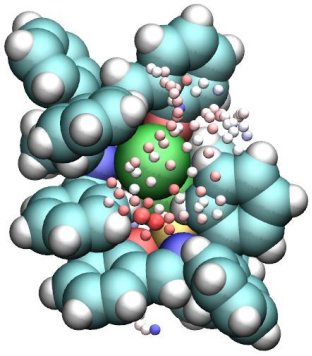

free energy landscape for ACN

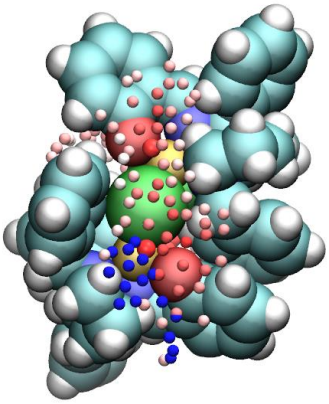

free energy landscape for H2O

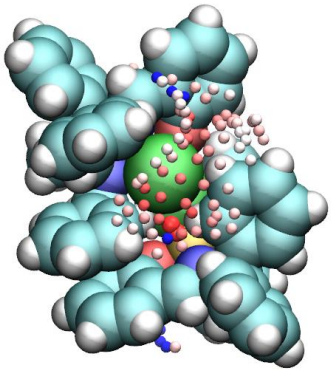

free energy landscape for H2O

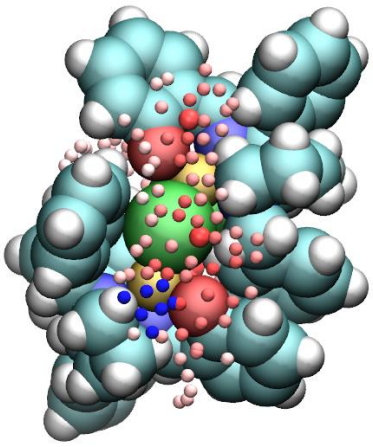

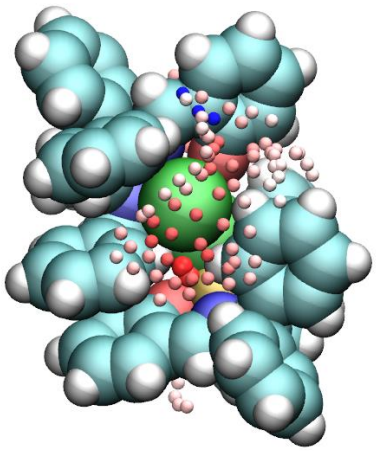

free energy landscape for MeOH free energy landscape for MeOH

Figure S81 – Translation grid along surface accessible area (SAS) of the dimeric complex (transparent purple spheres) at singlet state. Points within 5.0 A of Cu^{2+} or Cl^{-} ions are highlighted (opaque purple spheres) and were used to sample the surface (first row). Free energy landscapes obtained at the GFN1-xTB level: AcN molecule (second row); H2O molecule (third row) and MeOH molecule (fourth row). Colorscale for the landscapes correspond to free energy values ranging from –32 kJ/mol (dark red) to +32 kJ/mol (dark blue). While color correspond to 0 kJ/mol.

Free energy landscape for ACN presented 2 translation points that amount to a 55.31 % probability, with free energy values ranging from –25.81 kJ/mol (p = 41.17 %) to –23.14 kJ/mol (p = 14.14 %).

Free energy landscape for H_2O presented 4 translation points that amount to a 52.04 % probability, with free energy values ranging from –28.91 kJ/mol (p = 15.14 %) to –27.71 kJ/mol (p = 9.35 %).

Free energy landscape for MeOH presented 4 translation points that amount to a 50.91 % probability, with free energy values ranging from –30.02 kJ/mol (p = 24.81 %) to –26.10 kJ/mol (p = 5.15 %).

The 50 most probable dimer (singlet)/ACN structures amounted to a cumulative probability of 55.56 %, with interaction energies ranging from –36.03 kJ/mol (p = 4.92 %) to –28.87 kJ/mol (p = 0.28 %).

The 50 most probable dimer (singlet)/H2O structures amounted to a cumulative probability of 23.73 %, with interaction energies ranging from –41.63 kJ/mol (p = 1.64 %) to –36.97 kJ/mol (p = 0.25 %).

The 50 most probable dimer (singlet)/MeOH structures amounted to a cumulative probability of 43.21 %, with interaction energies ranging from –42.36 kJ/mol (p = 2.31 %) to –37.23 kJ/mol (p = 0.30 %).

Results for Dimer (triplet)/molecules

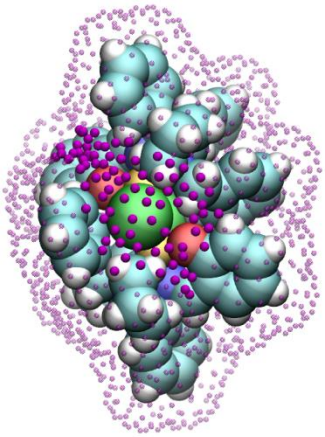

translation grid points near Cu^{2+} and Cl^{-} ions

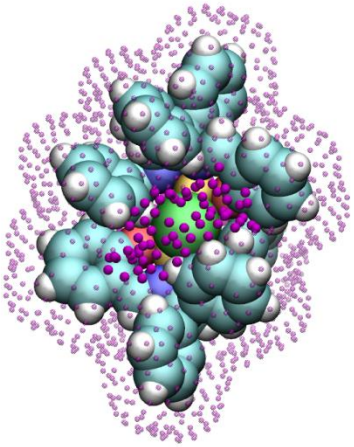

translation grid points near Cu^{2+} and Cl^{-} ions

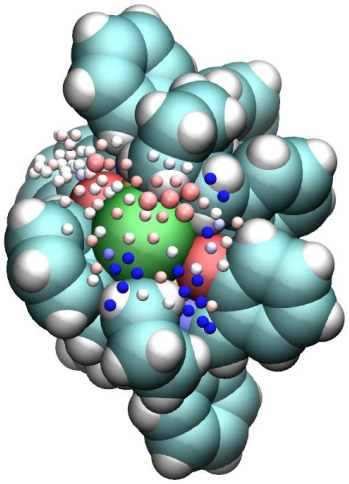

free energy landscape for can

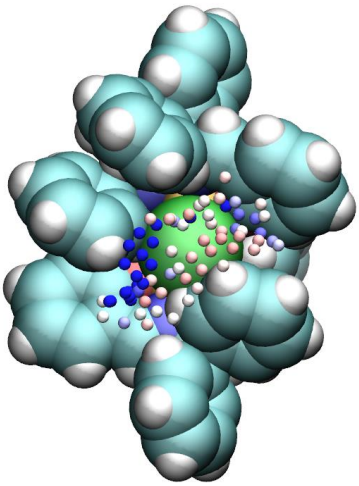

free energy landscape for AcN

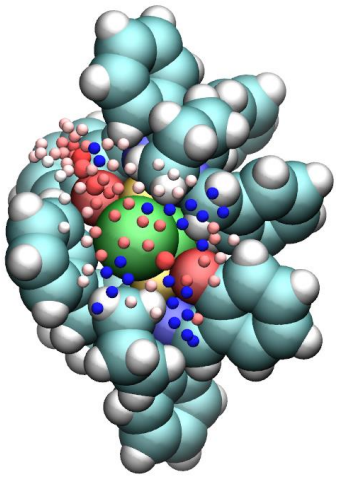

free energy landscape for H2O

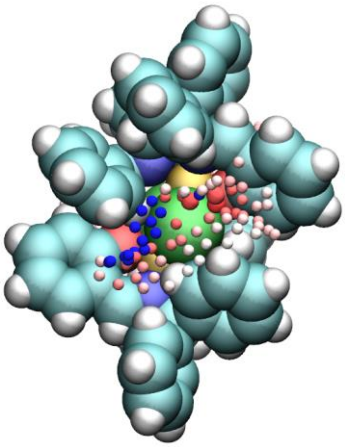

free energy landscape for H2O

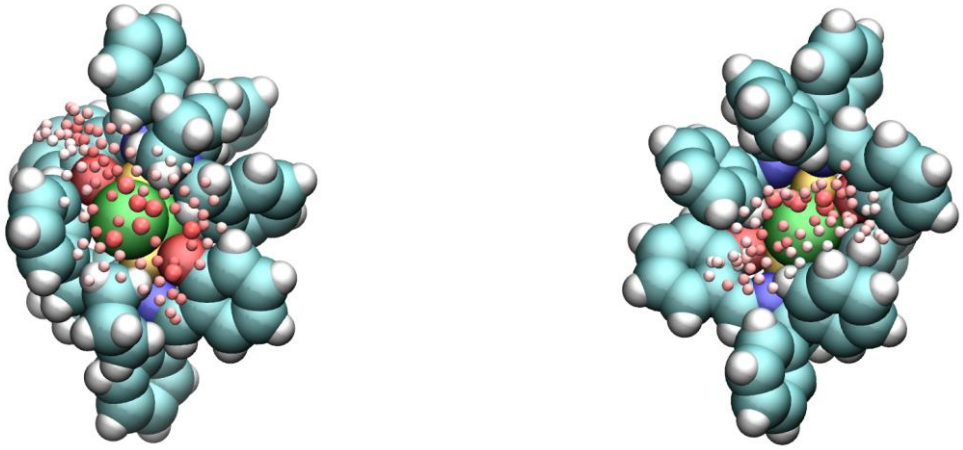

free energy landscape for MeOH free energy landscape for MeOH

Figure S82 – Translation grid along surface accessible area (SAS) of the dimeric complex (transparent purple spheres) at triplet state. Points within 5.0 A of Cu^{2+} or Cl^{-} ions are highlighted (opaque purple spheres) and were used to sample the surface (first row). Free energy landscapes obtained at the GFN1-xTB level: AcN molecule (second row); H2O molecule (third row) and MeOH molecule (fourth row). Colorscale for the landscapes correspond to free energy values ranging from –32 kJ/mol (dark red) to +32 kJ/mol (dark blue). While color correspond to 0 kJ/mol.

Free energy landscape for ACN presented 5 translation points that amount to a 51.46 % probability, with free energy values ranging from –18.69 kJ/mol (p = 14.22 %) to –16.36 kJ/mol (p = 5.58%).

Free energy landscape for H2O presented 7 translation points that amount to a 53.25 % probability, with free energy values ranging from –26.99 kJ/mol (p = 13.74 %) to –23.89 kJ/mol (p = 3.97 %).

Free energy landscape for MeOH presented 12 translation points that amount to a 51.95 % probability, with free energy values ranging from –24.47 kJ/mol (p = 8.66 %) to –21.58 kJ/mol (p = 2.84 %).

The 50 most probable dimer (triplet)/AcN structures amounted to a cumulative probability of 42.24 %, with interaction energies ranging from –29.29 kJ/mol (p = 1.97 %) to –24.46 kJ/mol (p = 0.29 %).

The 50 most probable dimer (triplet)/H2O structures amounted to a cumulative probability of 15.38 %, with interaction energies ranging from –37.11 kJ/mol (p = 0.52 %) to –34.63 kJ/mol (p = 0.19 %).

The 50 most probable dimer (triplet)/MeOH structures amounted to a cumulative probability of 21.74 %, with interaction energies ranging from –37.89 kJ/mol (p = 1.30 %) to –33.81 kJ/mol (p = 0.25 %).

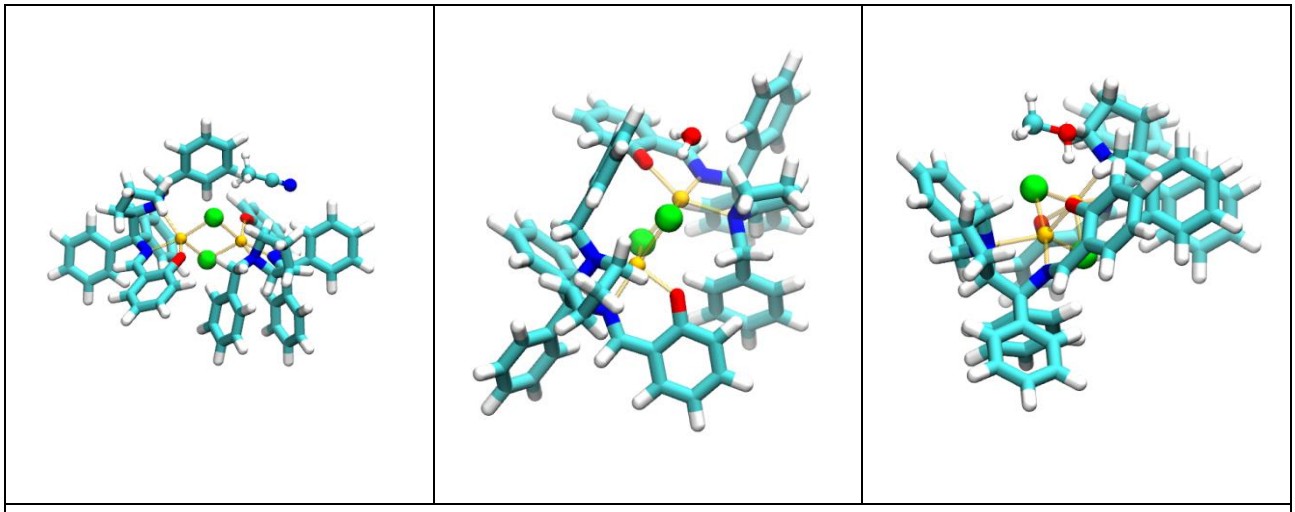

Figure S83 – Most probable complex/molecule structures after Themis search followed by a full geometry optimization: dimer (triplet)/AcN (left); dimer (singlet)/H2O (center) and dimer (singlet)/MeOH (right).

Table S12. Thermochemical data obtained from the DFT calculations of the $Cu^{II}L1$ monomer or dimer interacting with a single solvent molecule. Spin multiplicityis indicated for each complex and the stabilization energies (in kJ/mol) amount to the difference between the most stable singly-solvated complex and the energies of the separated solvent molecule and complex.

ACN	
$Cu^{II}L1$ monomer (doublet)	-33.1
$Cu^{II}L1$ dimer (singlet)	-41.9
$Cu^{II}L1$ dimer (triplet)	-35.9
H_2O	
$Cu^{II}L1$ monomer (doublet)	-57.2
$Cu^{II}L1$ dimer (singlet)	-50.4
$Cu^{II}L1$ dimer (triplet)	-47.0
MeOH	

Cu^{II}L1 monomer (doublet)	-54.1
Cu^{II}L1 dimer (singlet)	-49.6
Cu^{II}L1 dimer (triplet)	-44.0

References

67. Colombari, F. M., Bernardino, K., Gomes, W. R., Lozada-Blanco, A., Moura, A. F. Themis: a Software to Assess Association Free Energies Via Direct Estimative of Partition Functions. Unpublished.
68. Sun, M.; Xu, L.; Qu, A.; Zhao, P.; Hao, T.; Ma, W.; Hao, C.; Wen, X.; Colombari, F. M.;de Moura, A. F.; Kotov, N. A.; Xu, C.; Kuang, H. Site-selective photoinduced cleavage andprofiling of DNA by chiral semiconductor nanoparticles. *Nature Chemistry***2018**, 10, 821–830.
69. Bernardino, K.; Lima, T. A.; Ribeiro, M. C. C. Low-Temperature Phase Transitions of the Ionic Liquid 1-Ethyl-3-methylimidazolium Dicyanamide. *The Journal of Physical Chemistry B***2019**, 123, 9418–9427.
70. Bernardino, K.; Goloviznina, K.; Gomes, M. C.; Pádua, A. A. H.; Ribeiro, M. C. C. Ion pair free energy surface as a probe of ionic liquid structure. *The Journal of Chemical Physics***2020**, 152, 014103.
71. Colombari, F. M.; da Silva, M. A. R.; Homsi, M.; Souza, B. R. L.; Araujo, M.; Francisco, J. L.;Silva, G. T. S. T.; Silva, I. F.; de Moura, A. F.; Teixeira, I. F. GraphiticCarbonNitrides asPlatforms for Single-Atom Photocatalysis. *Faraday Discussions***2020**, Accepted Manuscrit.